

AD

00000000

USAAVLABS TECHNICAL REPORT 68-17

**MODEL STUDIES OF
HELICOPTER ROTOR FLOW PATTERNS**

By

August F. Lehman

April 1968

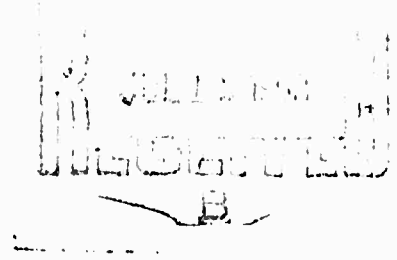
**U. S. ARMY AVIATION MATERIEL LABORATORIES
FORT EUSTIS, VIRGINIA**

CONTRACT DA 44-177-AMC-426(T)

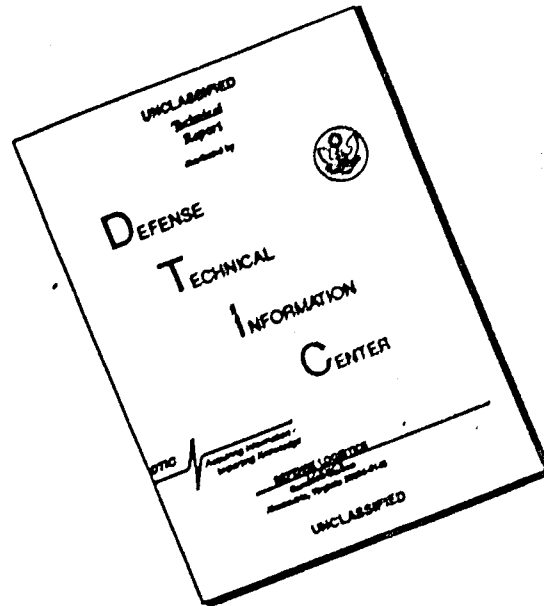
OCEANICS, INC.

PLAINVIEW, NEW YORK

*This document has been approved
for public release and sale; its
distribution is unlimited.*



DISCLAIMER NOTICE



THIS DOCUMENT IS BEST QUALITY AVAILABLE. THE COPY FURNISHED TO DTIC CONTAINED A SIGNIFICANT NUMBER OF PAGES WHICH DO NOT REPRODUCE LEGIBLY.



DEPARTMENT OF THE ARMY
U. S. ARMY AVIATION MATERIEL LABORATORIES
FORT EUSTIS, VIRGINIA 23604

This investigation was initiated to determine the suitability of the water tunnel for rotary-wing flow visualization. The specific task attempted was the definition of isolated rotor wake boundaries at various disc loadings, numbers of blades, and advance ratios.

The results indicate that the technique can provide considerable insight into the rotor flow field and may subsequently be used for studying the complex flow interactions of main rotors, tail rotors, propulsion units, and airframes of rotary-wing derivative aircraft.

Task 1F125901A14232
Contract DA 44-177-AMC-426(T)
USAAVLABS Technical Report 68-17
April 1968

MODEL STUDIES OF
HELICOPTER ROTOR FLOW PATTERNS

Oceanics Report No. 67-38

by

August F. Lehman

Prepared by

Oceanics, Inc.
Plainview, New York

for

U. S. ARMY AVIATION MATERIEL LABORATORIES
FORT EUSTIS, VIRGINIA

This document has been approved for public
release and sale; its distribution is unlimited.

SUMMARY

This report discusses an experimental program undertaken in a water tunnel wherein the tip vortex patterns were made visible through air bubble injection at the rotor tips. The model was a scaled version of the 48-foot-diameter Bell UH-1D rotor. The rotor configuration was tested as a standard 2-bladed unit and also as a 1- and 3-bladed unit. Correlation was established by comparing full-scale vertical lift values (at hover conditions) with scaled model values, where the model was mounted above the tunnel floor at a distance equivalent to "out of ground" effects for the full-scale vehicle. Employing solely a Prandtl-Glauert correction factor produced excellent lift value agreement between the model and the full-scale vehicle. Different aspects of the tip vortex patterns were visible from 2 to 6 diameters downstream; thus the technique appears promising for both near and far field studies. High speed movies and stop and time exposure photographs were used to document the variation in vortex patterns. Discrete tip vortex patterns are created for forward flight regimes in the general ranges of hover to 10 knots, 10 to 50 knots, and above 50 knots. Tip vortices shed from one blade do intersect with following blades (under certain conditions), thus verifying a limitation in the commonly employed mathematical models, where this limitation has been hypothesized by certain other investigators.

FOREWORD

This program was sponsored by the U. S. Army Aviation Materiel Laboratories under Contract No. DA 44-177-AMC-426(T). The Army project engineer was Mr. William E. Sickles of the sponsoring agency, and appreciation is expressed to him and the agency for their interest in this area. Mr. Robert Romandetto of the Oceanics Water Tunnel Division played a key part in the testing program.

PRECEDING
PAGE BLANK

CONTENTS

	<u>Page</u>
SUMMARY	iii
FOREWORD	v
LIST OF ILLUSTRATIONS	ix
INTRODUCTION.	1
Program Objectives.	2
TECHNICAL APPROACH TO THE PROBLEM	4
Observation of Disturbed Flows	4
Model/Full-Scale Correlation	6
Model/Tunnel-Size Consideration.	7
TEST FACILITIES AND EQUIPMENT.	9
Rotor Lift Measurement.	10
Test Procedures	11
Photographic Documentation	13
Order of Recorded Data Accuracy.	13
TEST RESULTS - EVALUATION AND DISCUSSION	15
Vertical Lift Performance	16
Vortex Trail Observations - Hover and Forward Flight Conditions	23
Vortex Trail Observations - Inflow Patterns	27
Simulated Power Failure	28
Rotor Wake Spatial Coordinates	28
Additional Rotor Wake Observations	30
SUMMARY AND CONCLUSIONS.	35

PRECEDING
PAGE BLANK

	<u>Page</u>
RECOMMENDATIONS FOR FUTURE WORK	39
REFERENCES	40
APPENDIXES	
I Hover and Forward Flight Conditions .	89
II Air Bubble Streak Studies.	102
III Simulated Power Failure.	104
DISTRIBUTION	108

ILLUSTRATIONS

<u>Figure</u>		<u>Page</u>
1	Tip Vortex Cavitation on a Marine Propeller	42
2	Rotor Blades and Hub Assembly	43
3	Sketch of the Tunnel Test Installation.	44
4	Jig Used in Setting the Rotor Collective Pitch Angle.	45
5	Plot Comparing the Collective Pitch Angle Settings from Full-Scale Data with Model Settings	46
6	Plot Comparing the Collective Pitch Angle Settings from Full-Scale Data with Model Settings	47
7	Plot Comparing the Collective Pitch Angle Settings from Full-Scale Data with Model Settings	48
8	Plot Comparing the Collective Pitch Angle Settings from Full-Scale Data with Model Settings	49
9	Plot of 1-Bladed Rotor Lift as a Percentage of 2-Bladed Rotor Lift for Variations in Forward Velocity.	50
10	Plot of 3-Bladed Rotor Lift as a Percentage of 2-Bladed Rotor Lift for Variations in Forward Velocity.	51
11	2-Bladed Rotor Vortex Trails at Hover .	52
12	1-Bladed Rotor Vortex Trails at Hover .	53
13	2- and 3-Bladed Rotor Vortex Trails for Same Collective Pitch Angle Setting at 10 Knots.	54
14(a)	3-Bladed Vortex Trails at 35 Knots. . .	55
14(b)	3-Bladed Vortex Trails at 35 Knots. . .	56

<u>Figure</u>		<u>Page</u>
15	2-Bladed Vortex Trails at 110 Knots . .	57
16	2-Bladed Rotor Vortex Trails at 120 Knots	58
17	Comparison of 2-Bladed Rotor Hover Trails at Vertical Lifts of 4,060 and 10,075 Pounds	59
18	Comparison of 2-Bladed Rotor Vortex Trails at 20 Knots for Vertical Lifts of 4,000 and 10,150 Pounds.	60
19	Comparison of 3-Bladed Rotor Vortex Trails at 20 Knots for Vertical Lifts of 4,960 and 13,250 Pounds.	61
20	Comparison of 2-Bladed Rotor Vortex Trails at 120 Knots for Vertical Lifts of 9,750 and 4,000 Pounds	62
21	Comparison of 1- and 3-Bladed Rotor Vortex Trails at Same Collective Pitch Angle Setting and Hover Conditions. . .	63
22	Comparison of 1-, 2-, and 3-Bladed Rotor Vortex Trails for Same Collective Pitch Angle Setting and Mast Angle at 25 Knots	64
23	Comparison of 1-, 2-, and 3-Bladed Rotor Trails for Same Collective Pitch Angle Setting and Mast Angle at 110 Knots	65
24(a)	Velocity Increase Sequence Showing Vortex Trails Passing Above the Rotor; 2-Bladed Rotor.	66
24(b)	Velocity Increase Sequence Showing Vortex Trails Passing Above the Rotor; 2-Bladed Rotor.	67
24(c)	Velocity Increase Sequence Showing Vortex Trails Passing Above the Rotor; 2-Bladed Rotor.	68

<u>Figure</u>		<u>Page</u>
25	Variation in Inflow Pattern with Rake Lateral Position; 2-Bladed Rotor, Hover Condition	69
26	Variation in Inflow Pattern with Velocity Increase; 2-Bladed Rotor, Rake On Fore and Aft Center Line of Rotor Shaft	70
27	Simulated Power Failure - Autorotation with 2-Bladed Rotor	71
28	Comparison of Tip Vortex Trails for 2-Bladed Rotor in Simulated Autorotation Condition at 70 Knots.	72
29	Comparison of Tip Vortex Trails for 2-Bladed Rotor in Simulated Autorotation at 150 Knots	73
30	Plot of Spatial Wake Coordinates as Radial and Axial Contraction Ratios, 2-Bladed Rotor at Hover	74
31	Comparison of Faired Experimental Data with Equation Values for Case of 1-, 2-, and 3-Bladed Rotors at Hover	75
32	Sketch of Terms Employed in Spatially Locating Flow Characteristics	76
33	Rotor Tip Path Orientation Versus Forward Velocity for Nominal 4,000-Pound Lift for 2-Bladed Rotor	78
34	Rotor Tip Path Orientation Versus Forward Velocity for Nominal 6,000-Pound Lift for 2-Bladed Rotor	79
35	Rotor Tip Path Orientation Versus Forward Velocity for Nominal 8,000-Pound Lift for 2-Bladed Rotor	80
36	Rotor Tip Path Orientation Versus Forward Velocity for Nominal 10,000-Pound Lift for 2-Bladed Rotor	81

<u>Figure</u>		<u>Page</u>
37	Plot of Radial Contraction Ratio Versus Collective Pitch Angle for 1-, 2-, and 3-Bladed Rotor at Hover	82
38	Plot of Radial Contraction Ratio Versus Equivalent Vertical Load for 1-, 2-, and 3-Bladed Rotor at Hover	83
39	Displacement of the Upper and Lower Boundaries of the Flow Through the Rotor Versus Forward Velocity for a Nominal 4,000-Pound Lift for the 2-Bladed Rotor	84
40	Displacement of the Upper and Lower Boundaries of the Flow Through the Rotor Versus Forward Velocity for a Nominal 6,000-Pound Lift for the 2-Bladed Rotor	85
41	Displacement of the Upper and Lower Boundaries Defining the Flow Through the Rotor Versus Forward Velocity for a Nominal 8,000-Pound Lift for the 2-Bladed Rotor	86
42	Displacement of the Upper and Lower Boundaries of the Flow Through the Rotor Versus Forward Velocity for a Nominal 10,000-Pound Lift for the 2-Bladed Rotor	87
43	Displacement of the "Wing Tip Type" Vortices Versus Forward Velocity . . .	88

INTRODUCTION

Within the past two decades, the design techniques employed as a means of predicting VTOL performance have evolved from those approximating an art to a stature more representative of a science. However, a rather soft spot in this science of VTOL performance prediction lies in the area encompassing the hover and transitional regimes of flight, although certain refinements in the prediction techniques applicable throughout the entire speed range would be useful.

In a paper (Reference 1, pages 282-283) published in 1966, White wrote that "... a major advance in the present state of the art will not be accomplished until some basic homework is done to obtain a better understanding of the fundamental parameters upon which all of the applied prediction techniques depend" and "... unless a concerted effort is now made to obtain this basic information the availability of adequate prediction methods will again seriously lag behind the development of flight articles. If this occurs, the rejection of soundly conceived configurations because of poorly understood peripheral problems then becomes possible." It is this thought which crystalizes the concern of many scientists and engineers working in the VTOL field.

Although the experimental work which will be discussed in this report primarily involves model studies covering the range from hover to a 120-knot forward speed, the major value of the studies may well be in the hover-transitional flight range simply because this is the area wherein the existing prediction methods have the poorest performance record.

Jenney, Olson and Landgrebe in Reference 2 presented an excellent summary of the various methods (and their limitations) used in calculating the hover performance of a rotor, progressing from the simplest analysis of conservation of energy and momentum change of the air mass passing through an actuator disk, to the more sophisticated three-dimensional models as evidenced by the work of Goldstein-Lock in References 3 and 4, Piziali and DuWaldt in Reference 5, and Erickson and Ordway in Reference 6. The report in Reference 2 culminated the summary by discussing the performance method developed at United Aircraft Corporation Research Laboratories, which is perhaps the most advanced method published to date.

From the survey of these methods, there seems to be little doubt that the accurate prediction of rotor performance, particularly in the hover-transitional range, must include as input, information about, or certain

assumptions about, the rotor wake geometry characteristics; at this writing, a satisfactory theoretical method for establishing these characteristics is not available. Thus, the situation has not changed significantly, in terms of affording adequate input of this nature, since 1966, when Oceanics proposed and received sponsorship from the U. S. Army Aviation Materiel Laboratories (USAAVLABS) for an experimental study of model helicopter rotors in a water tunnel.

PROGRAM OBJECTIVES

The general problem revolves about the apparent lack of a clear physical grasp of the actual rotor tip vortex trail configuration(s). This fact, coupled with the complexity and inflexibility of the existing mathematical models permitting rigorous solution, made visual observations of the downwash flow field particularly advantageous. The visualization of the tip vortex trails would establish one facet of the flow field and permit, in a qualitative manner, a determination of any differences existing between the predicted and actual rotor performance with reference to the space location of the shed tip vortex trails. With these differences known, it would be possible to hypothesize about the work required to evolve more accurate theories.

Specifically, the program involved:

1. Testing three rotor configurations (1-bladed, 2-bladed, and 3-bladed);
2. Measuring rotor thrust;
3. Taking black and white 16 mm high speed movie clips (50 ft exposures) of the tip vortex trails for each test condition (side and overhead view);
4. Taking stop action and time exposure still photographs of each wake pattern (side and overhead view).

The test conditions consisted of equivalent 4,000-, 6,000-, 8,000-, and 10,000-pound loads for the 2-bladed configuration, with these conditions (i.e., collective pitch, mast tilt) then employed for the 1- and 3-bladed configurations. Equivalent forward velocities of hover and 10, 20, 25, 35, 50, 60, 70, 90, 110, and 120 knots were investigated.

In addition, inflow patterns to the rotor were

observed through bubble streak techniques, and certain information about power failure performance was gained through simulated autorotation investigations.

As a last item, a short color and black and white 16 mm sound motion picture was made wherein this testing technique is presented and discussed. This film is available through USAAVLABS (Aeromechanics Division).

TECHNICAL APPROACH TO THE PROBLEM

The test program was undertaken in the Oceanics water tunnel. The use of a water tunnel for the visualization of airflows, in particular vortex trails, is not an altogether new approach, although the technique has been somewhat neglected in spite of its potential. If the airflow being simulated by water flow is in a low velocity regime, such that the airflow can be treated as an incompressible medium, no problem arises since water is incompressible and can therefore be satisfactorily substituted. If the flow velocity is such as to enter the regime where compressibility of the air must be considered, a correction such as the Prandtl-Glauert factor must be introduced. In any event, water tunnel-free air regime data correlation is possible. In addition, tests undertaken in a water tunnel possess the significant advantage of permitting smaller test models, since the operating Reynolds number in most water tunnel studies is roughly twenty times that in air for studies with the same size model and the normally employed throat velocities for each type of test facility.

OBSERVATION OF DISTURBED FLOWS

The disturbances which are created in incompressible airflows by an object will also exist in water. With the flow disturbances existing in water, the presence and location of the disturbed flow (vortex patterns) can be made visible in several ways. For the case of tip vortex patterns, cavitation and air bubble injection offer the greatest advantages. Cavitation is nothing more than the local vaporization of the water due to a local pressure reduction brought about by local velocity increases. The presence of the vapor- or gas-filled void offers an excellent way of viewing a vortex trail since nothing is added to the test medium. Tip vortex cavitation on a marine propeller is shown in Figure 1. The vaporization of the water in the cores of the vortices is brought about by decreasing the ambient pressure in the water tunnel until this phenomenon (cavitation) occurs.

An example of the application of water tunnel investigations wherein the study of airflow disturbances was undertaken by Oceanics through the use of the water tunnel cavitation technique is presented in Reference 7. In that investigation, visualization of the air wake disturbances encountered by aircraft during a carrier landing approach was obtained. The high speed movies taken of

disturbed flow patterns made visible through cavitation (while the aircraft carrier model underwent scaled pitch and heave motions) have been a significant aid in understanding the cause and nature of these disturbances. It was the success of that program which led to the formulation of the proposal for this study.

Under certain test conditions, while tip vortices exist, it may not be possible to reduce the ambient pressure in the tunnel to produce a vaporous core in the tip vortex trail* before causing cavitation on the upper portion of the lifting surface. If cavitation occurs, the lift and drag characteristics of the lifting surface may be altered to such a degree that they no longer adequately represent the normal operation of the lifting surface. In other words, if, for example, during water tunnel tests involving wing tip vortex trail studies, should the upper surface of the wing begin to cavitate, the cavitating region can be roughly compared to a "stall" condition, so that flow conditions over the wing no longer represent performance before the occurrence of the "stall". If that situation occurs, the ambient pressure can be raised to prevent the unwanted surface cavitation and, through proper instrumentation in the wing, air can be injected into the core of the tip vortex. The air bubbles remain trapped in the core of the vortex until the core strength of the vortex reduces to a level which permits the bubbles to leave the vortex formation. Air bubbles not remaining in the vortex will interfere with visual observation, so that the proper amount of air injection is important. However, it should be emphasized that the air bubbles trapped in the vortex core patterns do not distort the vortex pattern, just as the vaporous cavities do not distort it. Dye can also be employed to trace the vortex patterns, but the use of dye requires large amounts of dye injection (with any reasonable test velocity), together with the fact that the contrast level between the dye and the background is diminished as the dye gradually changes the color of the water throughout the test section. Dye does offer a useful technique when streamline patterns are to be observed, since in that case the buoyancy of the air bubbles may distort the "flow pattern" more than can be tolerated.

* A possible situation of this nature occurs when the loading at the tip is not "heavy" enough to cause a strong tip vortex.

To review briefly, it has been established at this point that:

1. Studies involving airflow can be undertaken in water and;
2. Vortex trails can be made visible either through the use of the cavitation or the air bubble release technique.

The next matter of concern involves model/full-scale correlation; and since these studies were undertaken in a closed test section, the influence of the model-size/tunnel-size ratio must also be established.

MODEL/FULL-SCALE CORRELATION

Ignoring for a moment any corrections required to the data because the testing is conducted in a tunnel, there remain two scaling parameters requiring consideration. One parameter involves geometric similarity; the other, dynamic similarity. Geometric similarity is maintained by linear scaling of the physical size of the rotor blade selected for tests. Dynamic similarity requires that the ratio of the force acting on the model and the prototype be the same for both systems. The forces acting on a solid surface and the flow characteristics associating with those forces are strongly dependent on the ratio of inertia to viscous forces, i.e., the Reynolds number, $R_e = \frac{V\ell}{\nu}$, where V is the velocity term, ν is the kinematic viscosity term and ℓ is the length term. The normal manner in which the Reynolds number is scaled for lifting surface investigations employs the chord length of the foil as the length dimension term.*

On the basis of a Reynolds number derived from the rotor chord length and a full-speed tip velocity of 800 fps, the prototype has a Reynolds number value of approximately 7.9×10^6 . For the tunnel test conditions, the model value is approximately 9.3×10^4 . Thus, for these studies, there is a difference in the two Reynolds number values. However, for a variation of this magnitude

* To be precise, what should be employed for the "length term" is some measure of the boundary layer or momentum thickness, because these are the true characteristic parameters directly associated with the viscous forces of the flow.

in the Reynolds number, the drag characteristics rather than the lift characteristics are affected. (See, for example, any symmetrical four-digit airfoil data in Reference 8.) In the present study, the lift characteristics are of primary concern since the lift is more closely aligned with the downwash than the drag; thus, the difference which does exist between the two Reynolds numbers should not affect the validity of the test data.

A further consideration in assuring data correlation involves operating the model at the same advance ratio as the full-scale vehicle. The advance ratio (μ) is defined as the free-stream velocity divided by the tip speed velocity. For this study, a constant full-scale tip velocity of 800 fps was assumed for the entire full-scale speed range from hover to 120 knots.

The last consideration in assuring correlation of the test data lies in the correction to the data obtained in the water tunnel to a value representative of the air-flow performance where the speed of the rotor introduces compressibility effects. A reasonable approximation for estimating the compressibility effect on incompressible data is to employ the Prandtl-Glauert factor, which is $\sqrt{1-M^2}$. Payne in Reference 9 shows that the thrust coefficient obtained with an incompressible flow situation divided by the Prandtl-Glauert factor, where the Mach number (M) is taken as that occurring at the 0.7 radius of the rotor, provides good agreement with compressible flow thrust coefficient data. This approximation is the one used as the basis for correlation in the present study.

MODEL/TUNNEL-SIZE CONSIDERATION

The effects of model/tunnel size for the case of downward deflected wakes can become relatively involved, depending upon the specific information desired from the test data. For this particular study, the interest centered about:

1. The practicability of viewing vortex trails in a water tunnel;
2. Correlation of model rotor thrust with full-scale measurements using the hover case as the primary means of data correlation, since the full-scale hover data contain the least possible chance of error.

The manner of formation and the location of the vortex trails were of major concern, although some distortion in the flow signature could possibly be tolerated in an essentially qualitative study of this nature. In view of the criteria established for this test study, the model size of a 12-inch-diameter rotor was selected on the basis of:

1. Physical size large enough to machine model rotor blades having sufficient strength while permitting retention of an airfoil shape truly representative of the desired profile;
2. Rotor-diameter/tunnel-size ratio such that the model could be mounted relatively close to the center line (i.e., somewhat above) while retaining the floor-rotor distance such that it was essentially out of ground effect according to the full-scale data.

Full-scale evaluation of the 48-foot-diameter rotor in Reference 10 indicated that the rotor performance was out of ground effect when the center of the rotor hub was higher than the range of 52 feet to 60 feet above the ground, depending upon the rotor loading. In this test installation, the equivalent rotor height was 52 feet (hover condition); thus, from Reference 10 it was believed that there would be negligible ground effect from the tunnel floor, although the presence of the side wall and ceiling could have some effect on the results. However, Heyson shows in Reference 11 that the wall(s) and ceiling effects are small compared to the floor (or ground) effect. Thus, the net effect of the presence of the tunnel constraint should be negligible.

At the hover and transitional flight stages, the flow pattern established in a tunnel circuit by the action of the rotor downwash field impinging against the floor, then moving laterally to the side walls, up the side walls, across the ceiling of the tunnel, and once again into the rotor disk area, is not truly representative of free air patterns. This establishment of flow circulation in the tunnel has been reported by Rae in Reference 12. The effects of this unwanted rotor-induced circulation in the tunnel were minimized as much as possible in these tests by taking photographs, movies and data before this circulation was well established.

TEST FACILITIES AND EQUIPMENT

The tests were run in the Oceanics water tunnel. This tunnel is a recirculating, closed jet type tunnel having both the water velocity and the test section static pressure as controllable variables. The test section has a cross section approximately 20 inches on each side (with rounded corners) and a length of about 7 feet. The maximum water velocity is about 40 fps, and the static pressure can be independently controlled over a range from about 0.1 to 2 atmospheres absolute.

In the settling section, just ahead of the nozzle, there exists a rather fine grid honeycomb to improve the flow conditions before the water enters the nozzle and passes through the test section. At the entrance to the test section, screens can be inserted to create a particular wake profile or some desired level of turbulence. For these investigations, no screens were employed and a uniform flow approached the rotor system.

The model helicopter rotor blades consisted of scaled versions of the UH-1D rotor using information from the Bell Helicopter Corporation drawings. The increase in thickness at the root end was achieved in the model blade by a uniform linear increase in profile thickness to the appropriate grip thickness rather than through a true scaling of the doubler plates employed on the real rotor.

The model rotor blades were 5.42 inches long and had an NACA 0012 profile with a maximum thickness of 0.052 inch. The uniform twist from the root of the blade to the tip was 9 degrees 50 minutes (corresponding to twist from the rotor center to the tip of 10 degrees 54 minutes).

Designing the blades brought about several problems. The first was selecting a stainless material having an appropriate strength, since the bending stress level (at the beginning of the taper to the grip station) could approach 100 ksi. The material selected was Armco 17-4 Ph stainless steel having an ultimate strength of 200 ksi and a yield strength of 185 ksi in condition H 900. Machining was a difficult undertaking because of the length and thinness of the airfoil section. Ordinary blade machining techniques introduce a certain amount of tool pressure along the blade such that the nonuniformities were introduced along the blade span. Satisfactory blades were finally obtained through the use of chemical machining. This work was undertaken by Aerospace Techniques, Inc., of Connecticut. The final blades and hubs are shown in Figure 2.

The test assembly consisted of a drive motor, a strain-gaged lift measuring coupling, a drive shaft, a pylon fairing, and a rotor. The rotor pylon projected through a slot in the tunnel floor and was fastened to a pivoted mounting plate. The plate could be adjusted in the fore-and-aft direction by the use of a lead screw. The setting of a particular angle was possible through a pointer-scale arrangement. Since this study involved only the main rotor, i.e., no tail rotor was involved, the blade pitch variation around the azimuth includes only collective pitch and fore-and-aft cyclic pitch variations, as lateral pitch variations need not be introduced. Thus, the action of the test rotor is not truly representative of helicopter operation, since lateral cyclic is not introduced to the blade as it travels about the azimuth. Fore-and-aft cyclic, mast tilt, and fuselage orientation (in the pitch direction) can all be properly introduced through a given mast tilt setting, with collective pitch set on each individual blade. A sketch of the installation is shown in Figure 3. The desired collective pitch was established for each blade using the angular setting jig shown in Figure 4.

ROTOR LIFT MEASUREMENT

The lift of the rotor in a direction along the rotor drive shaft was sensed by a strain-gaged force coupling which connected the drive motor to the rotor drive shaft. This coupling incorporated a strain-gaged beam capable of detecting the force with considerable sensitivity and accuracy. Calibration of the force unit was performed by removing the motor and coupling as an assembly, inverting it, and hanging various weights from the coupling. In this manner, the applied calibration load was in the same direction as the lift force applied in test operations. The strain gages were powered by a Sanborn 650 system, and the output from the Sanborn unit was fed into an X-Y plotter; thus, a known weight could be associated with a given deflection. The sensitivity of the strain-gaged coupling was quite high, permitting various degrees of attenuation to be inserted into the signal to keep the deflection range within that allowable for the X-Y plotter. The force sensing arrangement permitted the measurements to be in the order of 10 inches for any particular test condition. This magnitude of deflection permitted rather good accuracy in determining the actual rotor load as it was undergoing tests.

TEST PROCEDURES

The initial portion of this program consisted of establishing test conditions equivalent to full-scale loads of 4,000, 6,000, 8,000 and 10,000 pounds for the 2-bladed rotor configuration. Information from USAAVLABS established the conditions of mast tilt (which included the mast tilt, fuselage orientation, and fore-and-aft cyclic) and collective pitch for each of the vertical load conditions, at forward velocities ranging from 0 knots to 120 knots. The information obtained from USAAVLABS is shown in Table I.

The USAAVLABS data were based on considerable interpolation of full-scale data, and through discussion with USAAVLABS, it was agreed that the mast tilt angle was to remain as specified and the collective pitch angle was to be adjusted if the desired lift coefficient was not achieved with the original collective pitch settings. The desired advance ratio (forward velocity/tip speed) for model testing was achieved by employing a constant full-scale tip speed of 800 fps and a constant model tip speed of 25.21 fps (8 rps). For the hover condition, the same model speed was employed, i.e., 8 rps.

For those studies involving simulated power failure, the test conditions consisted of a constant collective pitch angle of 2.75 degrees at the 0.75 span station, with the mast angle established as 8 degrees less than that employed in forward flight. In these studies, the rotor rotational speed was adjusted for the specified collective pitch and mast tilt angles to provide three different lift values. From these data, it should be possible to estimate sink rates as a function of rotor speed for given load conditions.

Actual testing procedures involved a check of the force unit calibration which was performed each day. Following this, the desired collective pitch angle was set on the blades, and the proper mast tilt was introduced. The required tunnel velocity and model rotational speeds were then established for the particular test condition being simulated. The rotor lift value was then obtained from the amount of deflection recorded on the X-Y plotter and the appropriate force calibration sheet. This lift value was converted into a lift coefficient value employing the Prandtl-Glauert factor mentioned earlier.

Trigonometric considerations were employed to convert the rotor lift as measured along the rotor shaft

TABLE I. INITIAL MAST TILT AND COLLECTIVE PITCH ASSUMPTIONS

TABLE I. INITIAL MAST TILT AND COLLECTIVE PITCH ASSUMPTIONS					
6,000 lb Gross Weight			10,000 lb Gross Weight		
V_{kt}	Collective Pitch Angle (deg)	Mast Tilt* (deg)	V_{kt}	Collective Pitch Angle (deg)	Mast Tilt* (deg)
0	+13.4	0	0	+16.2	0
10	12.4	- .9	10	14.8	- 1.1
20	11.7	- 1.9	20	14.2	- 2.2
25	11.4	- 2.5	25	14.1	- 2.8
35	11.4	- 3.6	35	13.9	- 3.9
50	11.5	- 5.4	50	13.8	- 5.6
60	11.7	- 6.7	60	14.0	- 6.8
70	12.0	- 8.4	70	14.1	- 7.8
90	12.9	-11.9	90	14.7	- 8.9
110	14.6	-13.8	100	15.2	-11.6
120	16.0	-15.6	110	15.8	-13.4

* Mast tilt represents the angle between the tip path plane and the free stream, the minus sign signifying nose down. The mast tilt angle accounts for the aggregate of cyclic pitch, flapping, fuselage tilt, and mast tilt with respect to fuselage.

Additional points for 4,000 pounds and 8,000 pounds gross weight may be computed on a linear basis.

to the vertical direction. If the lift coefficient value was not within approximately 3 percent of the desired value, the collective pitch angle was changed and the tests were repeated until the lift coefficient value obtained was within the tolerance range. In this manner, the acceptable collective pitch conditions were established for the 2-bladed rotor design. These same conditions were then employed for investigations involving the 1- and 3-bladed rotor configurations.

PHOTOGRAPHIC DOCUMENTATION

High speed motion picture and still camera photographs were taken of all test conditions. Still camera exposures were taken at 1/500 second (essentially stop action) and 1/25 second, wherein the bubbles appear as streaks in the photographs to supply an indication of the tip vortex pattern with time. The movies and still camera exposures were taken with the camera essentially centered on the rotor when the unit was in the hover orientation. Photographs were taken both from the side and from overhead. In addition, as noted earlier, a 15-minute-long, color and black and white 16 mm sound film depicting the test techniques was made and is available from USAAVLABS.

ORDER OF RECORDED DATA ACCURACY

The weights used in the calibrating of the force cell coupling were certified accurate according to National Bureau of Standards Tolerance Class C. Each division on the scale and indicator of the mast tilt unit was calibrated to within 3 seconds of arc, the total scale of 17 degrees within 6 seconds of arc. Each division on the scale and indicator for the jig used in aligning collective pitch for the blade was calibrated to 6 seconds of arc, the total scale of 30 degrees, calibrated to a tolerance of 6 seconds. The setting accuracy was within 0.2 degree. Rotor speed was held within 1 percent of the desired value employing a 10-second count on an electronic counter. The tunnel velocity entering the test section had a maximum of 2 percent error above 25 knots and a somewhat greater error below that, except at hover conditions, where there was zero error.

The use of a given hover setting as the daily check condition for the force sensing system resulted in a variation in the measured lift of less than 3 percent.

This variation in value includes any deviations included in the lift calibration, rpm, and collective pitch setting. On the basis of the check conditions repeatability, it can be concluded that the repeatability and accuracy of the raw data are within 3 percent of the given value. Note that this is the accuracy of the recorded raw lift condition and does not include refinements to this raw value required because of Mach number or model/tunnel-size considerations. These refinements will be discussed in the next section.

TEST RESULTS - EVALUATION AND DISCUSSION

The bulk of the raw data consists of high speed movie clips and still camera photographs. The tabulation of all test conditions is contained in Appendix I. All of these data are at USAAVLABS, and any serious consideration of this information relative to the implementation of existing theory (or theories) will require an examination of these data. In this report, certain general comments are presented as well as an indication of the observed flow conditions substantiating these conclusions.

Before entering into further data presentation and discussion, it is perhaps wise to review the conditions and assumptions employed in the test program:

1. Geometric rotor similarity was achieved by direct scaling.
2. Dynamic flow differences as indicated by the difference in the operating Reynolds number (7.9×10^6 vs. 9.3×10^4) will affect the rotor drag characteristics, but not the lift characteristics, and the lift characteristics are the dominant factor in determining the tip vortex trail configuration.
3. The same advance ratio (μ) was maintained in the model tests as existed during full-scale operation.
4. Model/full-scale lift correlation was established by comparing the vertical lift coefficients obtained at hover operating conditions.
5. Compressibility effects were accounted for by using the Prandtl-Glauert factor existing at the 0.7 radial section for a full-scale rotor at a tip speed of 800 fps.
6. The model was oriented in the tunnel slightly above the center line and at a distance corresponding to 1.1 rotor diameters above the floor. This rotor-floor spacing places the rotor out of ground effect according to full-scale data, and thus no corrections were made to the model data for the presence of the floor.

7. The presence of the tunnel ceiling should have considerably less effect than the presence of the tunnel floor (or ground - according to Heyson's work); thus, since (essentially) no ground effect exists for the given installation, no appreciable ceiling effect exists, and no corrections were made to the data as a result of the presence of the ceiling.
8. Corrections to the load as measured along the rotor drive shaft axis to the vertical direction were based on trigonometric considerations.

What the above condenses to is this: the rotor size was selected such that it was oriented near the center line of an equal height-width tunnel and at a distance equivalent to a full-scale distance which placed the rotor out of ground effect according to full-scale data. The resulting corrections to the data as measured in the tunnel, while maintaining the same advance ratio, thus resolved solely to a correction for Mach number considerations based on the Prandtl-Glauert factor.

VERTICAL LIFT PERFORMANCE

The validity of the data evaluation technique just presented is based upon a comparison of the full-scale hover performance for given collective pitch settings with model performance. This comparison is shown in Table II.

The rather remarkable good agreement between model and full-scale data for the hover case was essentially repeated throughout the speed range. Figures 5 through 8 present the suggested collective pitch settings and those actually required during model tests to obtain the desired equivalent vertical lift. Examination of these figures shows that, in general, slightly higher collective pitch angles were required in the model studies for equivalent full-scale performance.*

* It is possible that at least part of the difference between the suggested full-scale collective pitch settings and the model settings is a result of error in the mast tilt value, which includes a combination of rotor shaft tilt, fuselage orientation, flapping, and fore-and-aft cyclic pitch; but as noted earlier, adjustments were made only to the collective pitch settings.

TABLE II. COMPARISON OF FULL-SCALE AND MODEL VERTICAL LOAD PERFORMANCE FOR THE HOVER CONDITION, 2-BLADED UH-1D ROTOR

Collective Pitch (deg)		Full-Scale (or Model Equivalent) Vertical Load (lb)	
Full Scale	Model	Full Scale	Model
16.2	16.2	10,000	10,075
14.8	14.5	8,000	8,090
13.4	13.3	6,000	5,950
12.0	12.0	4,000	4,060

A comparison of vertical lift values for the 1-, 2-, and 3-bladed rotors (all other conditions being equal) is presented in Table III. A plot of 1-bladed rotor lift performance as a percentage of 2-bladed rotor lift is shown in Figure 9. These data form a series of similarly shaped curves with a uniform trend existing between the data applicable to the different vertical load situations. A distinct change in the curve form is noted at the condition equivalent to a 25-knot forward velocity.

Figure 10 presents the 3-bladed rotor configuration vertical lift performance as a percentage of the 2-bladed rotor performance. Data are shown for the four different vertical load situations established during 2-bladed rotor operations. These data follow the same general trend exhibited by the 1-bladed/2-bladed rotor performance comparison, but the individual curves for each particular vertical load situation are not as uniformly oriented relative to one another as for the case of the 1-bladed/2-bladed rotor performance comparison. However, this is perhaps to be somewhat expected in view of the recognized complex interaction of blade-blade interference which must exist during operation of the 3-bladed rotor configuration. Note that these data also show a rather sudden and sharp decrease in the lift performance in the general forward velocity range of 20 to 30 knots. This characteristic follows that indicated in the 1-bladed studies; thus, these data reinforce the generally accepted knowledge of a pronounced variation in the lift performance of the rotor at some point in the transitional stage of flight.

The overall performance trends of the 1-, 2-, and 3-bladed rotor units follow those generally established in the marine propeller field (see Reference 13 for example), in that a 1-bladed rotor produces more than 50 percent of the total lift of a 2-bladed rotor (all other conditions being equal) while a 3-bladed rotor unit produces less than 150 percent of a 2-bladed unit (again, all other conditions being equal). It is interesting to note, however, in Figure 10 that the 3-bladed rotor configuration approaches the ideal (150 percent) of a 2-bladed unit at the higher forward advance velocities. A study of the vortex patterns indicates that the vortex trails are so widely spaced at these conditions that the possibility of significant interactions from one blade to another is almost nonexistent, which explains why wing theory can be successfully employed.

TABLE III. COMPARISON OF VERTICAL LIFT VALUES FOR 1-, 2-, AND 3-BLADED ROTOR (ALL OTHER CONDITIONS EQUAL) MODEL DATA PRESENTED IN TERMS OF FULL-SCALE PERFORMANCE

Basic 4,000-Pound Load (2-Bladed Rotor Configuration)						
Vel (kt)	Suggested Collective Pitch Angle (deg)	Test Collective Pitch Angle (deg)	Mast Tilt (deg)	Vertical Lift (lb)		
				Rotor Configuration		
				1- Bladed	2- Bladed	3- Bladed
0	12.0	12.0	0	3,020	4,060	5,400
10	11.2	11.7	- 0.8	3,060	3,940	5,240
20	10.5	10.8	- 1.8	3,060	4,000	4,960
25	10.0	10.5	- 2.35	2,940	4,010	4,760
35	10.2	10.4	- 3.45	3,050	4,070	5,000
50	10.3	10.5	- 5.3	2,640	3,985	5,240
60	10.5	10.8	- 6.65	2,540	4,025	5,440
70	11.0	11.2	- 8.7	2,520	3,910	5,400
90	12.0	12.9	-13.4	2,590	3,980	5,800
110	14.3	14.1	-14.9	2,580	3,970	5,890
120	16.1	16.7	-15.1	2,560	4,000	5,720

TABLE III - Continued

Basic 6,000-Pound Load (2-Bladed Rotor Configuration)						
Vel (kt)	Suggested Collective Pitch Angle (deg)	Test Collective Pitch Angle (deg)	Mast Tilt (deg)	Vertical Lift (lb)		
				Rotor 1- Bladed	Configuration 2- Bladed	3- Bladed
0	13.4	13.3	0	4,520	5,950	7,930
10	12.4	13.1	- 0.9	4,210	5,975	7,650
20	11.7	12.3	- 1.9	4,330	6,100	7,590
25	11.4	12.0	- 2.5	4,110	5,950	7,480
35	11.4	11.7	- 3.6	4,220	5,975	7,630
50	11.5	11.4	- 5.4	3,760	5,950	7,760
60	11.7	11.8	- 6.7	3,650	5,850	8,040
70	12.0	12.3	- 8.4	3,820	6,050	8,570
90	12.9	13.6	-11.9	4,210	5,800	8,540
110	14.6	14.8	-13.8	3,300	6,100	8,900
120	16.0	15.6	-15.6	3,690	5,850	8,530

TABLE III - Continued

Basic 8,000-Pound Load (2-Bladed Rotor Configuration)						
Vel (kt)	Suggested Collective Pitch Angle (deg)	Test Collective Pitch Angle (deg)	Mast Tilt (deg)	Vertical Lift (lb)		
				Rotor 1- Bladed	Configuration 2- Bladed	3- Bladed
0	14.8	14.5	0	5,050	8,090	10,480
10	13.6	14.3	- 1.0	5,100	7,750	10,450
20	13.0	13.7	- 2.0	4,140	7,900	10,250
25	12.8	13.4	- 2.65	5,540	7,950	10,200
35	12.6	12.7	- 3.75	5,180	7,930	9,800
50	12.7	12.7	- 5.5	4,980	8,175	10,520
60	12.9	12.7	- 6.75	4,900	8,000	10,230
70	13.0	13.1	- 8.1	4,680	7,825	10,720
90	13.8	14.2	-10.4	4,920	7,875	11,500
110	14.9	15.5	-12.7	5,000	7,900	11,180
120	15.9	16.2	-14.5	4,560	8,150	11,280

TABLE III - Continued

Basic 10,000-Pound Load (2-Bladed Rotor Configuration)						
Vel (kt)	Suggested Collective Pitch Angle (deg)	Test Collective Pitch Angle (deg)	Mast Tilt (deg)	Vertical Lift (lb)		
				Rotor 1- Bladed	Configuration 2- Bladed	3- Bladed
0	16.2	16.2	0	6,460	10,075	13,600
10	14.8	15.9	- 1.1	6,010	9,960	13,250
20	14.2	15.2	- 2.2	6,200	10,150	13,250
25	14.1	14.8	- 2.8	5,920	10,175	12,900
35	13.9	14.7	- 3.9	6,190	10,100	13,480
50	13.8	14.2	- 5.6	5,920	9,925	13,400
60	14.0	14.5	- 6.8	5,850	10,175	13,950
70	14.1	14.5	- 7.8	5,620	9,950	13,500
90	14.7	14.9	- 8.9	5,790	9,760	13,650
110	15.2	16.2	-11.6	5,580	9,940	13,700
120	15.8	17.0	-13.4	5,390	9,750	13,300

VORTEX TRAIL OBSERVATIONS-HOVER AND FORWARD FLIGHT CONDITIONS

In this section, the first characteristic to be discussed will be the general form of the wake. From observing with stroboscopic light, viewing of the high speed movies, and examining still photographs, it appears that the wake signature can include three major general forms, with any particular wake comprised of any combination of these forms.

For the hover conditions, the wake consists of a helix trail which could be considered as a series of ring vortices. This wake form is shown in Figure 11, wherein essentially stop action and time exposure photographs of the tip vortex trails associated with the 2-bladed rotor configuration at hover conditions and a 10,075-pound load are shown. Figure 12 shows the hover condition for a 1-bladed rotor configuration wherein the collective pitch setting is representative of a 6,000-pound load for 2-bladed rotor configuration. In both figures, note the starting vortex which has reflected from the tunnel floor. (The tunnel floor is at a level corresponding to the bottom of the data card.) The rebound pattern is particularly interesting in Figure 11 (time exposure), where the effects of the side walls are shown in that the rebound of the starting vortex constrained by the tunnel side walls causes the vortex to be at a higher level than that in the upstream and downstream directions along the tunnel where there is no constraint.

As the forward velocity is increased to 10 knots, the tip vortex trails can still be characterized as consisting of helix patterns. However, it is interesting to note Figure 13, where time exposure photographs of the tip vortex patterns created at 10 knots show that the skew angle of the vortex trail relative to the oncoming flow is larger for the upstream side of the vortex trail than it is for the downstream side.

As the forward velocity approaches 20 knots, the wake pattern changes from a rather simple helix trail to a rather complex three-component configuration, and this general form of the wake continues to exist until the forward velocity reaches the 60-knot range. One component of the wake consists of the general mass flow through the rotor disk. Another component consists of two vortex trails moving downstream parallel to the general flow direction. The third component consists of vortex trails shed by the rotor during that portion of

its revolution from 270-0-90 degree sweep,* with these vortex trails traveling essentially perpendicular to the flow direction as they move downstream with their outer ends joining the vortex trails moving parallel to the flow direction. Figure 14 illustrates these general wake patterns as they are created with the 3-bladed rotor configuration at a 35-knot forward velocity.

At velocities above the general range of 60 knots, the wake pattern again changes. The wake pattern can now be characterized as consisting of a skewed, coarse-pitch, helix trail formed by the vortices shed from the rotor tips. The mass flow through the rotor disk is encompassed in the volume enclosed by the vortex trail. The trailing vortex pattern moving in the direction of the flow is no longer created. This type of wake formation is shown in Figures 15 and 16 for forward velocities of 110 and 120 knots.

Now that the general vortex patterns have been established, certain particular wake patterns and the changes in those patterns for variations in loading and number of rotor blades will be discussed in somewhat more detail. The first characteristic to be discussed concerns the vortex pattern for a given rotor configuration as the vertical load is changed. For the hover situation, the final amount of wake contraction becomes slightly greater, and the spacing between successive helix trails varies as the collective pitch varies. For example, in Figure 17, compare the vortex pattern of the 2-bladed rotor at the condition of an equivalent 4,060-pound vertical load (12.0° collective pitch) with the condition at an equivalent 10,075-pound vertical load (16.2° collective pitch).

Again, for a given rotor configuration, the heavier the loading (the larger the vertical lift), the greater the downwash displacement beneath the rotor as the forward velocity increases. In other words, the lighter the load, the larger the skew angle for a given velocity in the general range from "out of hover" to about 60 knots. Figures 18 and 19 illustrate the wake patterns for both 2- and 3-bladed rotor configurations

* Zero degrees is defined as the position at which the rotor points directly aft and the rotation is counterclockwise when viewed from overhead. (The model had clockwise rotation.)

at a forward velocity of 20 knots for two different loading conditions. Note that the trail associated with the heavier vertical load is diverted primarily downward in both cases while that for the lighter vertical load moves essentially in a rearward direction as it leaves the rotor disk.

At forward speeds above the general range of 60 knots, the spacing of the vortex trails remains essentially constant regardless of the vertical load. Compare the photograph of an equivalent 10,000-pound load with that at a 4,000-pound load, both conditions having an equivalent 120-knot forward velocity (Figure 20).

Changing the number of rotor blades while keeping other conditions constant appears to influence the pitch of the helix trail at hover condition. In addition, the initial amount of radial and axial motion is influenced. Figure 21 illustrates the trails for the 1- and 3-bladed rotors at hover conditions and same collective pitch settings. Note that with the 3-bladed rotor, three trails are evident at the third grid line from the top, i.e., one rotor revolution. For the 1-bladed rotor, the third trail is at the fourth grid line, i.e., three rotor revolutions.

The downwash angle of the wake as indicated by the path of the tip vortex trails shed during the rearward portion of a rotor revolution is also influenced by the number of blades contained in the rotor. Figure 22 illustrates this change for the 1-, 2-, and 3-bladed rotor configurations at a forward velocity of 25 knots and the same collective pitch angle setting and mast angle. Note the rather significant change in the trail position on the grid as the trail moves out of the viewing area. Since the 1-bladed rotor is loaded more heavily than any 1 blade of the 2- and 3-bladed rotors, it appears that the downwash angle is influenced more by the rotor disk loading than by the rotor blade loading.

At the higher forward velocities (the general range above 70 knots), the number of blades in the rotor did not seem to influence the wake characteristics to any significant degree. The spacing between the tip vortex trails shed by the same blade on succeeding rotor revolutions is the same whether the rotor had 1, 2, or 3 blades. This observation, of course, reinforces the existing knowledge of rotor performance or operation at higher forward velocities. See Figure 23 for a comparison of the tip vortex trails spacing for the three different rotor blade configurations at 110 knots.

One of the more significant occurrences observed during this test program concerns the path of the tip vortex trails shed during the forward portion of a rotor revolution (approximately 90-180-270-degree travel sector). It is clearly evident from these studies that with the first beginnings of forward velocity, up to the general range to about 70 knots, portions of the tip vortex trails shed during the forward portion of a rotor revolution lie above the rotor in such a manner that the following rotor blade(s) intersect with one or more of the trails. The possibility of such interaction has been mentioned by a number of authors; for example, Spencer et al and Jenney et al, in References 14 and 2. Vapor trail studies in air (Reference 2) have also shown that a tip vortex trail can intersect a rotor blade. However, for the first time, the present water tunnel studies permitted the complete observation of the shed vortex trails and their position relative to the rotor blade(s) for extended ranges of rotor operation. Figure 24 presents a series of both side and overhead-view photographs showing the position of the vortex trail for a 2-bladed rotor operating at an equivalent 10,000-pound vertical load. Covering a forward velocity range from 20 to 70 knots, these photographs present a rather vivid illustration of the path of the vortex trails shed during the forward portion of a rotor revolution, but a view of the high speed movie is really a necessity to appreciate the nature of this rotor-vortex trail interaction.*

* One of the observers visiting Oceanics for the purpose of viewing this testing technique was Mr. Frank Davenport of Vertol Division of The Boeing Company. In viewing a number of test conditions, he questioned whether the deflection of the rotor blades at an equivalent 10,000-pound vertical load might not cause the shed vortex trails to be at a "higher" location in space than would exist for a rotor blade having a hinged end connection point. (The model rotor was rigid at the hub and had a coning angle of 4 degrees. Thus, the tips did deflect as the rotor was subjected to load.) Equivalent 10,000-pound vertical lift rotor load conditions were therefore run at reduced model rotational speeds and tunnel forward velocities. This technique permitted a reduction of the absolute loading on the model and thus the rotor tip deflection. Reducing the model rotational speed from the normally employed 8 rps to 3.25 rps (while maintaining the correct forward velocity/tip speed ratio) reduced the tip deflection by approximately 1/2 inch. However, the tip vortex patterns did not drop in space orientation a similar amount. Their position relative to the rotor blade changed by approximately 1/8 inch or 1/3 rotor chord.

VORTEX TRAIL OBSERVATIONS - INFLOW PATTERNS

The path that the oncoming flow takes as it enters the rotor disk area has been examined by a number of investigators. The studies undertaken by Jenney, Olson, and Landgrebe in Reference 2 using smoke trails presented a most interesting insight into stream element inflow trajectories. A short series of tests utilizing air bubble release from a forward rake was undertaken during this program to determine the usefulness of this technique in gaining additional insight into the helicopter rotor inflow character.

The test arrangement consisted of a rake positioned ahead of the rotor in such a manner that it was either on the fore-and-aft center line of the rotor shaft or moved laterally 0.45 rotor radii to either side of the rotor shaft line. A complete listing of the test conditions for which photographs were taken is given in Appendix II.

Since the air bubbles released in this manner are not trapped in finite vortex trails as they are when the tip vortex trails are examined, the buoyancy of the bubbles will distort the inflow pattern (determined by the bubble path) to a certain degree. Thus, while certain qualitative information is obtainable using this technique, its value as a test technique is considerably less than that of the tip vortex method discussed earlier.

The difference in the inflow pattern with rake lateral position is shown in Figure 25. Here the rotor inflow strength, as made evident by the bubble streaks, is greatest when the rake is aligned in the fore-and-aft direction with the rotor shaft. The strength appears somewhat less as the rake is moved laterally toward the

Thus, at an equivalent 35-knot forward velocity, rather than having three vortex trails lie above the blade when it was located at the 180-degree position for a rotor speed of 8 rps, two trails were above while the third was just beneath the blade at a rotor speed of 3.25 rps. It is therefore believed that the amount of distortion in the vortex patterns introduced by the fact that the test model blades deflected does not significantly detract from the general observations made. Should this test technique be employed for more rigorous wake analysis, corrections for this distortion could be introduced.

advancing blade and considerably less as it is moved laterally toward the retreating blade. A change in the forward velocity also affects the inflow pattern. Figure 26 illustrates the inflow condition as made evident by the bubble streak pattern at speeds of 10, 20, and 35 knots. In this latter figure, the rake is oriented on the fore-and-aft center line of the rotor shaft.

SIMULATED POWER FAILURE

The last experimental phase of this study involved a short series of tests employing the 2-bladed rotor wherein power failure was simulated by operating the rotor at reduced rotational speeds while maintaining a fixed collective pitch of +2.75 degrees at the 0.75 radial station. The mast angle was 8 degrees less than that employed at similar forward flight conditions.

A tabulation of these data is shown in Table IV, while Figure 27 presents these data as plots of equivalent full-scale vertical lifts as a function of rotor speed for varying forward velocities. The velocity range was 70 to 150 knots. From these plots, the lift curve appears to have a constant slope with rotor speed for given forward flight velocities. The data for lower velocities tend to approach a common curve (for conditions of a particular basic vertical load value), with the separation between curves becoming larger as the forward velocity is increased. For the most part, the side photographs of these test conditions presented little discernible information, as the wake traveled essentially straight back. However, the overhead view did offer certain indications of the tip vortex trail character. All photographed test conditions are listed in Appendix III.

The effect of rotor rotational speed (and consequently the vertical lift) on the vortex trail pattern is shown in Figure 28 for a 70-knot forward flight condition and in Figure 29 for a 150-knot forward flight condition. Note that the axial (or downstream) spacing between successive vortex trails shed by the same rotor blade becomes larger as the rotor rotational speed is reduced. This characteristic is particularly evident in Figure 29.

ROTOR WAKE SPATIAL COORDINATES

As mentioned earlier, the high speed movies were viewed primarily to gain a qualitative insight into the

TABLE IV. TABULATION OF SIMULATED POWER FAILURE DATA, 2-BLADED ROTOR - CONSTANT COLLECTIVE PITCH 10.1 DEGREES

Equip Fwd Vel (kt)	Mast Angle (deg)	Equip Tip Speed (fps)	Equip Vert Load (lb)	Mast Angle (deg)	Equip Tip Speed (fps)	Equip Vert Load (lb)
70	0.2	583	9,377	0.4	438	5,260
		565	8,775		420	4,901
		539	8,250		402	4,423
90	0.9	585	9,441	3.9	449	5,299
		554	8,610		428	4,969
		542	8,246		401	4,412
110	3.6	583	9,309	5.8	454	5,324
		546	8,542		428	4,806
		538	8,090		407	4,367
120	5.4	595	9,367	7.6	452	5,316
		568	8,671		439	4,855
		558	8,338		421	4,515
135	8.5	624	9,552	10.3	487	5,347
		600	8,888		467	4,937
		582	8,397		451	4,605
150	11.8	664	9,542	13.3	534	5,545
		640	8,913		511	5,055
		627	8,475		484	4,507

tip vortex trail patterns. However, three conditions did receive a rather complete analysis, wherein the spatial coordinates of a tip vortex element were determined for angular rotations of the blade up to 720 degrees beyond the point where the vortex filament was initially deposited. This analysis was undertaken by examining the high speed film strips with a time and motion projector. Using a projector of this type, the number of film frames required for known angular displacement can be used in deducing the angular position of the rotor for any particular frame in a given sequence. By examining an arbitrary number of individual frames throughout two rotor revolution sequences, it was possible, by viewing both the side and the overhead exposure views, to determine with reasonable precision the position of a particular vortex element in space.

The 1-, 2-, and 3-bladed rotor configurations were examined in this manner at hover conditions with a collective pitch setting of 14.5 degrees. Figure 30 is a plot of the radial and axial wake contraction ratios for the 2-bladed rotor. Note in particular how the axial contraction is affected by blade passing; i.e., azimuth positions of 180, 360, 540, and 720 degrees.

A comparison of these data with the equations presented in References 2 and 15 is illustrated in Figure 31, where a faired curve presents the data trends and symbols indicate computations using the equations and these model test data. From the information presented on this figure, it can be noted that, for at least the cases analyzed, the axial contraction as predicted by the empirical equations is quite good up to about 100 to 150 degrees of azimuth. At higher azimuth values, the equations predict consistently higher axial contraction values than those observed during the test. For the case of radial contraction, the equations consistently predict values indicating less radial contraction than that actually observed.

ADDITIONAL ROTOR WAKE OBSERVATIONS

As an additional method of documenting the wake flow patterns, a sheet of acetate was placed over the viewing window during each test run and a sketch of the wake flow patterns was made by tracing the patterns on the acetate sheet with a grease pencil. These sketches included the rotor position as well as the significant wake characteristics. The purpose of the sketches was to augment the other data obtained during the tests in analyzing the data and preparing the report. However, the

USAAVLABS project engineer suggested that these sketches be used to establish certain spatial positions of the dominant wake characteristics.

Figure 32 identifies the principal wake characteristics and terms which are discussed in this section. Here can be noted the "wing tip type" vortex trails, the upper boundary of the flow "ring" tip vortices, and the lower boundary of the flow through the rotor, as well as the angles defining the tip path plane and the skew of the flow through the rotor.

Figures 33 through 36 present the measured model tip path plane angle as a function of velocity for the 1-, 2-, and 3-bladed rotors for different equivalent lift values. These figures also show the full-scale tip path plane, assuming that the plane was perpendicular to the mast position employed during these tests. In general, the model tip path plane angles are less than the full-scale angles, particularly at the higher forward velocities. This general reduction in angle value is at least partially accounted for by the fact that the model rotor was rigid; thus, there was deflection of the rotor blade in the spanwise direction. This deflection was particularly noticeable during the forward part of a rotor revolution, and the maximum deflection appeared to occur at a rotor position of 180 degrees. During the rear portion of a rotor revolution, the rotor blade did not exhibit noticeable deflections. At the higher velocities, the outer portion of the rotor blade in a spanwise direction was always aligned parallel to the oncoming flow at the 180-degree rotor position.

The amount of radial contraction of the wake at hover conditions is of considerable interest, and certain observations were presented earlier in the section "VORTEX TRAIL OBSERVATIONS - HOVER AND FORWARD FLIGHT CONDITIONS". Figure 37 presents the contraction ratio r/R (radius to the tip vortex/rotor radii) as a function of the rotor blade collective pitch angle for the 1-, 2-, and 3-bladed rotor blades as determined from the acetate sketches. This figure shows that the same trend of contraction ratio exists for a variation in collective pitch angle for all rotors tested but that increasing the number of rotor blades increases the magnitude of radial contraction.

Since it has been shown earlier in this report that the absolute lift per rotor blade at a given collective pitch angle varies with the number of blades in the rotor,

it is of interest to plot the radial contraction ratio as a function of absolute load for the various rotors. This information is shown in Figure 38. These data show, as one might expect, that the radial contraction of the wake is primarily dependent upon the disk loading and not on the individual blade loading.

From the hover conditions to approximately 10 knots, the tip vortex wake can be characterized as a deformed helix trail, with the upstream boundary of the flow forming an angle, relative to the oncoming flow, different from that of the downstream boundary. Figure 13 is a photograph illustrating such flow conditions, while Figure 32(b) defines the method of establishing the skew angle. Table V presents the measured skew angle for the different conditions tested. These data reinforce conclusions that the skew angle reduces as the collective pitch increases, i.e., as the rotor load increases.

To spatially locate the flow boundary defined by the "ring" tip vortices shed during the rear portion of a rotor revolution, and that boundary defined by the lower surface of the flow through the rotor, an extension was made of the tip path plane. At a location of 1.2 rotor radii, measurements were made normal to the tip path plane to determine the distance to the flow boundary in question. Figure 32(a) illustrates the manner in which these measurements were made.

Figures 39 through 42 show how these flow boundaries vary with disk loading and the number of blades in the rotor. What is evident from these figures is that, for a given disk loading and forward velocity, the spatial location of the upper flow boundary is relatively independent of the number of blades in the rotor. On the other hand, the spatial location of the lower flow boundary is rather strongly influenced by the solidity. Also, as the disk loading increases, the differences in the spatial location of the lower flow boundaries become more pronounced with a variation in the number of rotor blades. For example, compare Figure 39 with Figure 42 to note the increase in curve separation.

At forward velocities below 50 knots, the upper flow boundary is clearly influenced by the disk loading, and the increasing displacement of the boundary surface with increasing vertical lift can be easily seen by examining the appropriate figures.

TABLE V. SKEW ANGLES OF ROTOR FLOW AT 10 KNOTS
(Measured From Rotor Tip Path Plane)

No. of Rotor Blades	Collective Pitch Angle (deg)	Skew Angle β_1 (Upstream) (deg)	Skew Angle β_2 (Downstream) (deg)
1	11.7	117	102
1	13.1	113	107
1	14.3	101	95
1	15.9	101	93
2	11.7	110	99
2	13.1	108	97
2	14.3	106	95
2	15.9	102	94
3	11.7	108	97
3	13.1	108	100
3	14.3	99	93
3	15.9	98	91

The last of the flow characteristics to be spatially located are the vortices emanating from the 90- and 270-degree azimuth positions which resemble those shed from the tips of fixed-wing aircraft. These vortices can be seen in the photographs presented in Figure 14(b) and are defined in Figure 32(a). This type of wake characteristic existed in the forward velocity range from about 20 to 50 or 60 knots. The measurements of the spatial location of these vortices were taken in the same manner as those measurements defining the upper and lower boundaries of the flow through the rotor. The strength of these vortices varied, depending upon whether they were shed as the rotor blade was advancing or retreating. This variation in vortex strength was noted not only by observing the "core" size and action of the air bubbles trapped in the vortex trail but also by observing the position of the trail above the tunnel flow as both trails moved downstream. The vortex trail shed from the advancing rotor blade tip was always deflected to a position nearer the tunnel floor than that shed from the retreating blade. However, in defining the location of the vortices for these measurements, i.e., at 1.2 rotor radii, the difference in downward deflection had not yet developed.

Figure 43 presents the spatial location of one point in the vortex trail(s) for this flow characteristic. These data indicate a trend of increasing displacement with increasing disk loading, as might be expected. Any variation in vortex deflection associated with the number of blades in the rotor cannot be clearly established.

SUMMARY AND CONCLUSIONS

The use of water tunnel testing as a technique for visualizing the tip vortex trails shed by a helicopter rotor appears to offer one of the most useful tools yet employed in understanding the nature of the helicopter tip vortex wake. The clarity in which the character of the wake can be viewed leaves little to be desired. This report emphasizes the testing technique aspects of the program and presents only enough data, movie, and photograph analysis to establish the validity of the test techniques and to indicate how the viewed wake differs from the currently employed mathematical models. A detailed analysis of all movies and photographs will be a rather comprehensive undertaking.

The more significant conclusions which can be drawn from this investigation are:

1. Air bubbles emitted in a tip vortex core during water tunnel studies do not distort the core path and do permit its observation for several rotor diameters downstream. Thus, this technique can be successfully employed for both near and far field investigations.
2. The tip vortex wake can be characterized as possessing or passing through three separate and distinct pattern sequences as the flight conditions go from hover to speeds above the 50- to 60-knot range.
3. The tip vortex pattern existing at hover conditions and to forward velocities of perhaps 10 knots can be correctly characterized as a helix trail, providing both the radial contraction and changes in the axial spacing of succeeding helixes are considered. The initial rapid radial contraction of the tip vortex with the associated slight axial translation results in vortex interference with the following blade (in some cases) such that the generalized lifting line representation of the blade appears to be unacceptable, except for specialized cases.
4. At forward flight velocities above the 50-

to 60-knot range, the tip vortex trail can also be characterized as a helix pattern. In this mode, the helix has an extremely coarse pitch, such that notable interaction of one trail with a preceding or succeeding one is not possible. It is this fact which permits conventional wing theory to be employed at these operating conditions with such good success.

5. The forward flight regime beginning at the 10- to 60-knot range is the one wherein the wake is a most complex arrangement. Mass flow through the rotor disk is deflected downward. Tip vortices shed when the rotor blades are roughly in the 90 ± 15 and 270 ± 15 degree orientation during a rotor revolution coalesce and form a pair of parallel vortex trails which move downstream much in the manner of the tip vortex trails shed by fixed-wing aircraft. The arc segment of the tip vortex trail formed during the forward portion of a rotor revolution loses its identity (strength) rapidly, usually disappearing by the time it reaches the center of the rotor as it travels downstream. On the other hand, the arc segment of the tip vortex trail formed during the rear portion of a rotor revolution retains its identity and its ends join the parallel tip vortex trails mentioned earlier. These latter segments of the tip vortex trails retain their identity for perhaps two rotor diameters downstream.
6. At forward speeds in the general range of 10 to 50 knots, the tip vortices shed by the rotor blade during the forward portion of a rotor revolution cycle pass above the rotor blade, and thus the following blade intersects with one or more of the preceding trails. This observation makes it appear mandatory that any rigorous analysis of rotor performance in this range of forward flight include finite core and finite blade chord effects.

7. For the hover condition, the final amount of wake contraction appears related to the rotor load rather than the number of rotor blades, and, for a given rotor configuration, the successive spacing of the vortex trails varies with the collective pitch angle.
8. The skew angle of the downwash is related to the disk loading for a given rotor configuration. The heavier the load, the smaller the skew angle; i.e., the mass flow through the rotor is directed more strongly downward.
9. The number of rotor blades influences the downwash (skew) angle for a given collective pitch and mast angle setting. The greater the number of rotor blades, the smaller the skew angle. From this, it appears as if the rotor disk loading influences this characteristic of the wake rather than the blade loading.
10. By selecting a model size such that when the blade is located slightly above the center line of an equal height-width tunnel (with rounded corners), with this position scaled to be "out of ground effect" according to full-scale performance data, excellent agreement between model and full-scale rotor lift values can be achieved employing only a Prandtl-Glauert correction factor to account for compressibility effects.
11. The use of air bubbles as "tracers" in defining inflow characteristics to the rotor provides a longer path of visualization than smoke studies, but the buoyancy of the individual bubbles distorts the trace path whereas smoke does not. Thus, this technique has a decided limitation. Corrections can be introduced for the buoyant effect (knowing the bubble size), but this is rather laborious.
12. For the three cases analyzed, the equations as presented in References 2 and 15 predict

values showing good axial contraction agreement to azimuth angles of 100 to 150 degrees. At higher azimuth angles, the equations predict higher axial contraction values than those measured. All measured radial contraction values indicated larger contractions than the value predicted by the equations and these model data.

RECOMMENDATIONS FOR FUTURE WORK

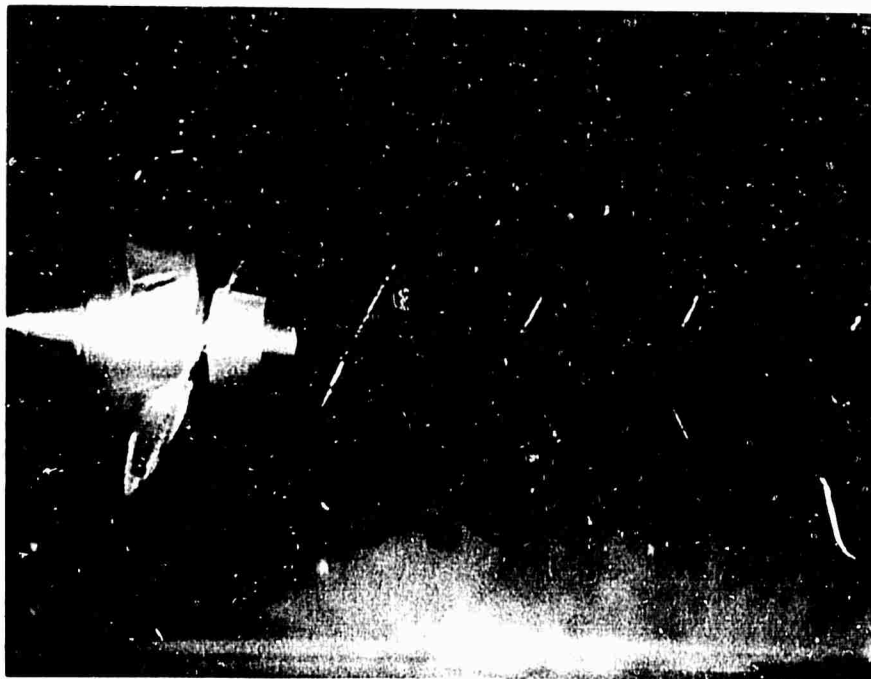
This testing technique appears to be capable of contributing to several areas concerned with a better understanding of rotor performance. The following recommendations for additional study oriented toward this general area are therefore made:

1. Detailed analysis of all movie and photographic data for integration, insofar as possible, with advanced rotor prediction methods such as those developed at Cornell, United Aircraft, Therm, and Vertol.
2. Additional tunnel studies employing tip vortex visualization to illustrate the effect of:
 - a. Tandem rotors
 - b. Fuselage
 - c. Rotor blade deflection (on this technique)
3. Development of this general test technique wherein the vortex sheet shed by the rotor, as well as the tip vortex, can be visualized.

REFERENCES

1. White, R. P.: "VTOL Periodic Aerodynamic Loadings: The Problems, What is Being Done and What Needs to be Done," Journal of Sound Vibration, p. 282-304, September 1965.
2. Jenney, D. S., Olson, J. R., and Landgrebe, A. J.: "A Reassessment of Rotor Hovering Performance Prediction Methods," American Helicopter Society 23rd Annual National Forum, Sikorsky Aircraft Division of United Aircraft Corporation, May 10-12, 1967.
3. Goldstein, S.: "On the Vortex Theory of Screw Propellers," Proceedings, Royal Society of London, Vol. A 123, No. A 792, 1929.
4. Lock, C. N. H.: "The Application of Goldstein's Theory to the Practical Design of Airscrews," British ARC R & M No. 1377, 1931.
5. Piziali, R., and DuWaldt, F.: "Computation of Rotary Wing Harmonic Airloads and Comparison with Experimental Results," Proceedings of AHS Forum, May 1962.
6. Erickson, J. C., and Ordway, D. E.: "A Theory for Static Propeller Performance," CAL/AVLABS Symposium Proceedings, Vol. 1, June 1966.
7. Lehman, August F.: "An Experimental Study of the Dynamic and Steady State Flow Disturbances Encountered by Aircraft During a Carrier Landing Approach," Oceanics, Inc., Report No. 64-16, September 1964.
8. Abbott, Ira H., von Doenhoff, Albert E., and Stivers, Louis S., Jr.: "Summary of Airfoil Data," NACA Report No. 824, 1945.
9. Payne, P. R.: Helicopter Dynamics and Aerodynamics, Sir Isaac Pitman & Sons, Ltd., London, 1959.
10. Porter, David W., and Flanigen, Edwin G.: "Category II Performance Tests of the YUH-1D with a 48-Foot Rotor," Air Force Flight Test Center, Edwards Air Force Base, California, Air Force Systems Command, Technical Documentary Report No. 64-27, November 1964, AD No. 452710.

11. Heyson, Harry H.: "Jet-Boundary Corrections for Lifting Rotors Centered in Rectangular Wind Tunnels," NASA TR R-71, 1960.
12. Rae, W. H., Jr.: "Limits on Minimum-Speed V/STOL Wind-Tunnel Tests," Journal of Aircraft, Volume 4, No. 3, p. 249, May-June 1967.
13. Lehman, August F.: "Further Experimental Studies of Propeller Blade Thickness and Appendage Asymmetry Effects on Propeller-Appendage Interaction," Oceanics, Inc., Report No. 67-35, May 1967.
14. Spencer, R. H., et al: "Tip Vortex Core Thickening for Application to Helicopter Rotor Noise Reduction," The Boeing Company, Morton, Pennsylvania, September 1966, AD 644 317.
15. Gray, R. B.: "On the Motion of the Helical Vortex Shed from a Single-Bladed Hovering Model Helicopter Rotor and its Application to the Calculation of the Span-wise Aerodynamic Loading," Princeton Aeronautical Engineering Dept., Report No. 313, September 1955.
16. Lehman, August F.: "Some Cavitation Observation Techniques for Water Tunnels and a Description of the Oceanics Tunnel," ASME Symposium on Cavitation Research Facilities and Techniques, May 1964.



Ordnance Research Laboratory Photograph
(From Reference 16 by the Author)

Figure 1. Tip Vortex Cavitation on a Marine Propeller

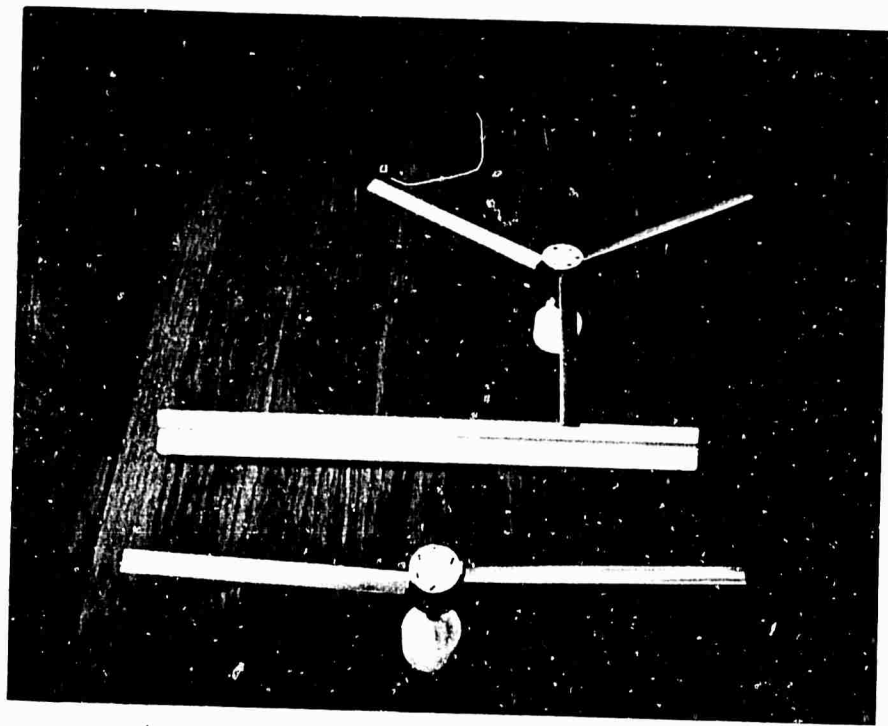


Figure 2. Rotor Blades and Hub Assembly

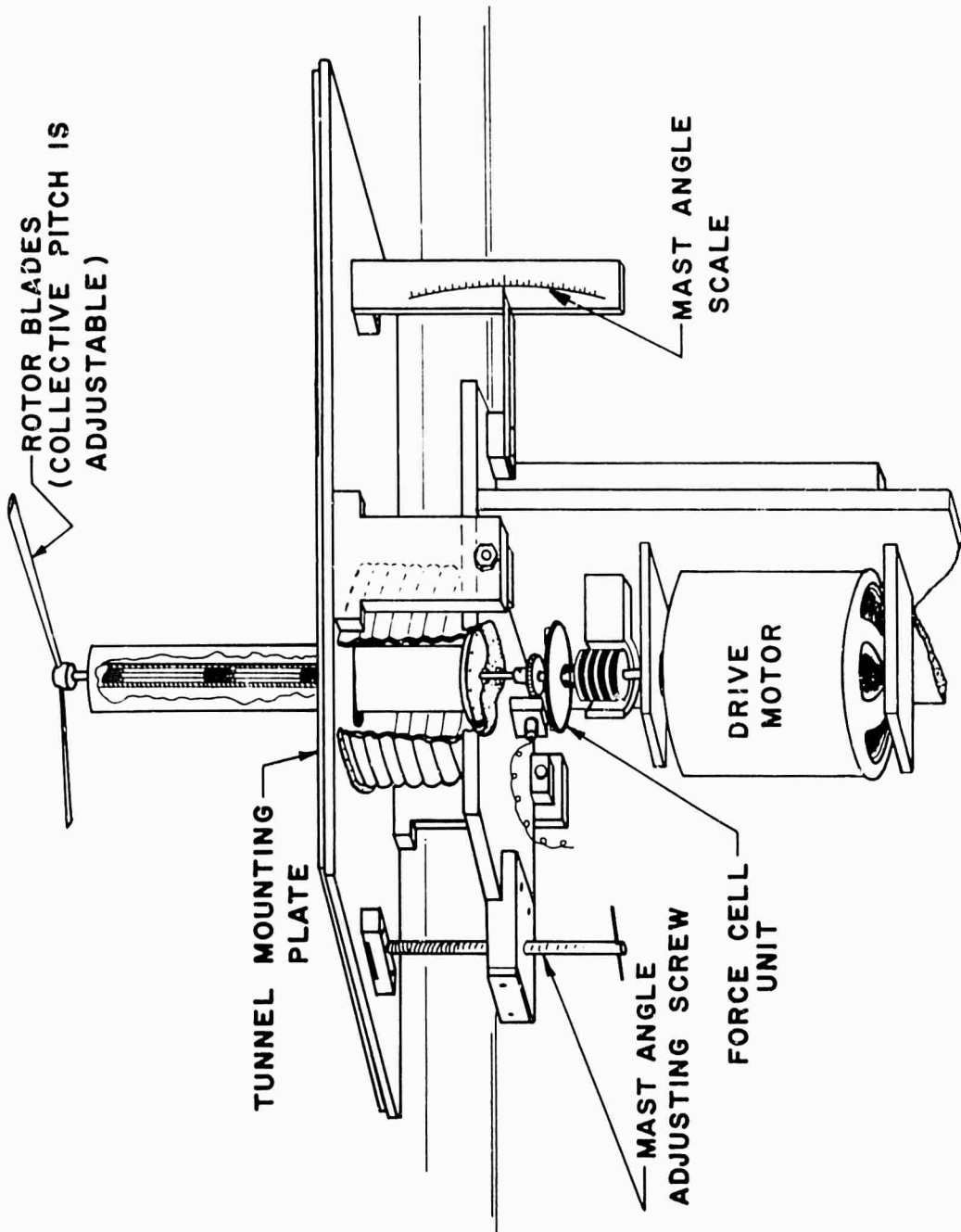


Figure 3. Sketch of the Tunnel Test Installation

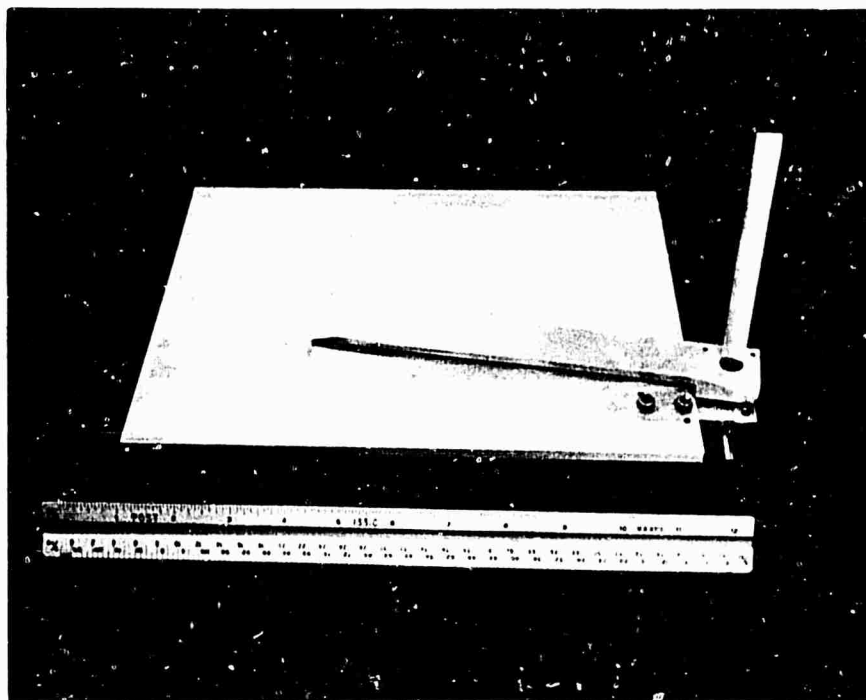


Figure 4. Jig Used in Setting the Rotor Collective Pitch Angle

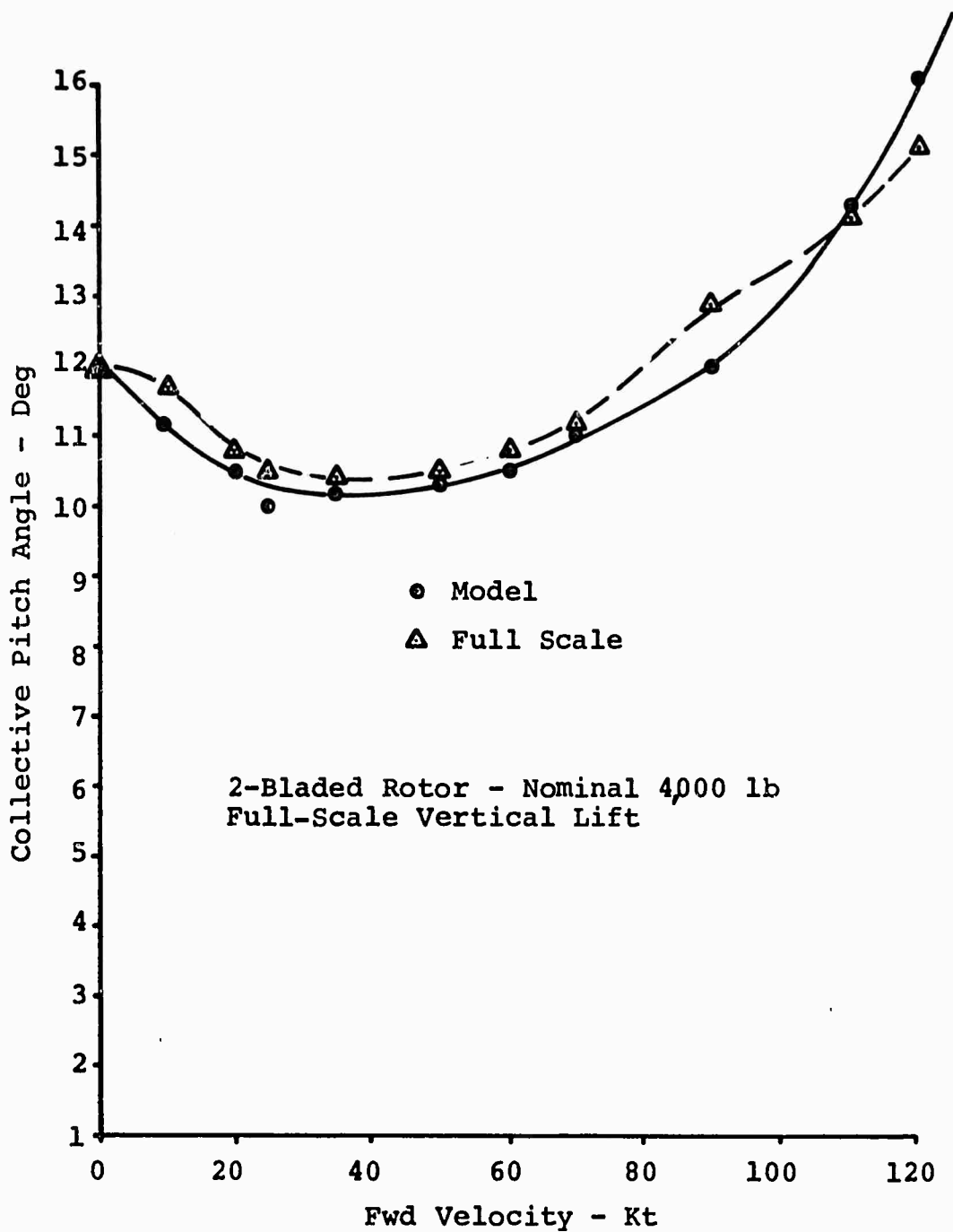


Figure 5. Plot Comparing the Collective Pitch Angle Settings from Full-Scale Data with Model Settings

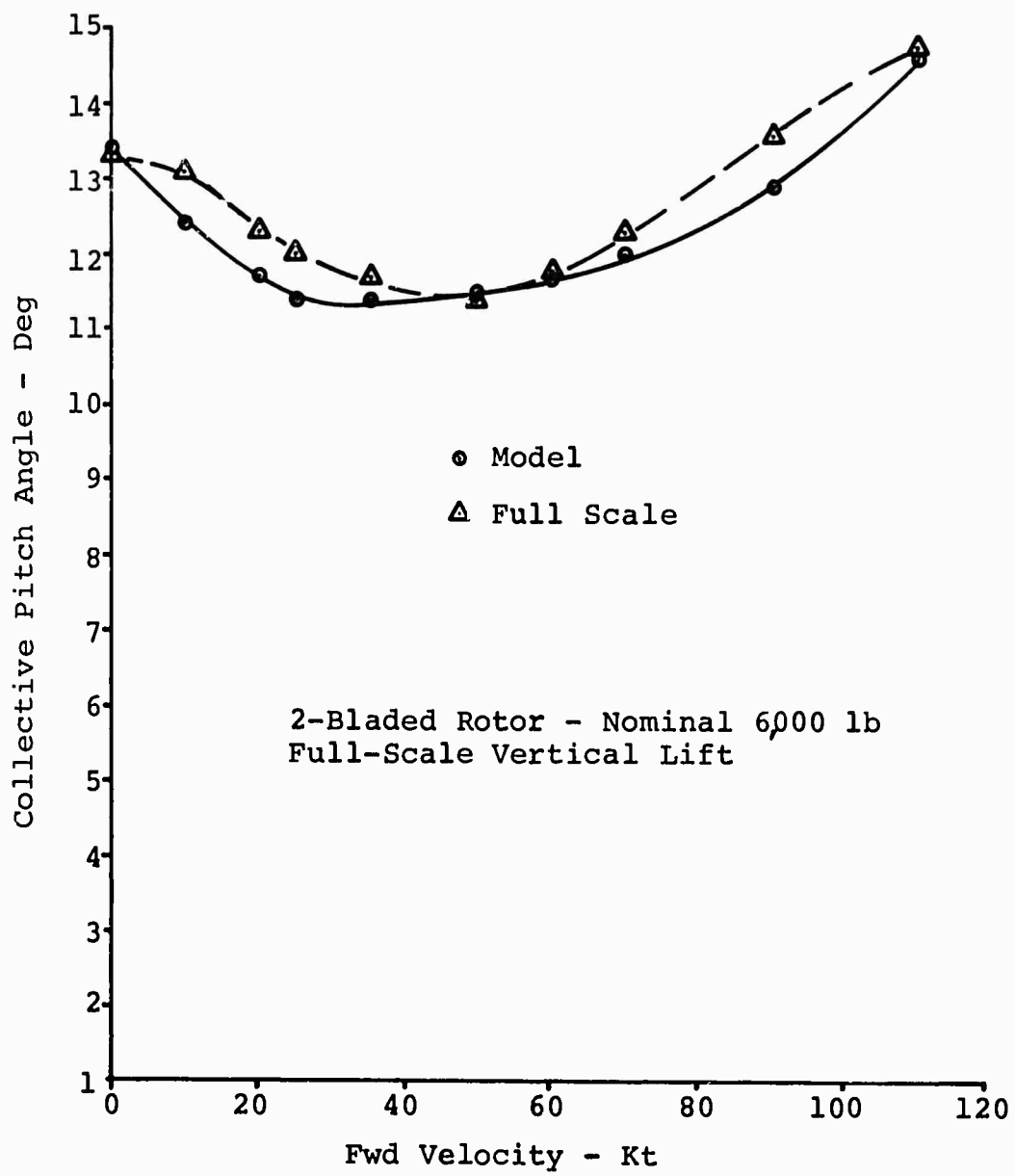


Figure 6. Plot Comparing the Collective Pitch Angle Settings from Full-Scale Data with Model Settings

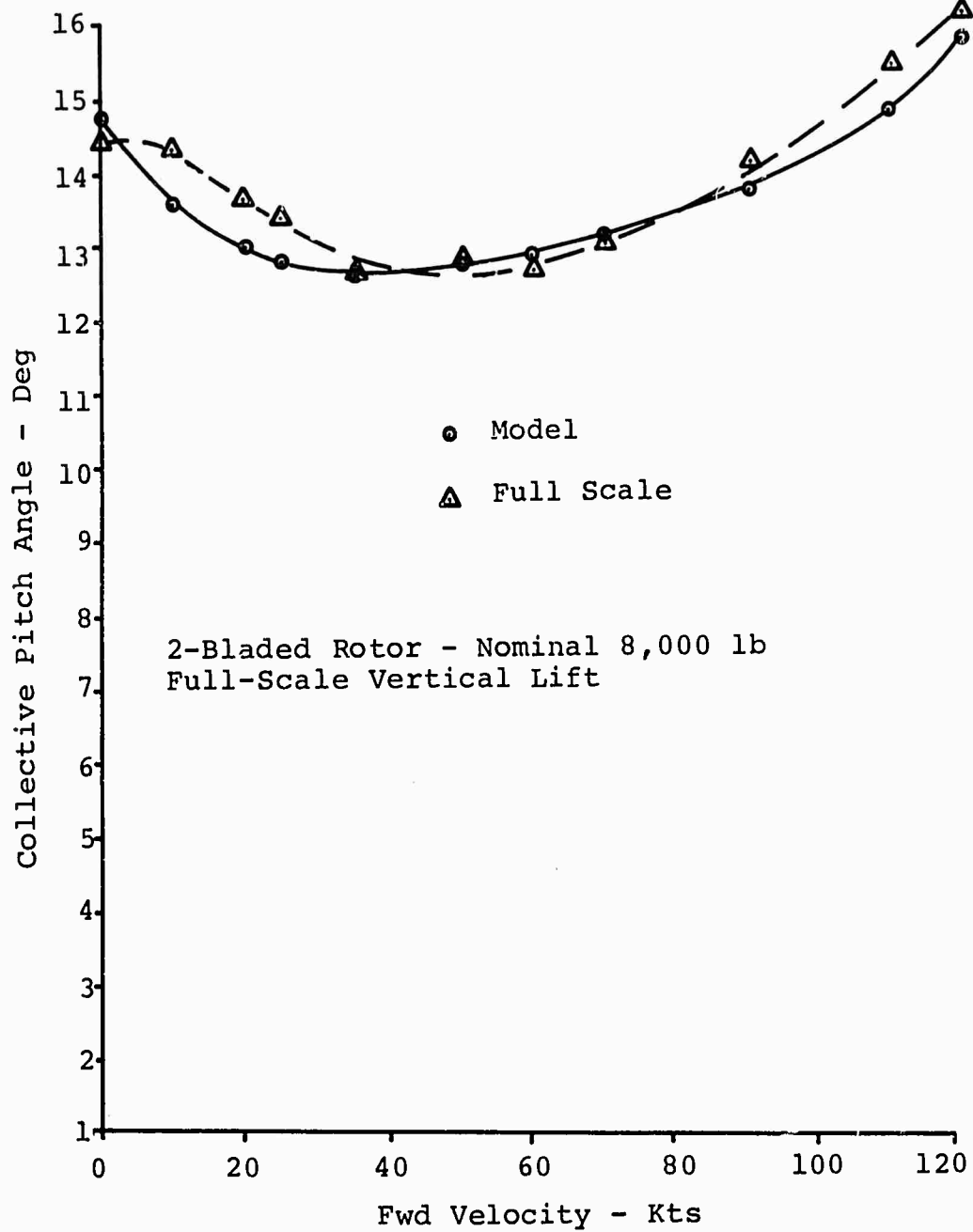


Figure 7. Plot Comparing the Collective Pitch Angle Settings from Full-Scale Data with Model Settings

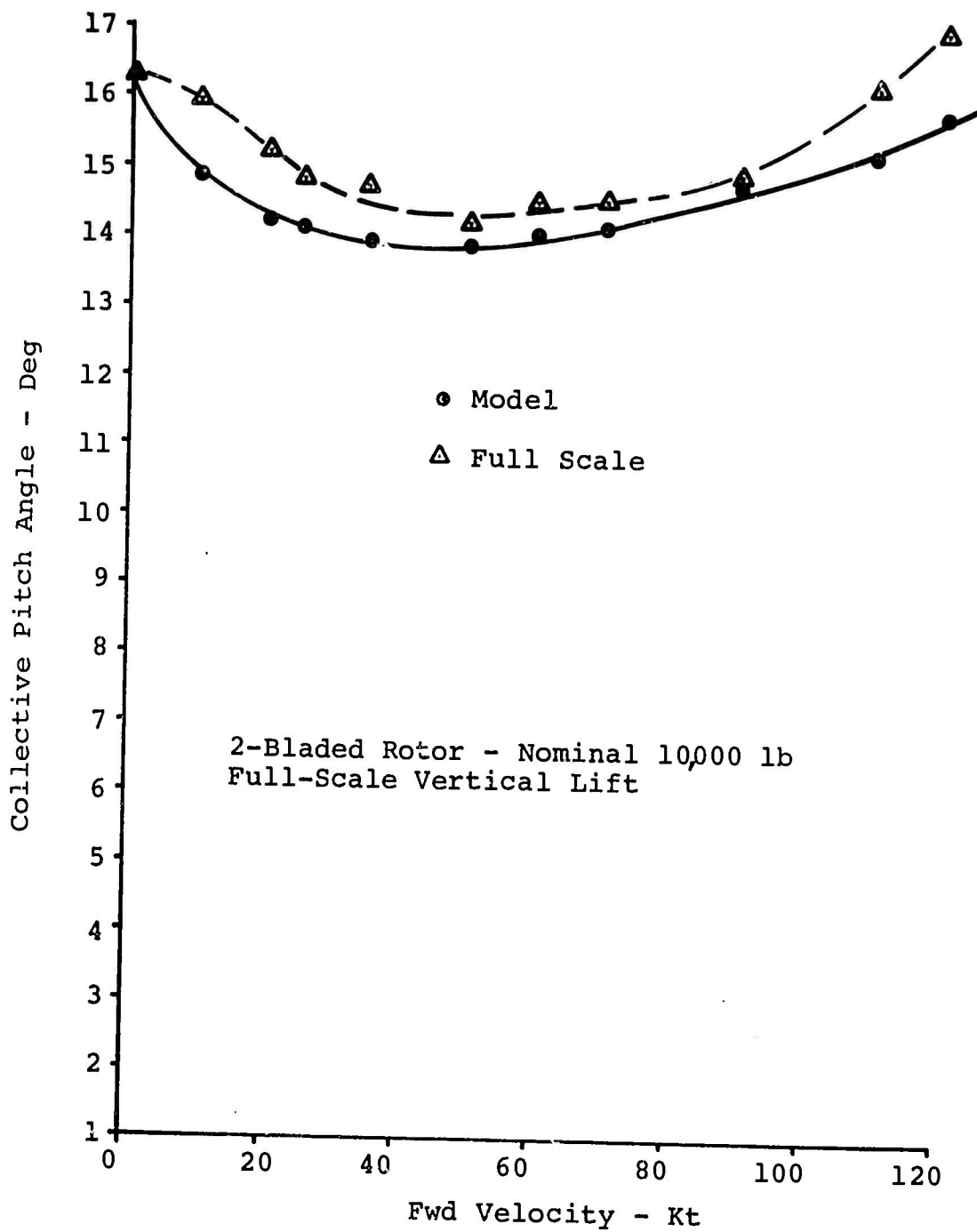


Figure 8. Plot Comparing the Collective Pitch Angle Settings from Full-Scale Data with Model Settings

Conditions for 2-Bladed Rotor
Producing:

- ≈ 4,000 lb Vertical Lift
- △ ≈ 6,000 lb Vertical Lift
- ≈ 8,000 lb Vertical Lift
- ≈ 10,000 lb Vertical Lift

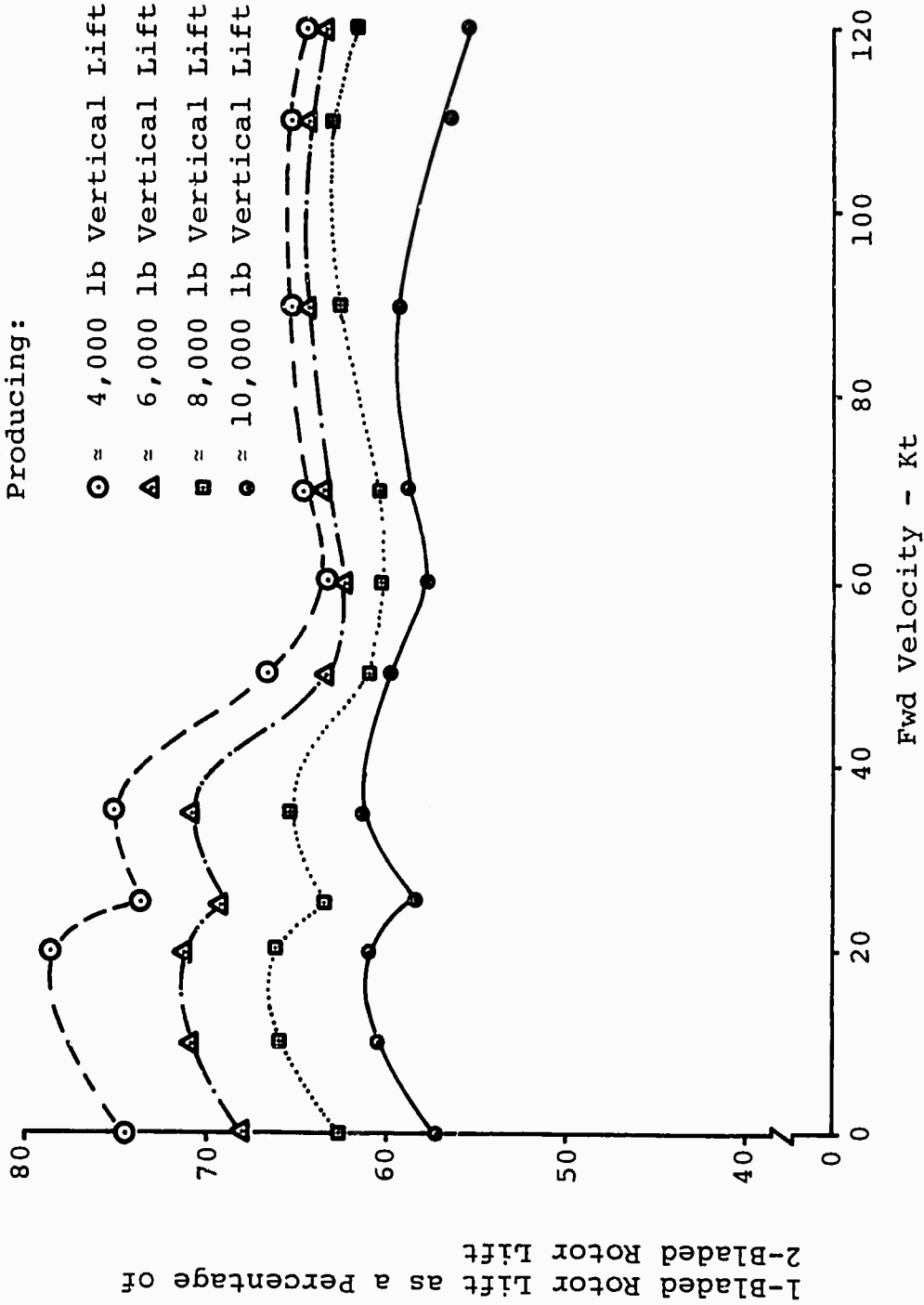


Figure 9. Plot of 1-Bladed Rotor Lift as a Percentage of 2-Bladed Rotor Lift for Variations in Forward Velocity

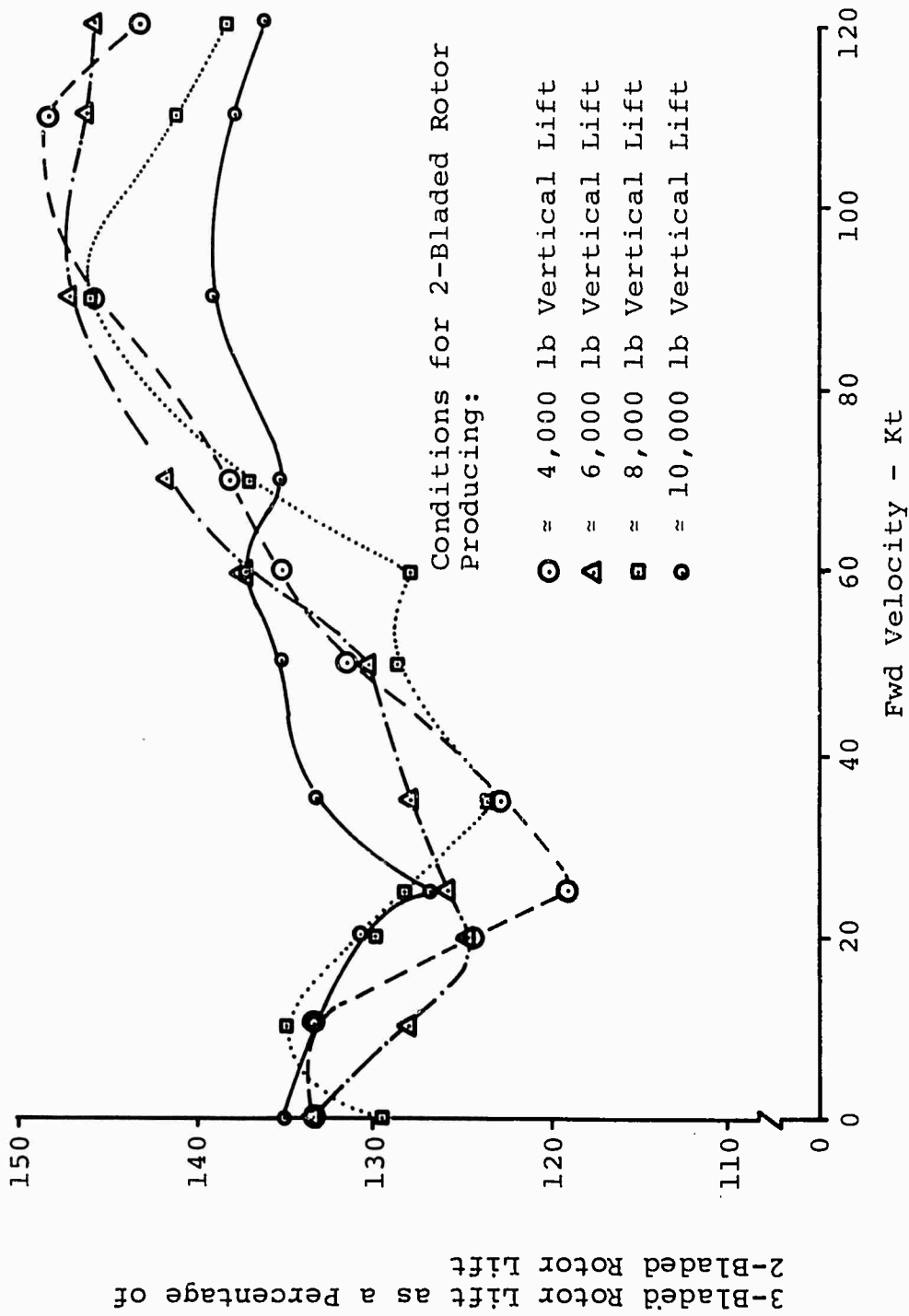
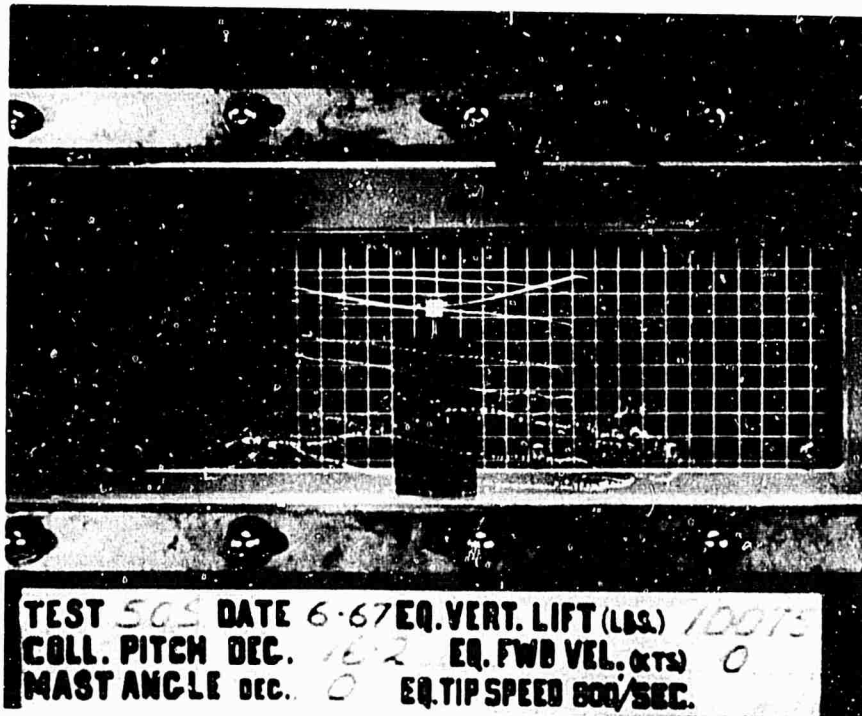


Figure 10. Plot of 3-Bladed Rotor Lift as a Percentage of 2-Bladed Rotor Lift for Variations in Forward Velocity

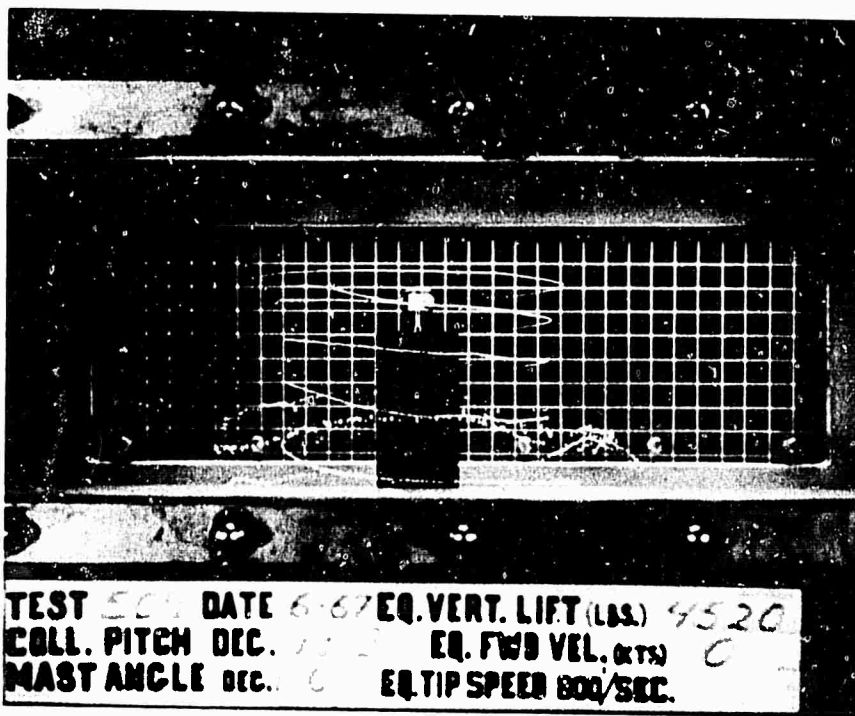


Stop Action
 (Starting
 Vortex Has
 Reflected
 From Tunnel
 Floor)

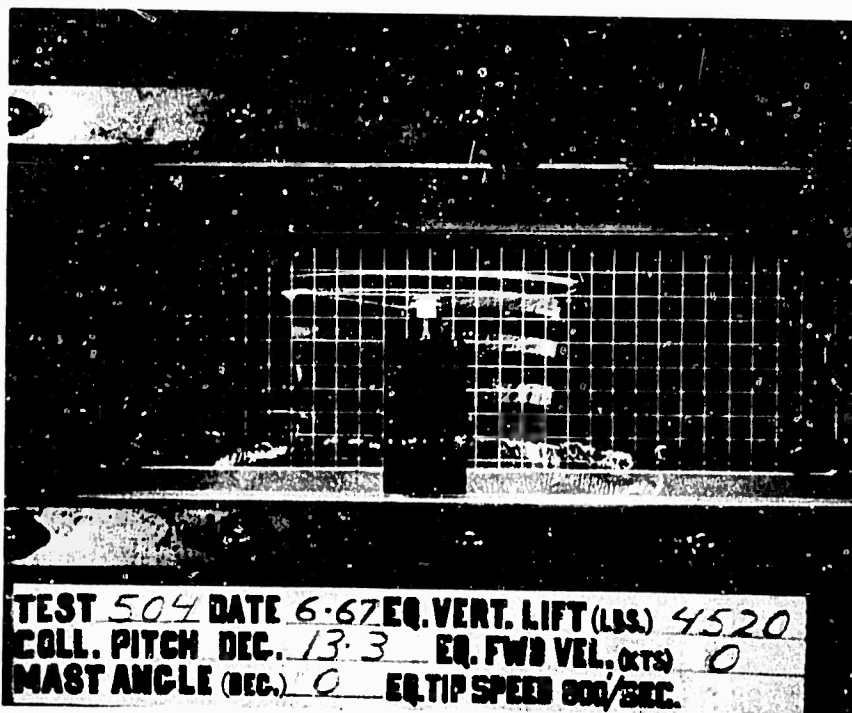


Time
 Exposure
 (Starting
 Vortex Has
 Reflected
 From Tunnel
 Floor)

Figure 11. 2-Bladed Rotor Vortex Trails at Hover



Stop
 Action
 (Starting
 Vortex Has
 Reflected
 From
 Tunnel
 Floor)

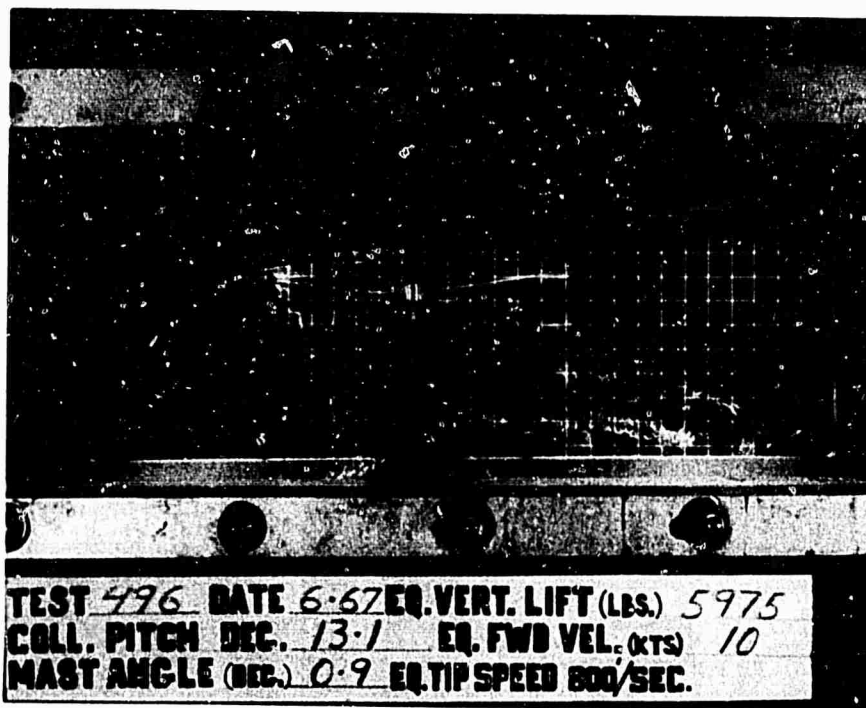


Time
 Exposure
 (Starting
 Vortex Has
 Reflected
 From
 Tunnel
 Floor)

Figure 12. 1-Bladed Rotor Vortex Trails at Hover

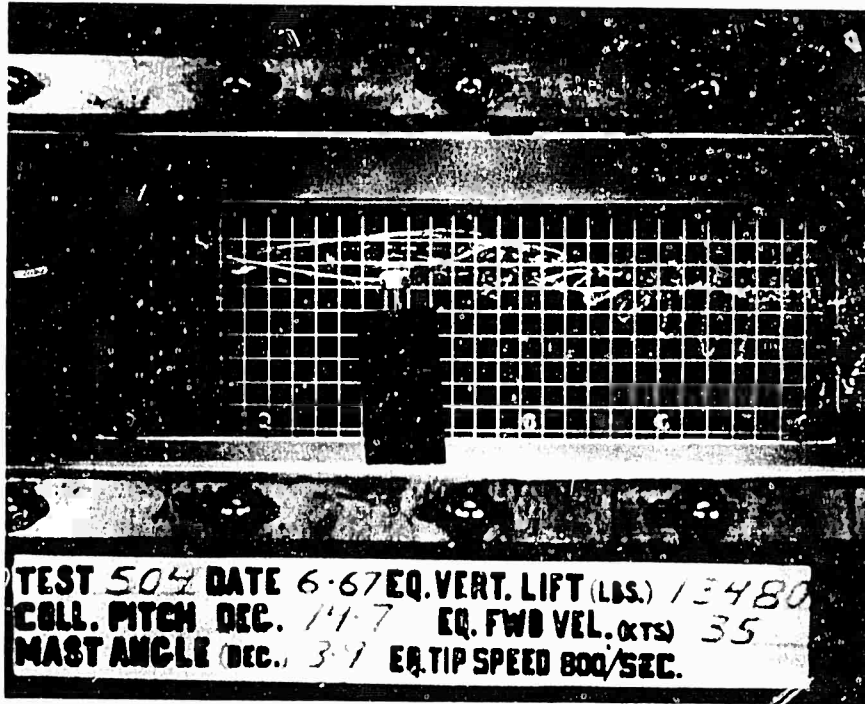


3-Bladed
 Rotor
 Time
 Exposure
 (Starting
 Vortex
 Has Not
 Traveled
 to Tunnel
 Floor)

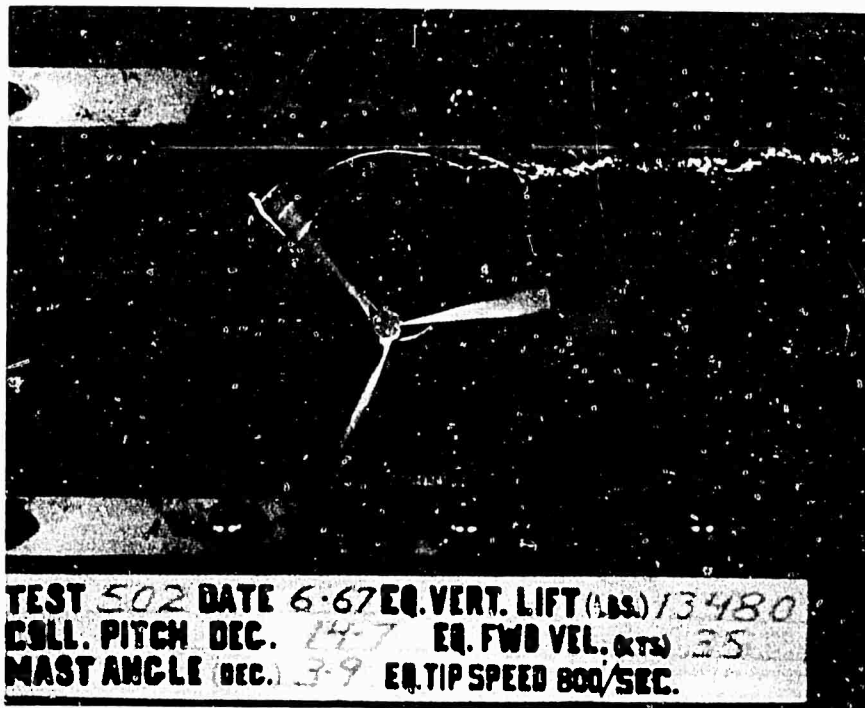


2-Bladed
 Rotor
 Time
 Exposure
 (Starting
 Vortex Has
 Reflected
 From Tunnel
 Floor)

Figure 13. 2- and 3-Bladed Rotor Vortex Trails
 for Same Collective Pitch Angle Setting
 at 10 Knots

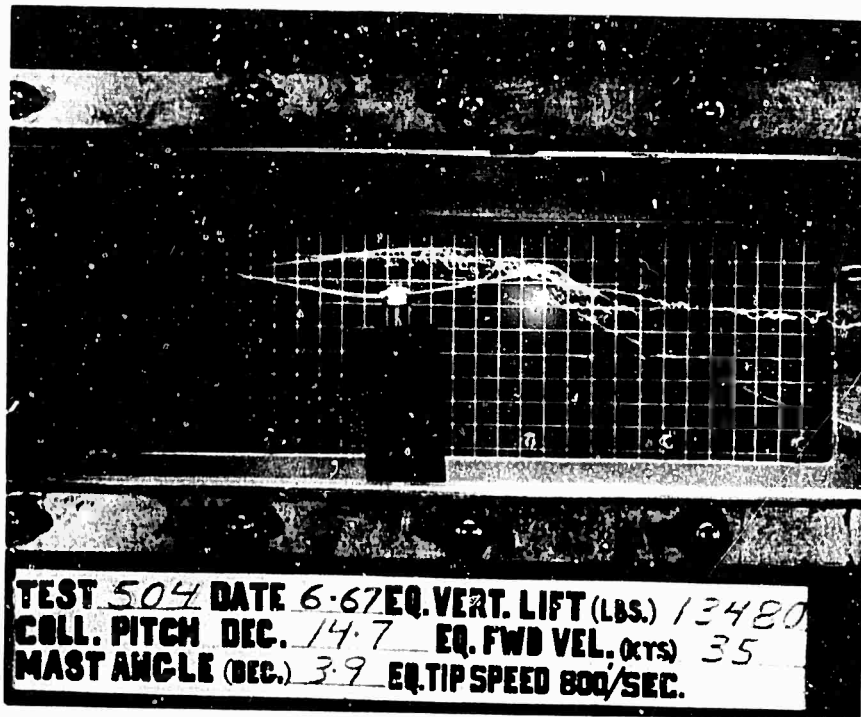


Stop
Action

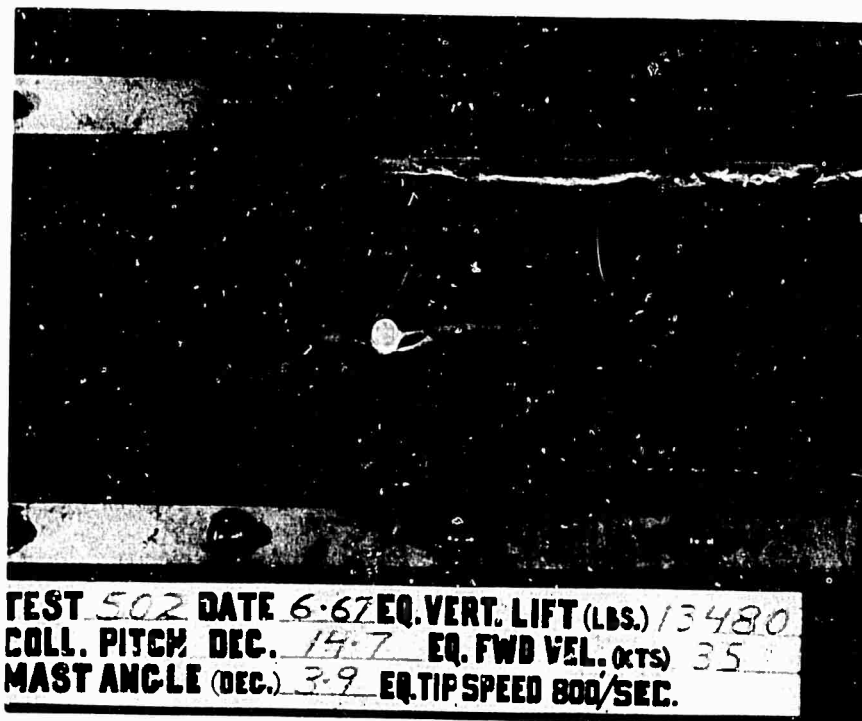


Stop
Action

Figure 14(a). 3-Bladed Vortex Trails at 35 Knots

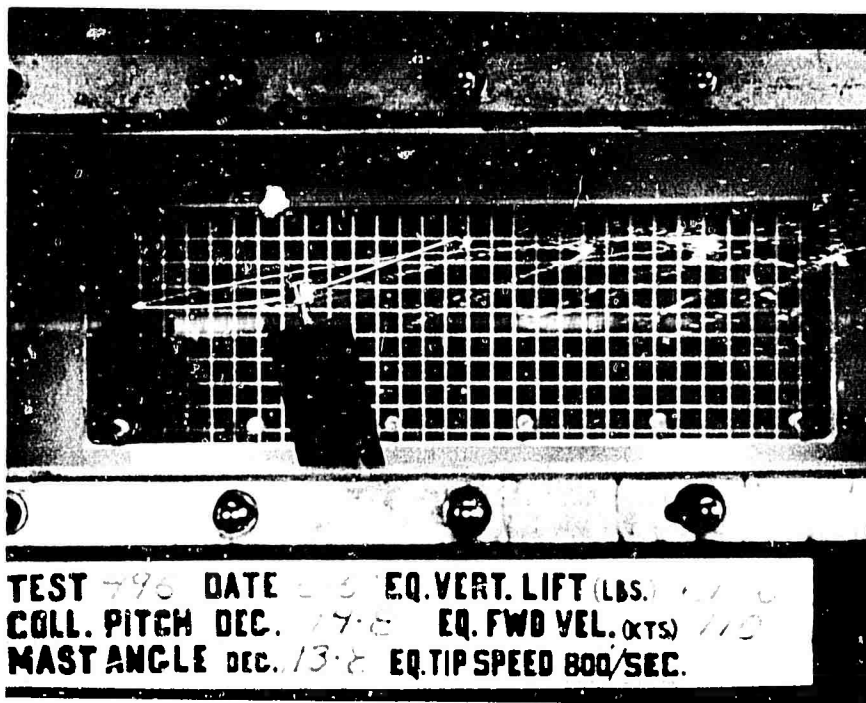


Time
Exposure

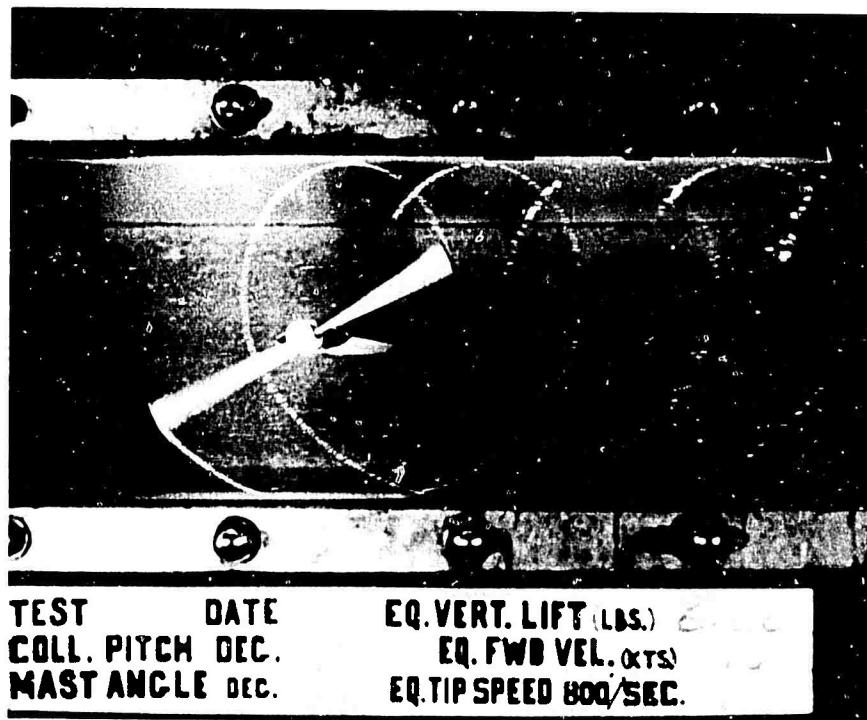


Time
Exposure

Figure 14(b). 3-Bladed Vortex Trails at 35 Knots

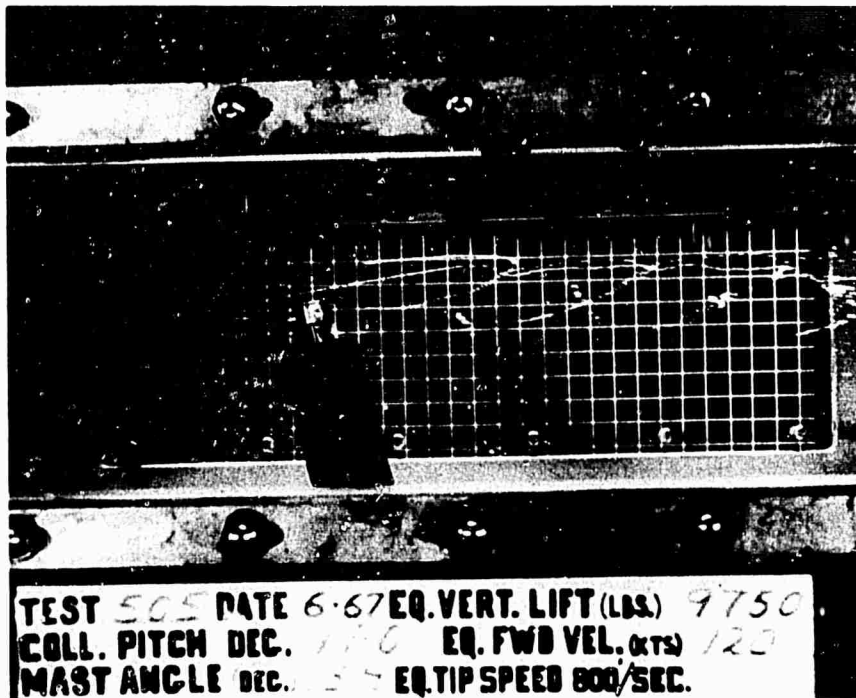


Stop
Action

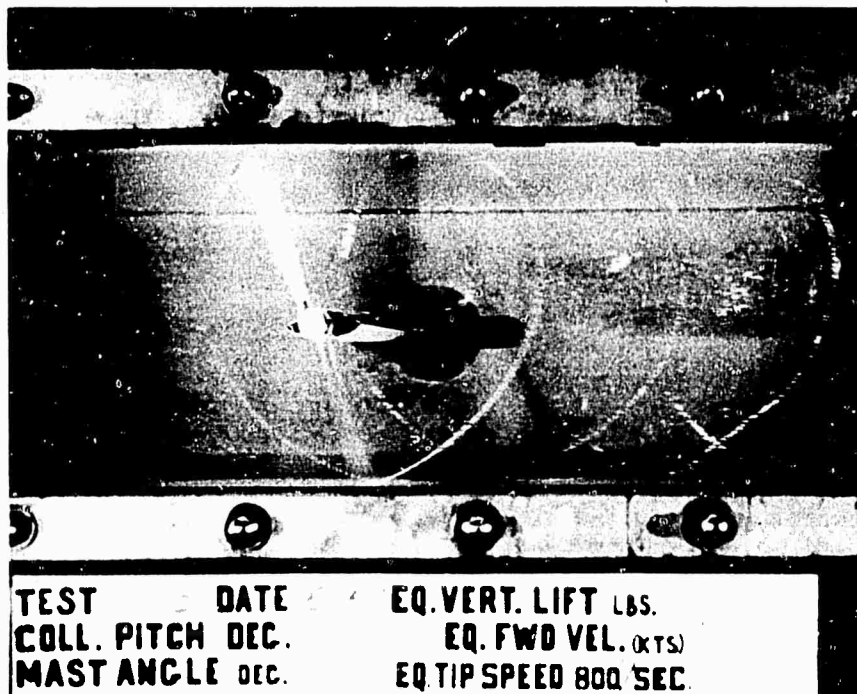


Stop
Action

Figure 15. 2-Bladed Vortex Trails at 110 Knots

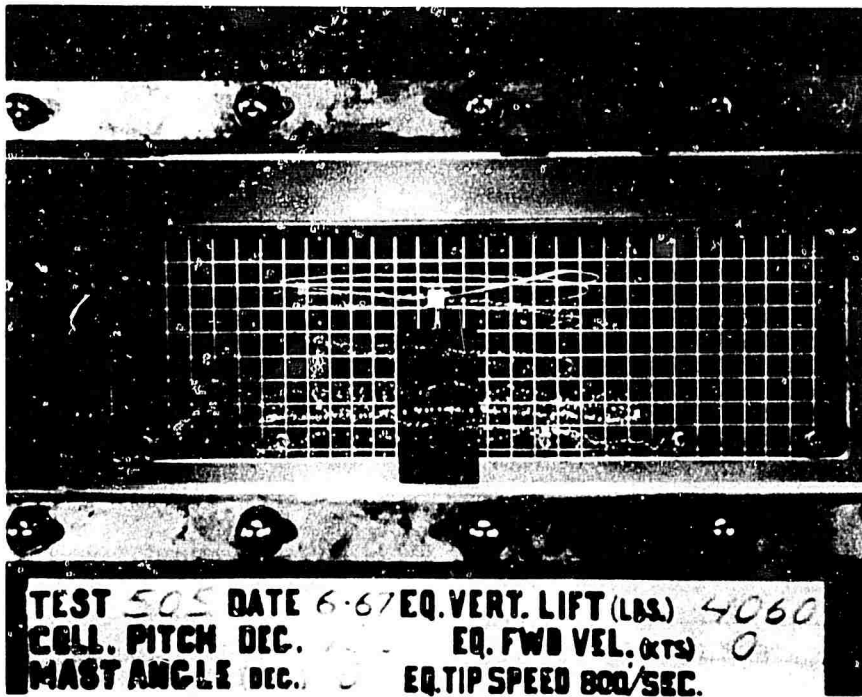


Stop
Action

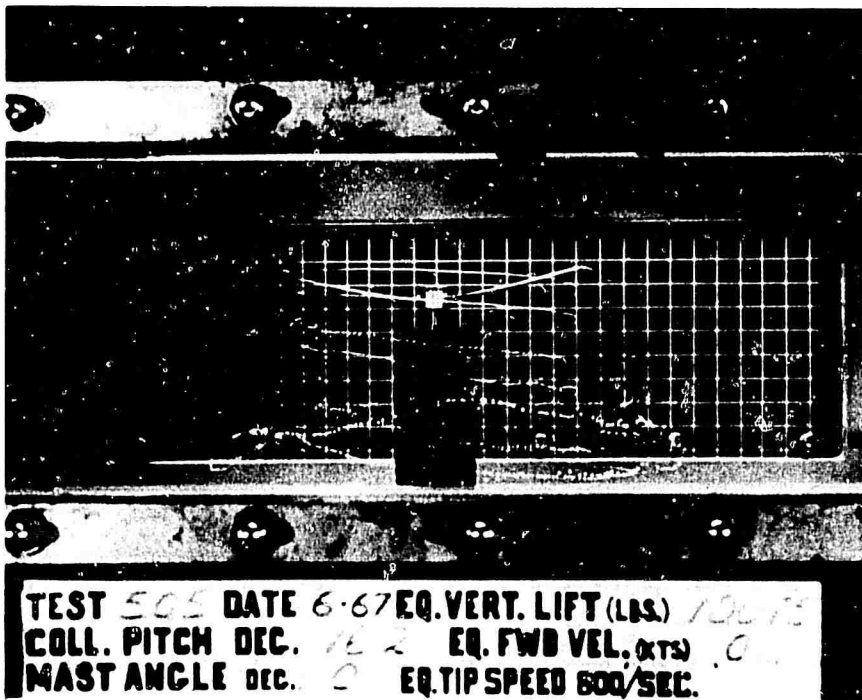


Stop
Action

Figure 16. 2-Bladed Rotor Vortex Trails at 120 Knots

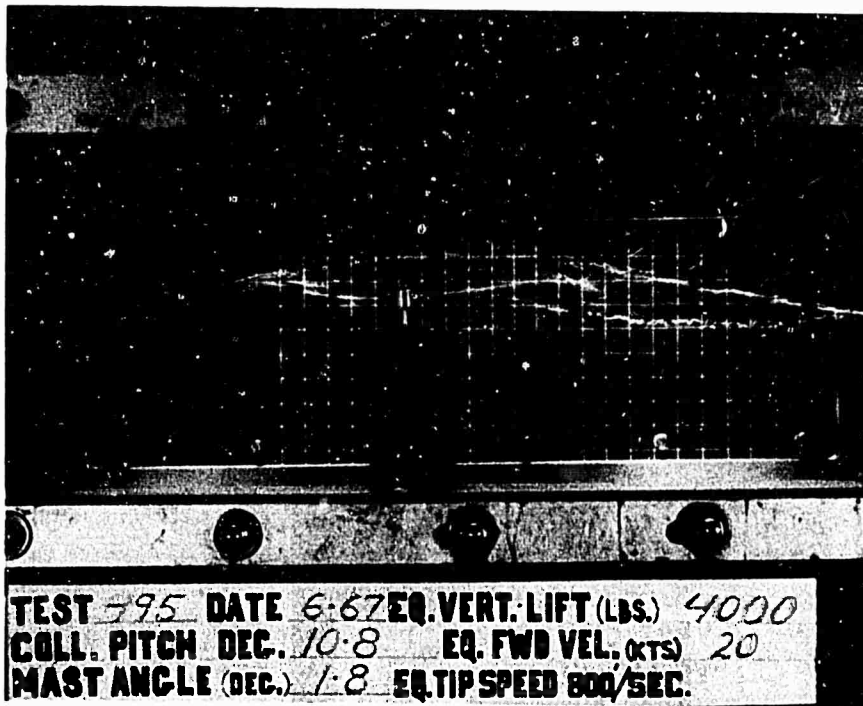


Stop
Action
(Starting
Vortex
Has Not
Traveled
to Tunnel
Floor)

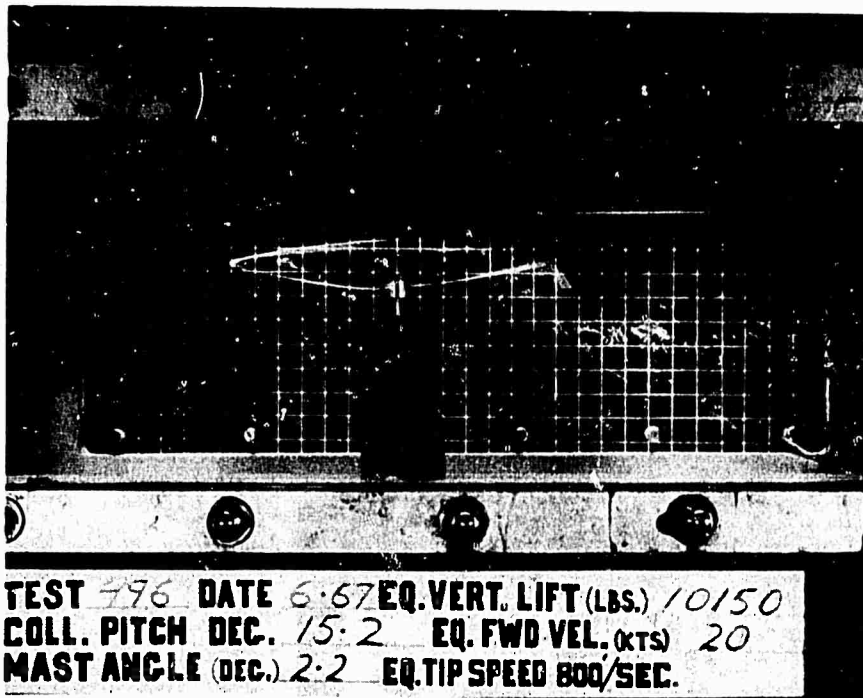


Stop
Action
(Starting
Vortex
Has
Reflected
From
Tunnel
Floor)

Figure 17. Comparison of 2-Bladed Rotor Hover Trails at Vertical Lifts of 4,060 and 10,075 Pounds

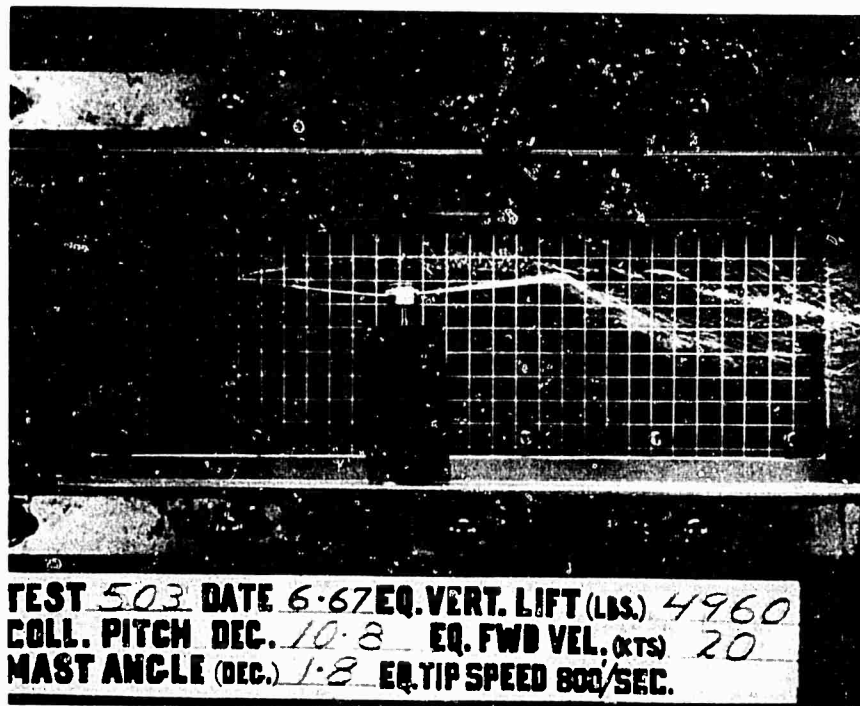


Time
 Exposure

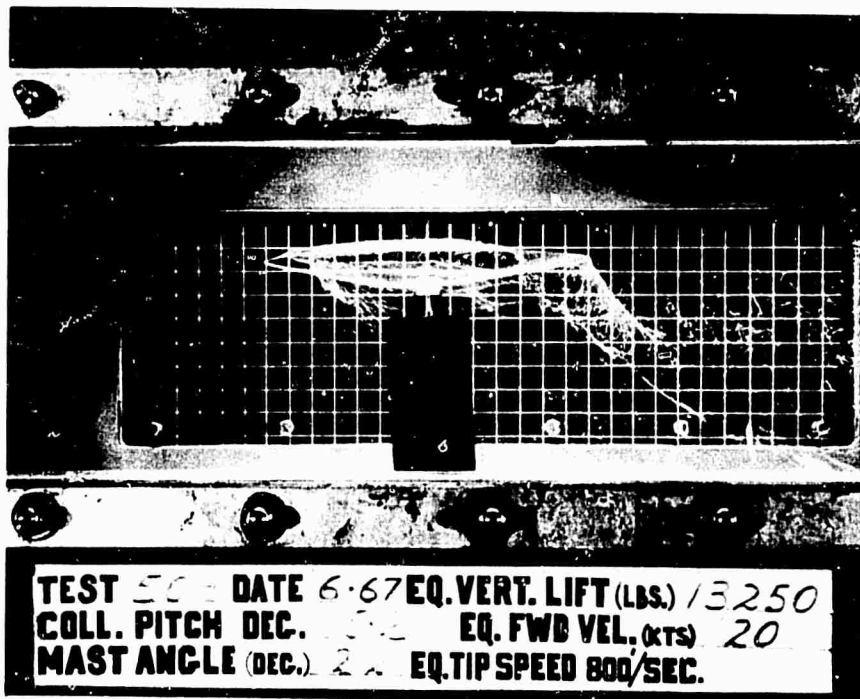


Time
 Exposure

Figure 18. Comparison of 2-Bladed Rotor Vortex Trails at 20 Knots for Vertical Lifts of 4,000 and 10,150 Pounds

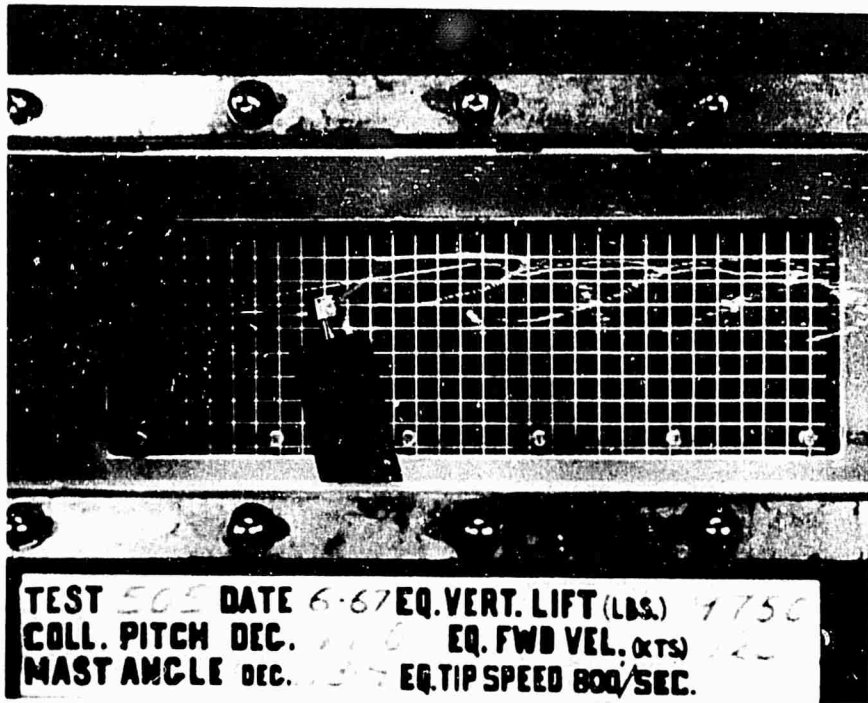


Time
Exposure

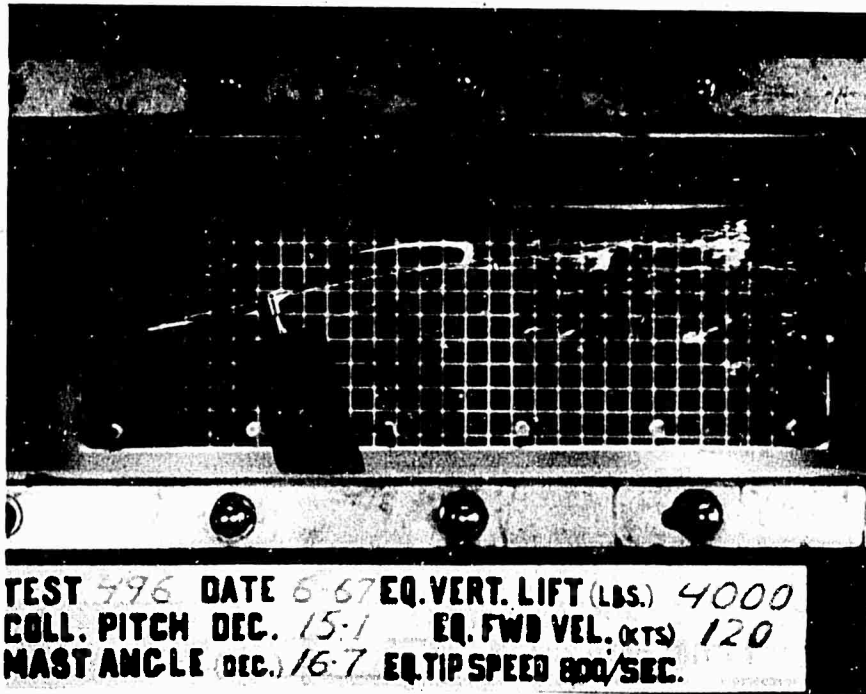


Time
Exposure

Figure 19. Comparison of 3-Bladed Rotor Vortex Trails at 20 Knots for Vertical Lifts of 4,960 and 13,250 Pounds

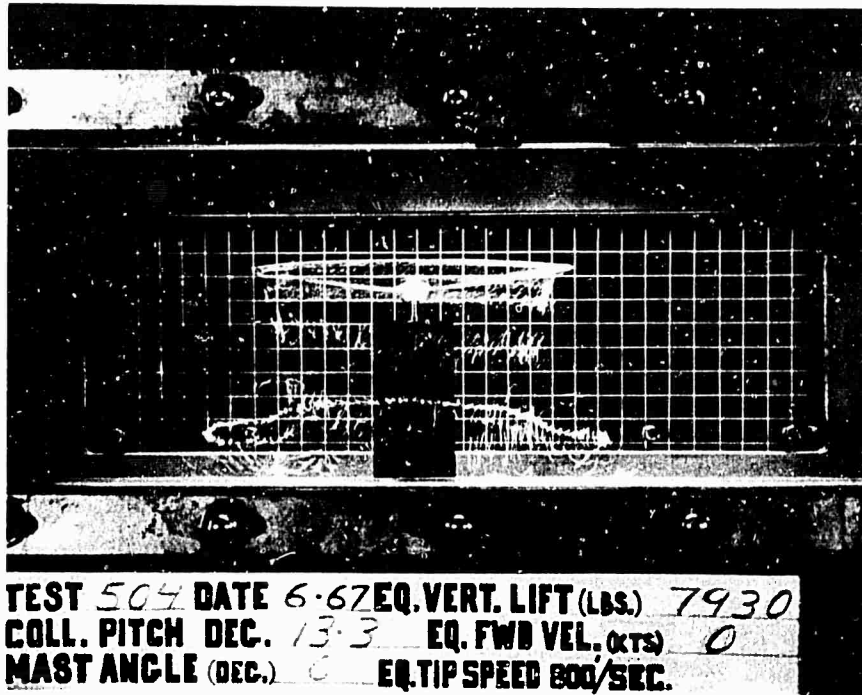


Stop
Action

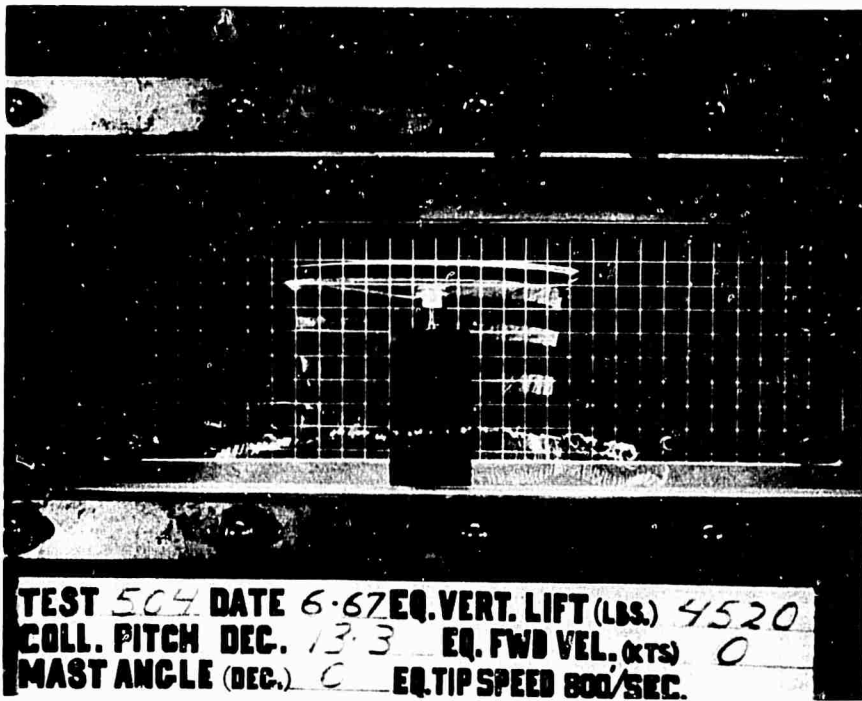


Stop
Action

Figure 20. Comparison of 2-Bladed Rotor Vortex Trails at 120 Knots for Vertical Lifts of 9,750 and 4,000 Pounds

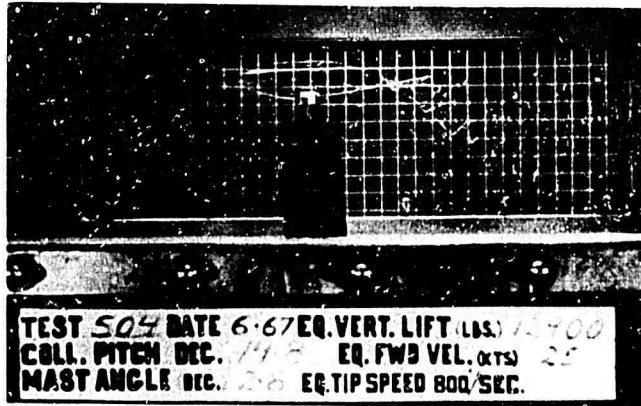


3-Bladed
Rotor
Time
Exposure
(Starting
Vortex Has
Reflected
From Tunnel
Floor)

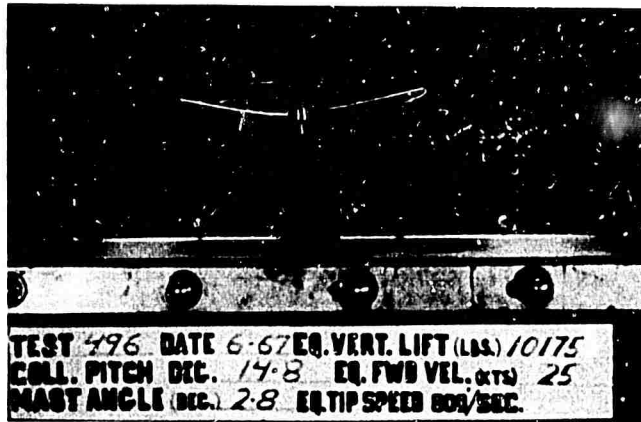


1-Bladed
Rotor
Time
Exposure
(Starting
Vortex Has
Reflected
From Tunnel
Floor)

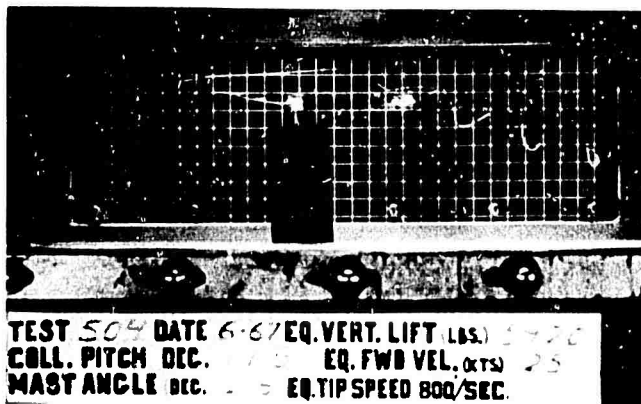
Figure 21. Comparison of 1- and 3-Bladed Rotor Vortex Trails at Same Collective Pitch Angle Setting and Hover Conditions



3-Bladed
Rotor

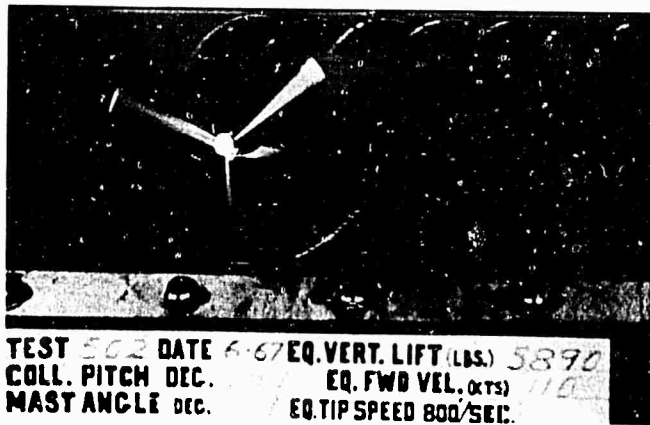


2-Bladed
Rotor

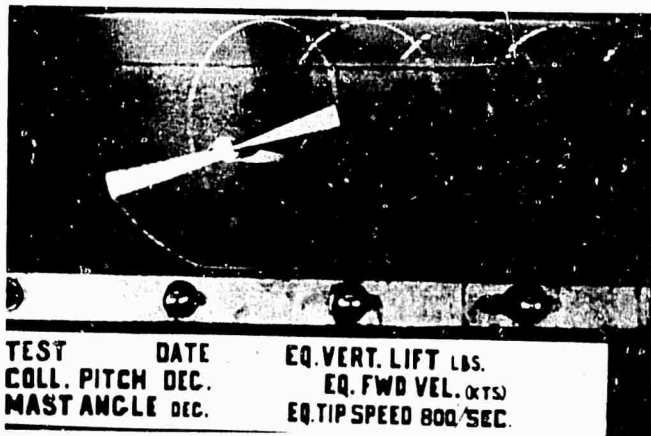


1-Bladed
Rotor

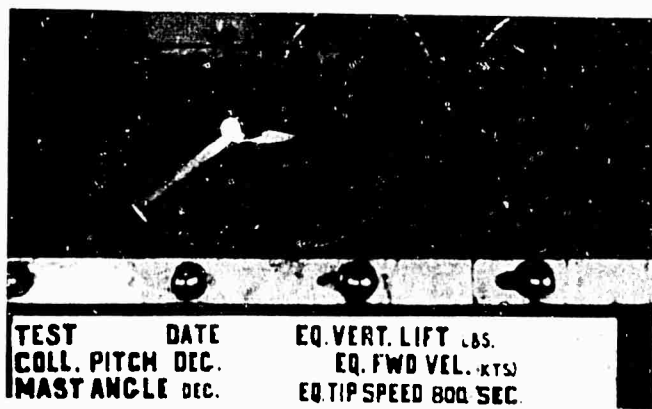
Figure 22. Comparison of 1-, 2-, and 3-Bladed Rotor Vortex Trails for Same Collective Pitch Angle Settings and Mast Angle at 25 Knots



3-Bladed Rotor



2-Bladed Rotor



1-Bladed Rotor

Figure 23. Comparison of 1-, 2-, and 3-Bladed Rotor Trails for Same Collective Pitch Angle Setting and Mast Angle at 110 Knots

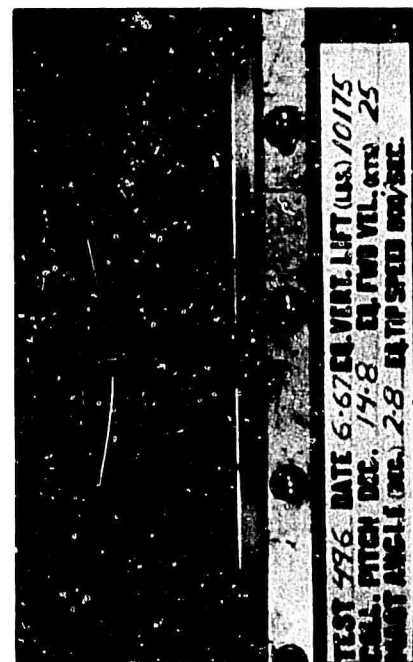
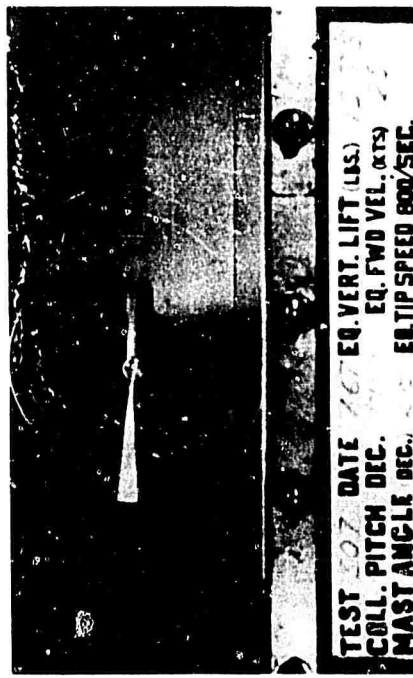


Figure 24(a). Velocity Increase Sequence Showing Vortex Trails Passing Above the Rotor; 2-Bladed Rotor

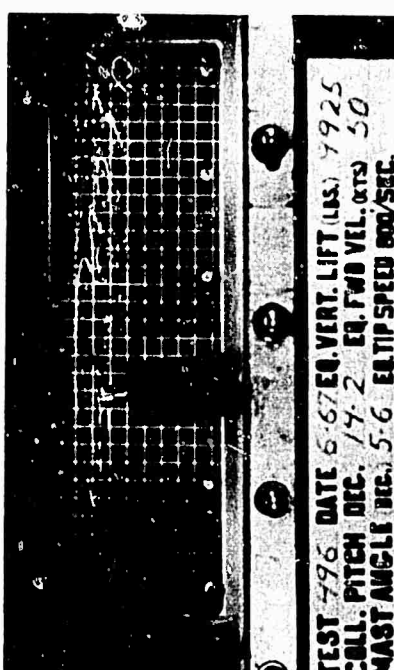
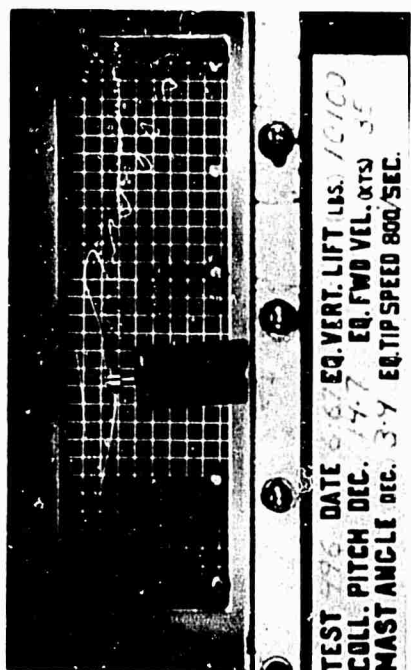


Figure 24 (b). Velocity Increase Sequence Showing Vortex Trails Passing Above the Rotor; 2-Bladed Rotor

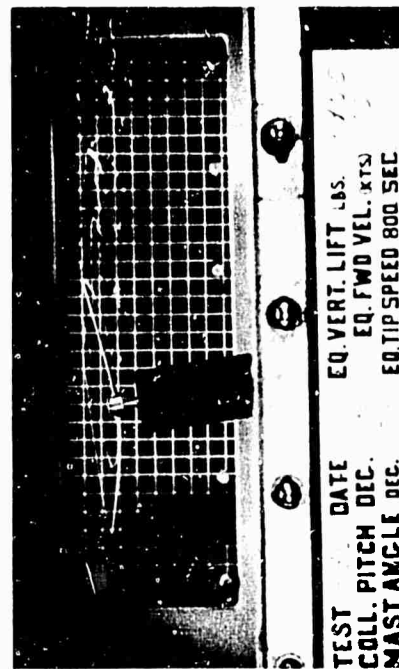
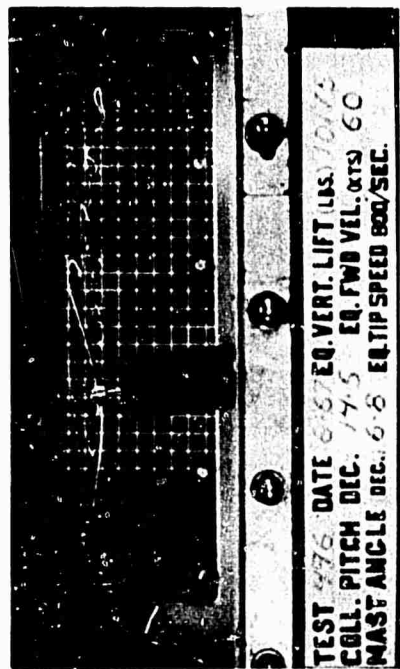
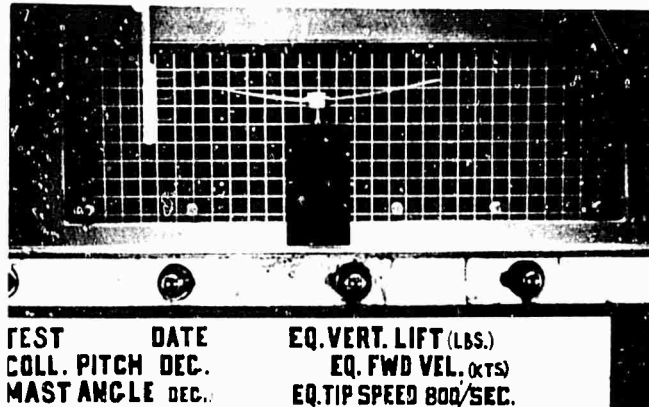
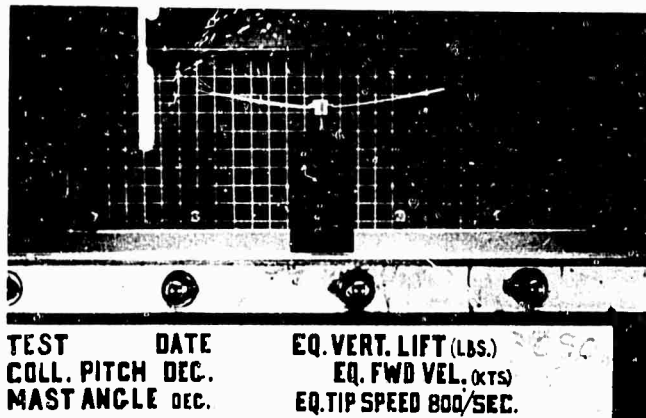


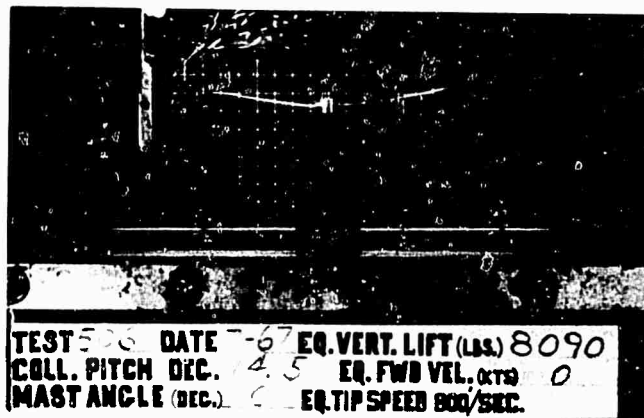
Figure 24(c). Velocity Increase Sequence Showing Vortex Trails Passing Above the Rotor; 2-Bladed Rotor



Rake 0.45 R
Laterally
from Shaft
Center Line
Toward
Retreating
Blade



Rake on
Shaft
Center
Line



Rake 0.45 R
Laterally
from Shaft
Center Line
Toward
Advancing
Blade

Figure 25. Variation in Inflow Pattern with Rake Lateral Position; 2-Bladed Rotor, Hover Condition

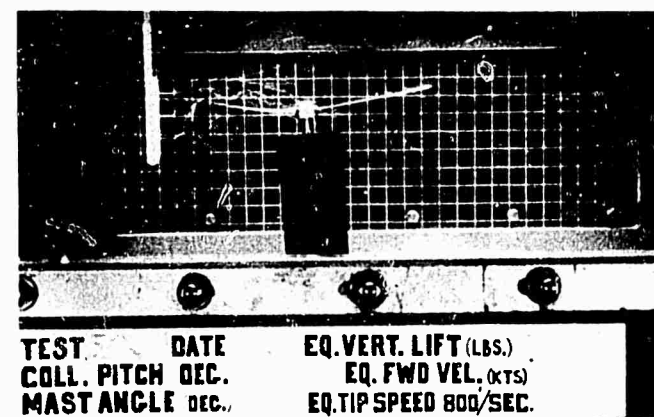
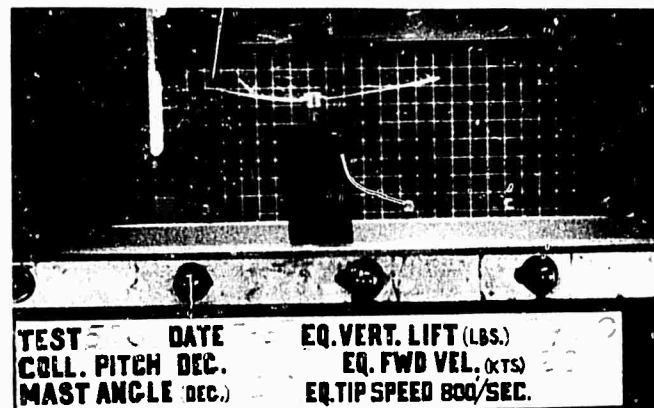
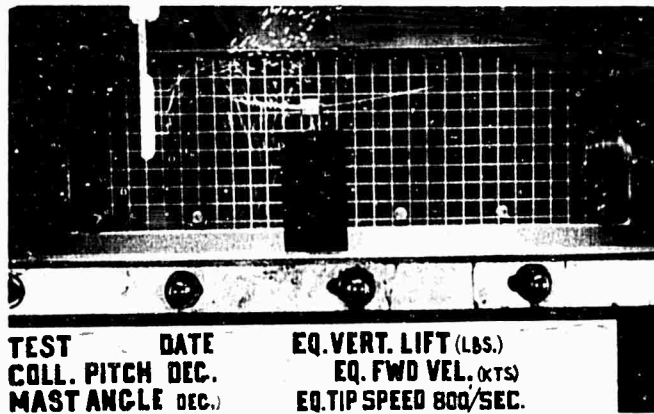


Figure 26. Variation in Inflow Pattern with Velocity Increase; 2-Bladed Rotor, Rake on Fore and Aft Center Line of Rotor Shaft

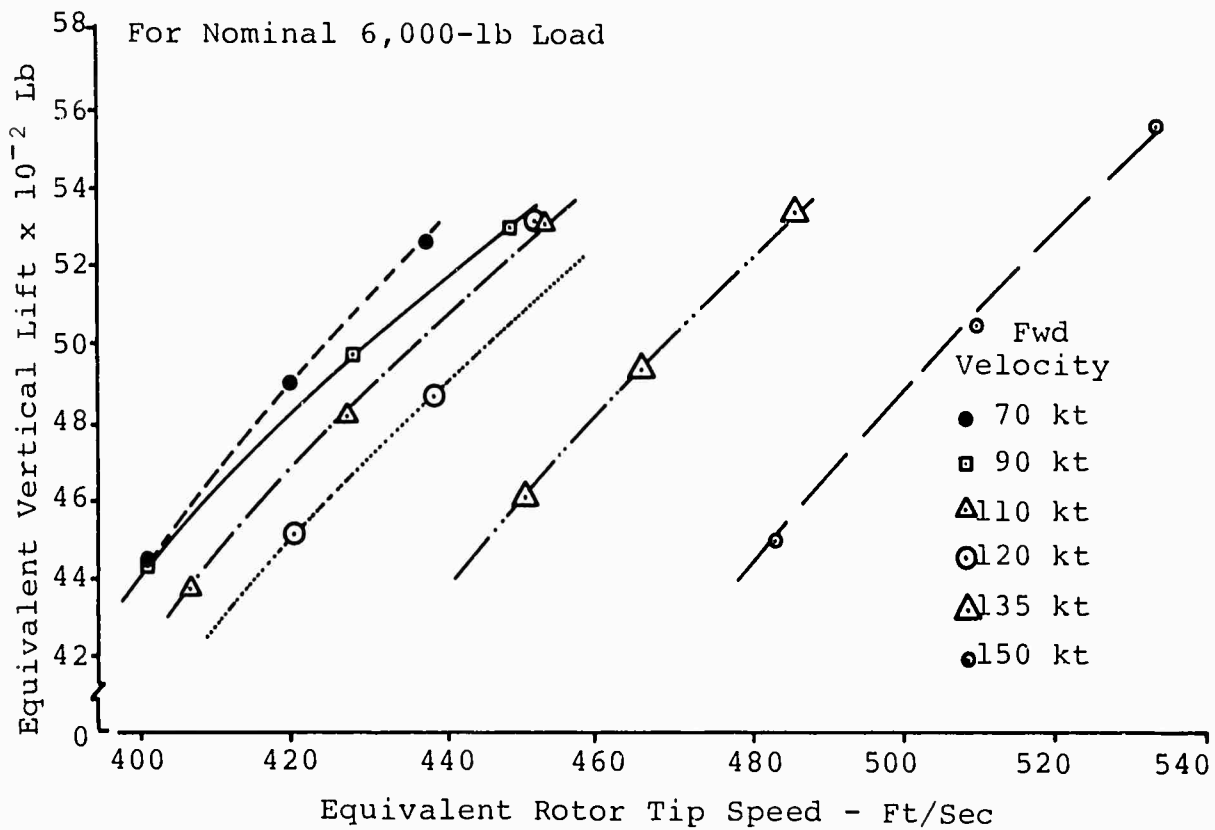
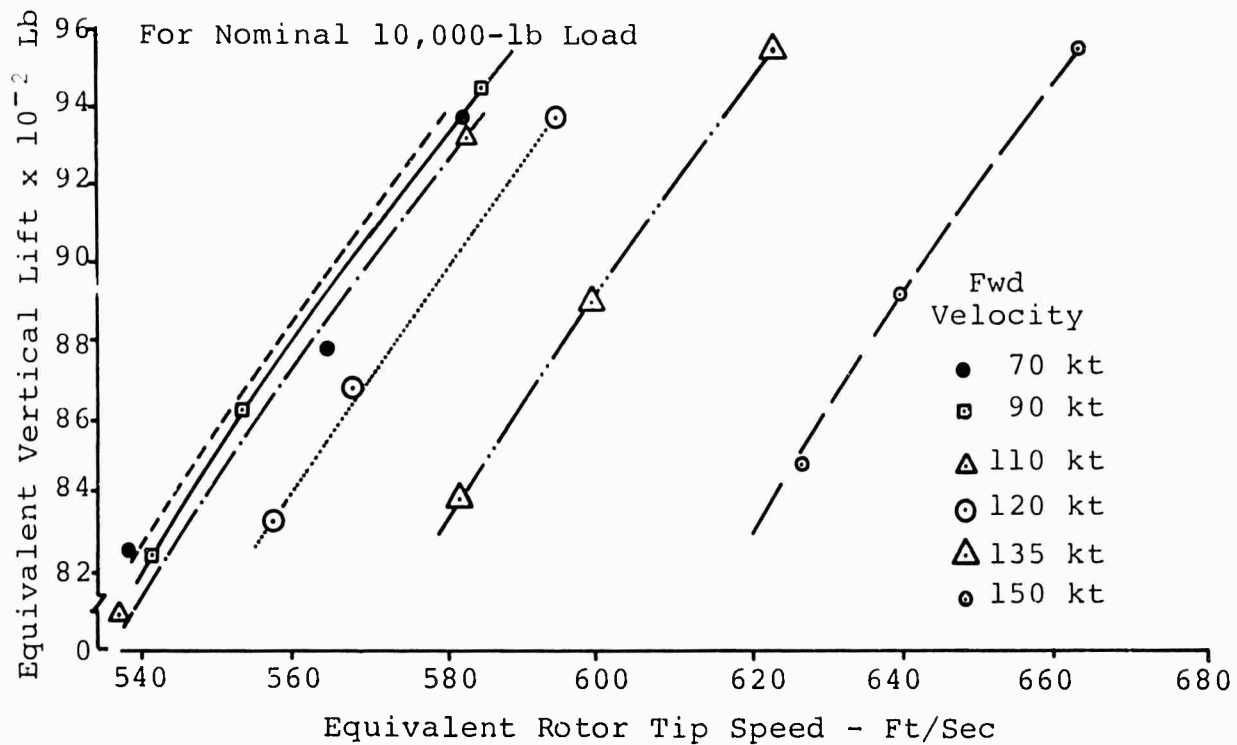


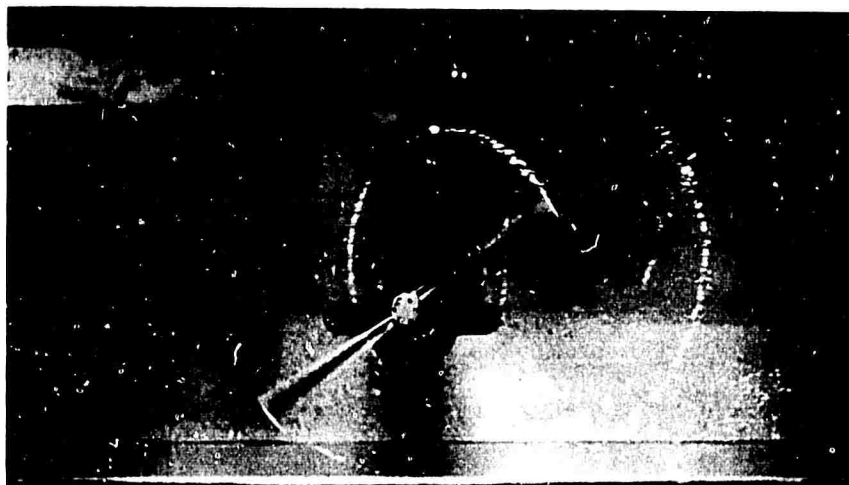
Figure 27. Simulated Power Failure - Autorotation with 2-Bladed Rotor



Equivalent
Rotor Tip
Speed
583 fps

Lift: 9,377 lb

TEST	DATE	EQ. VERT. LIFT	LBS.
COLL. PITCH	DEC.	EQ. FWD VEL.	(KTS)
MAST ANGLE	DEC.	EQ. TIP SPEED	SEC.



Equivalent
Rotor Tip
Speed
438 fps

Lift: 5,266 lb

TEST	DATE	EQ. VERT. LIFT	LBS.
COLL. PITCH	DEC.	EQ. FWD VEL.	(KTS)
MAST ANGLE	DEC.	EQ. TIP SPEED	SEC.

Figure 28. Comparison of Tip Vortex Trails for 2-Bladed Rotor in Simulated Autorotation Condition at 70 Knots



Equivalent
Rotor Tip
Speed
664 fps

Lift: 9,542 lb

TEST	DATE	EQ. VERT. LIFT	LBS.
COLL. PITCH	DEC.	EQ. FWD VEL.	(KTS)
MAST ANGLE	DEC.	EQ. TIP SPEED	/SEC.



Equivalent
Rotor Tip
Speed
484 fps

Lift: 4,507 lb

TEST	DATE	EQ. VERT. LIFT	LBS.
COLL. PITCH	DEC.	EQ. FWD VEL.	(KTS)
MAST ANGLE	DEC.	EQ. TIP SPEED	/SEC.

Figure 29. Comparison of Tip Vortex Trails for 2-Bladed Rotor in Simulated Autorotation Condition at 150 Knots

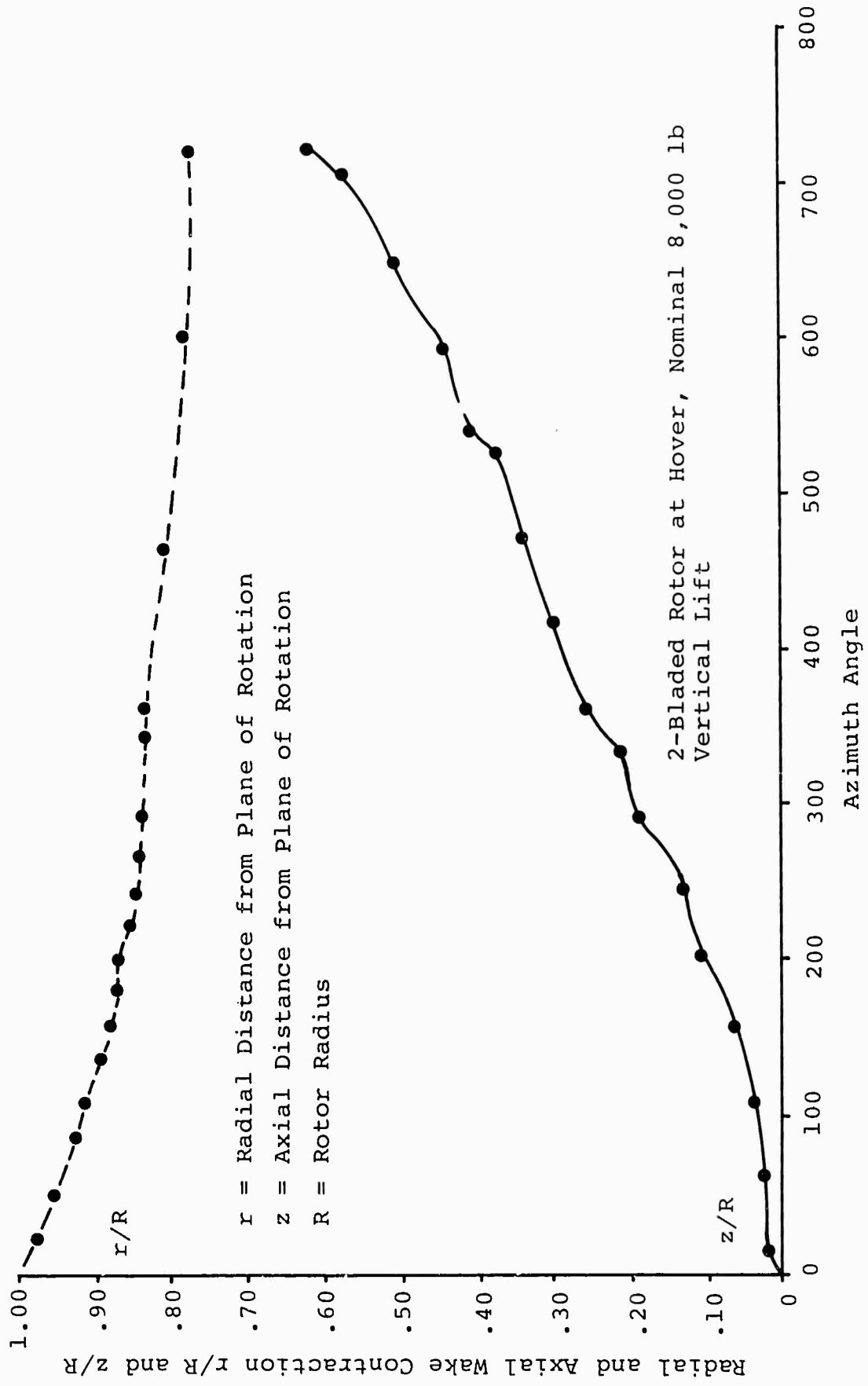


Figure 30. Plot of Spatial Wake Coordinates as Radial and Axial Contraction Ratios, 2-Bladed Rotor at Hover

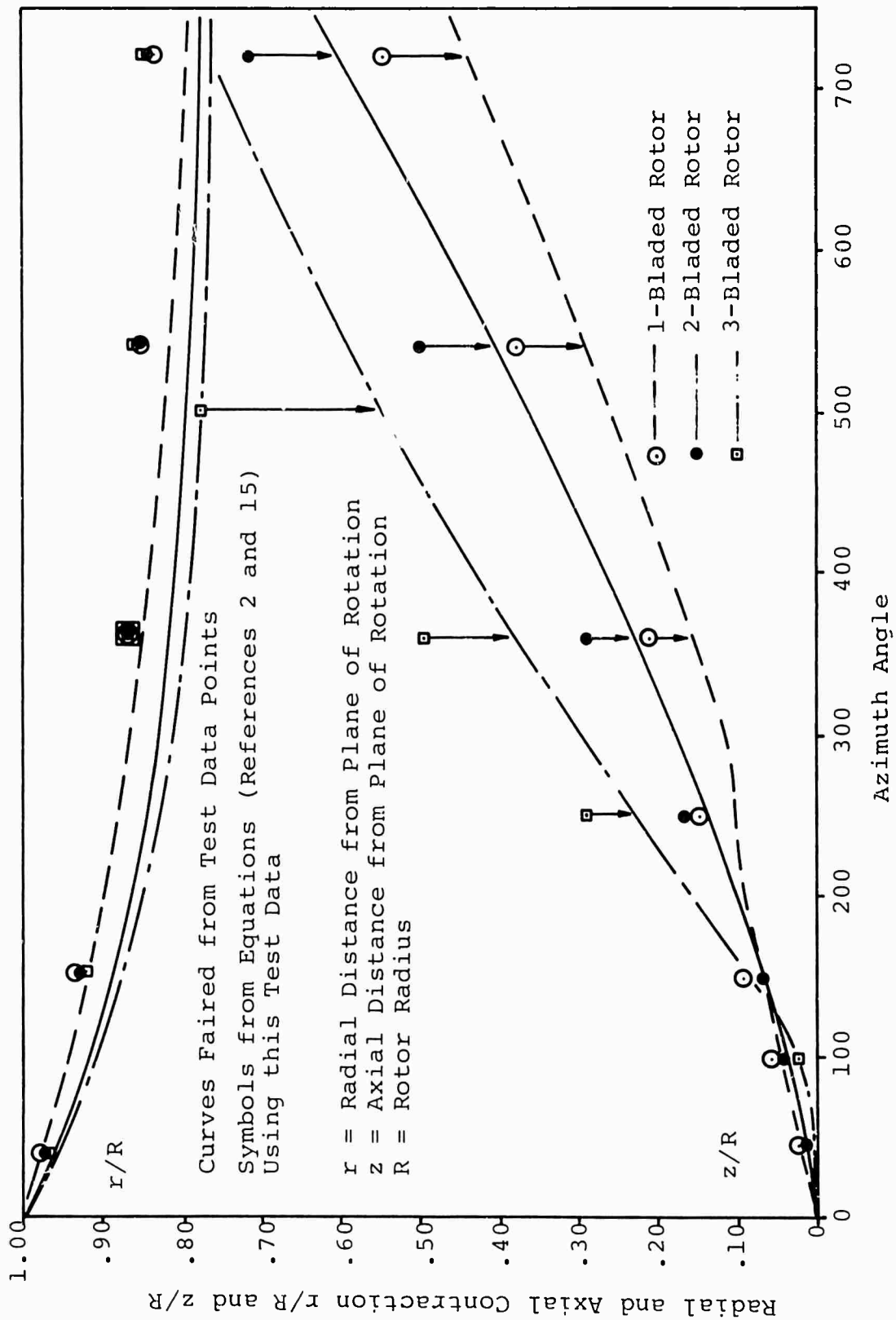
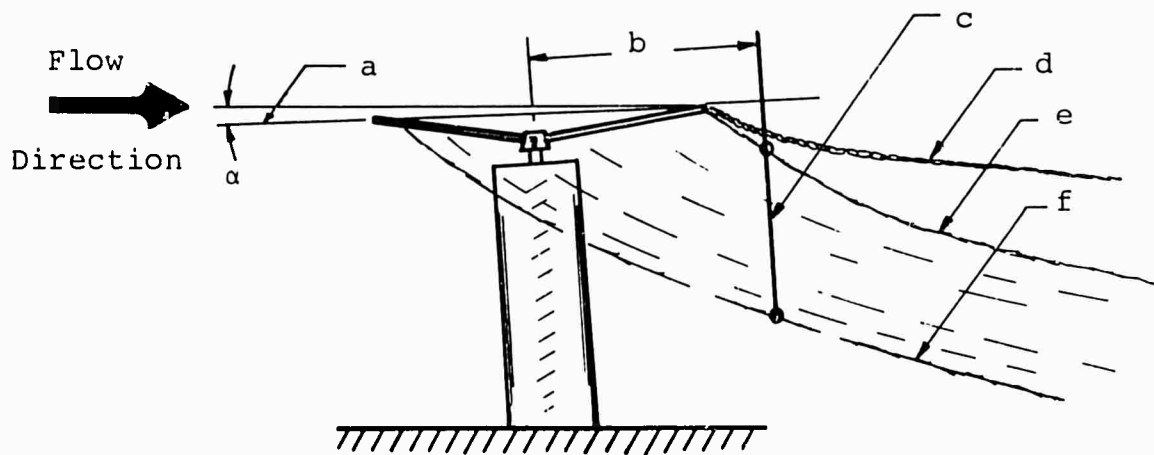


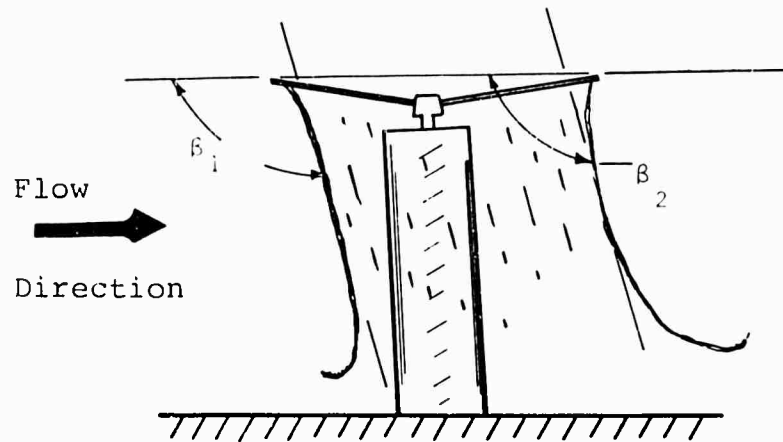
Figure 31. Comparison of Faired Experimental Data with Equation Values for Case of 1-, 2-, and 3-Bladed Rotors at Hover



- a Tip path plane
- b 1.2 rotor radii, distance to plane c
- c Plane perpendicular to the tip path plane along which distances to d, e, and f are measured
- d "Wing tip type" tip vortex trail [see Figure 14(a)]
- e Upper boundary of "ring" vortices shed during rear portion of a rotor revolution measured at center line [see Figure 14(a) and upper photograph of Figure 14(b)]
- f Lower boundary of flow through the rotor [see Figure 19] measured at center line
- α Angle of tip path plane with oncoming flow

(a) Wake Flow Definition (except skew angle)

Figure 32. Sketch of Terms Employed in Spatially Locating Flow Characteristics



- β_1 Skew angle that the upstream boundary of flow through the rotor makes with the tip path plane
- β_2 Skew angle that the downstream boundary of the flow through the rotor makes with the tip path plane

(b) Skew Angle Definition

Figure 32. Continued

All Rotor Blade Orientations
Correspond to $\approx 4,000\text{-lb}$ Vertical
Lift with 2-Bladed Rotor

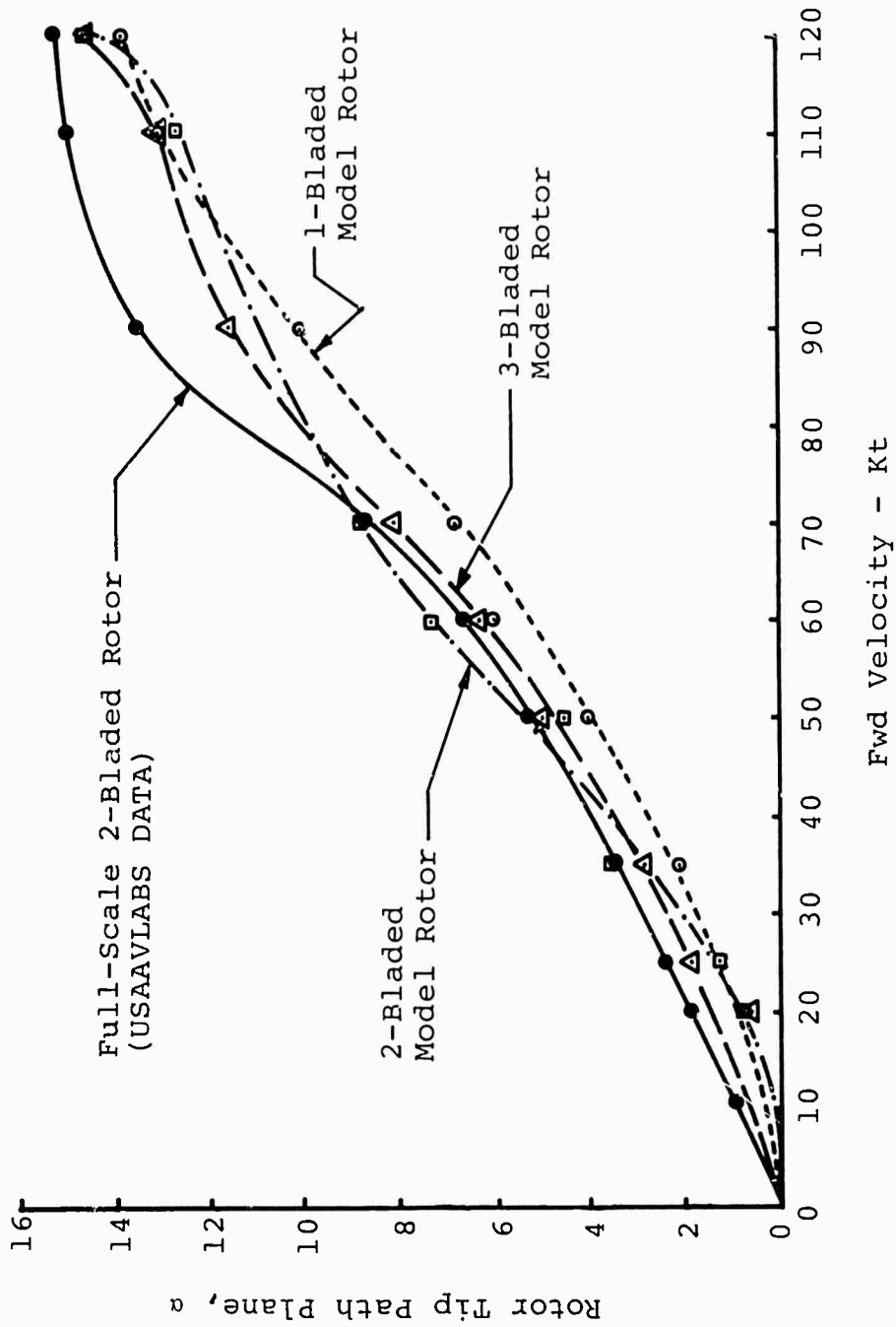


Figure 33. Rotor Tip Path Orientation Versus Forward Velocity for Nominal 4,000-Pound Lift for 2-Bladed Rotor

All Rotor Blade Orientations
Correspond to $\approx 6,000$ -lb Vertical
Lift with 2-Bladed Rotor

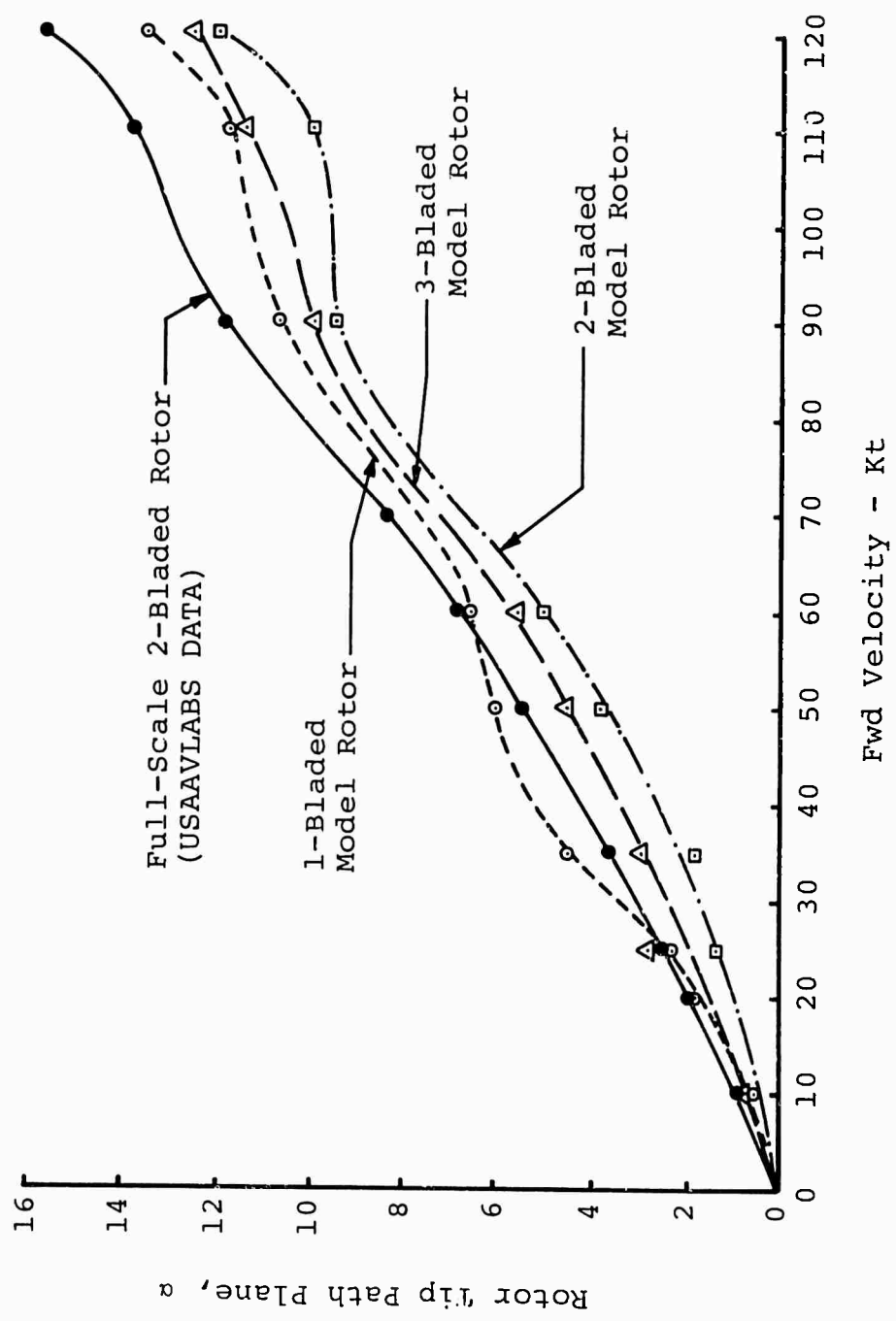


Figure 34. Rotor Tip Path Orientation Versus Forward Velocity for Nominal 6,000-Pound Lift for 2-Bladed Rotor

All Rotor Blade Orientations
Correspond to \approx 8,000-lb Vertical
Lift with 2-Bladed Rotor

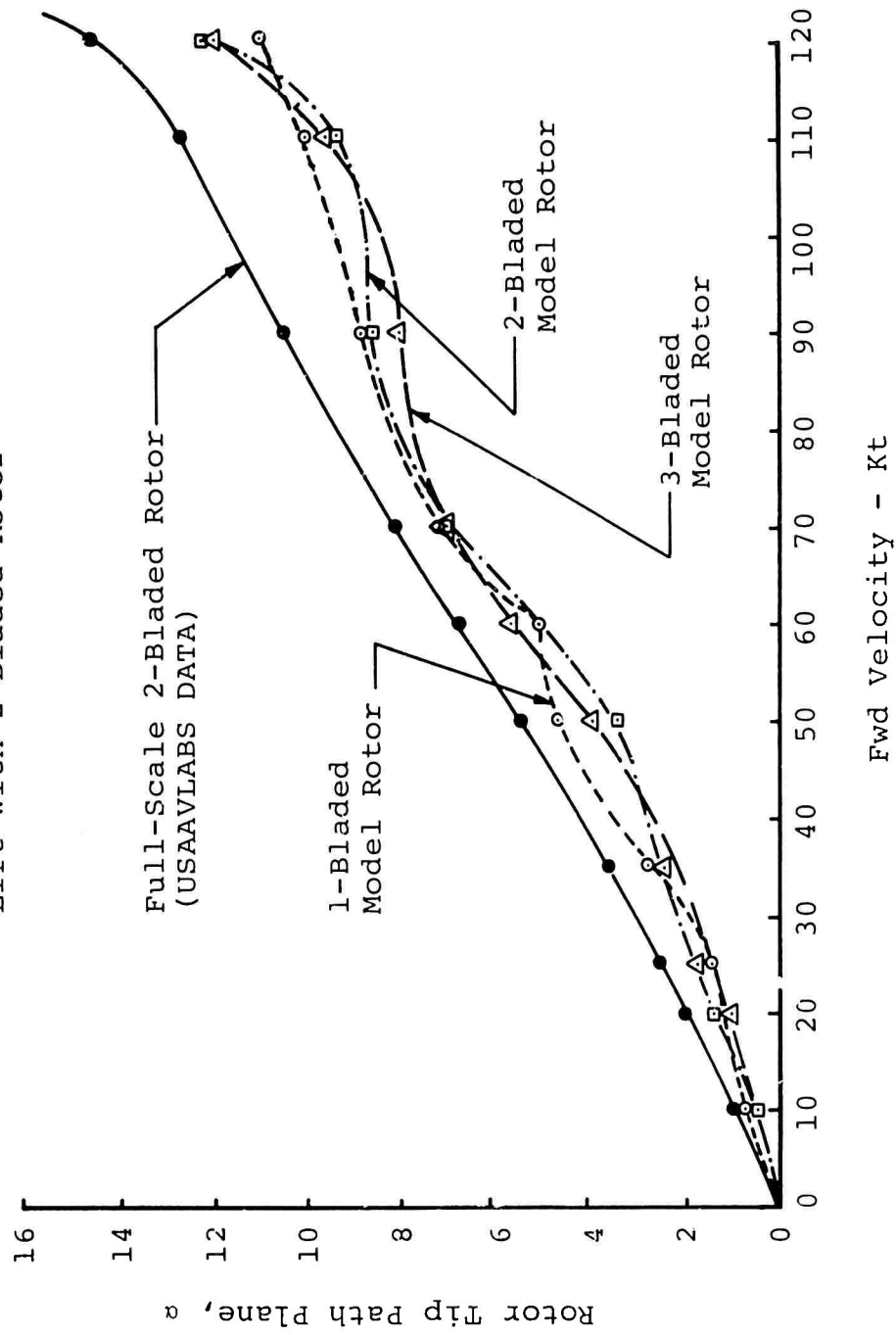


Figure 35. Rotor Tip Path Orientation Versus Forward Velocity for Nominal 8,000-Pound Lift for 2-Bladed Rotor

All Rotor Blade Orientations
 Correspond to $\approx 10,000\text{-lb}$ Vertical
 Lift with 2-Bladed Rotor

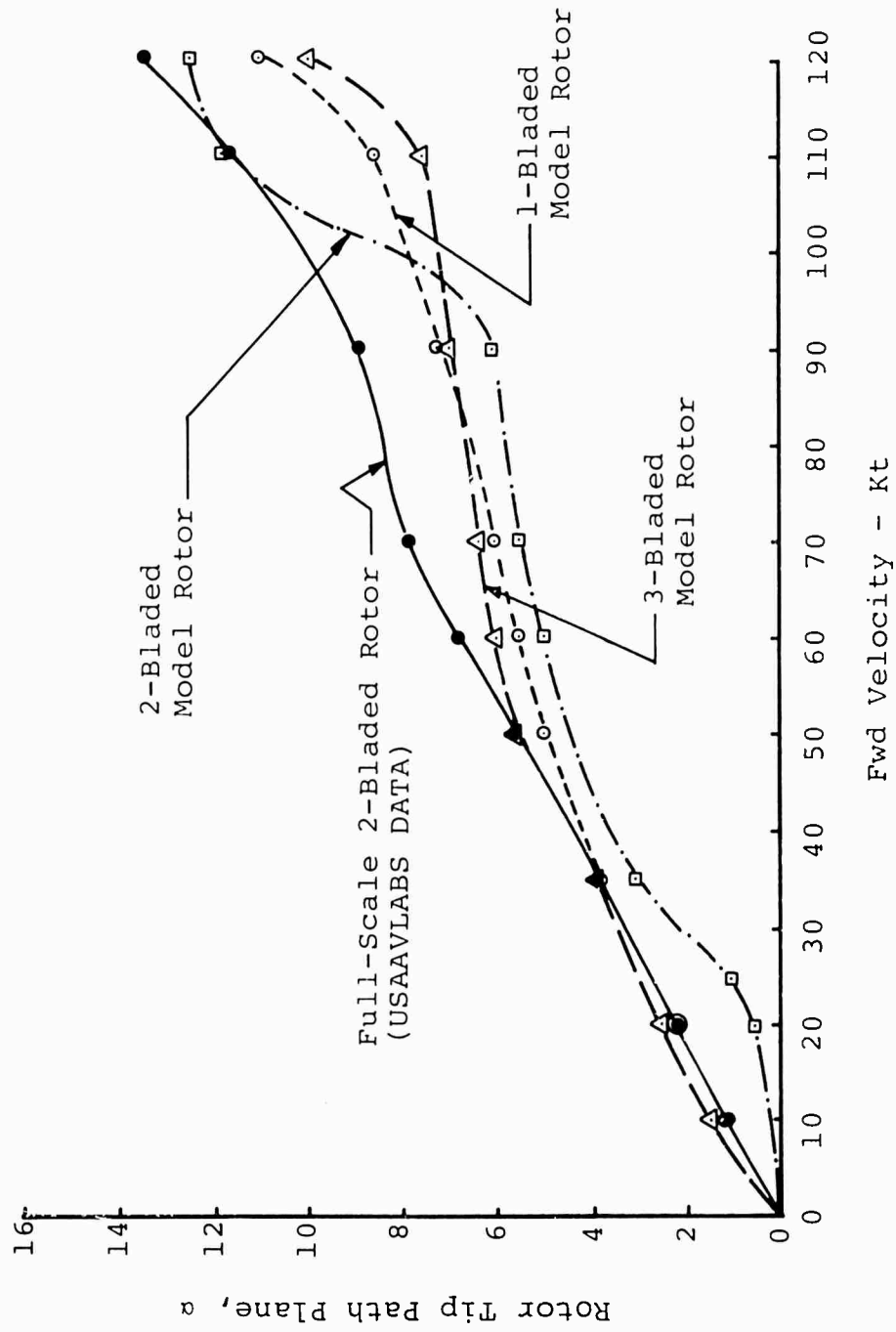


Figure 36. Rotor Tip Path Orientation Versus Forward Velocity for Nominal 10,000-Pound Lift for 2-Bladed Rotor

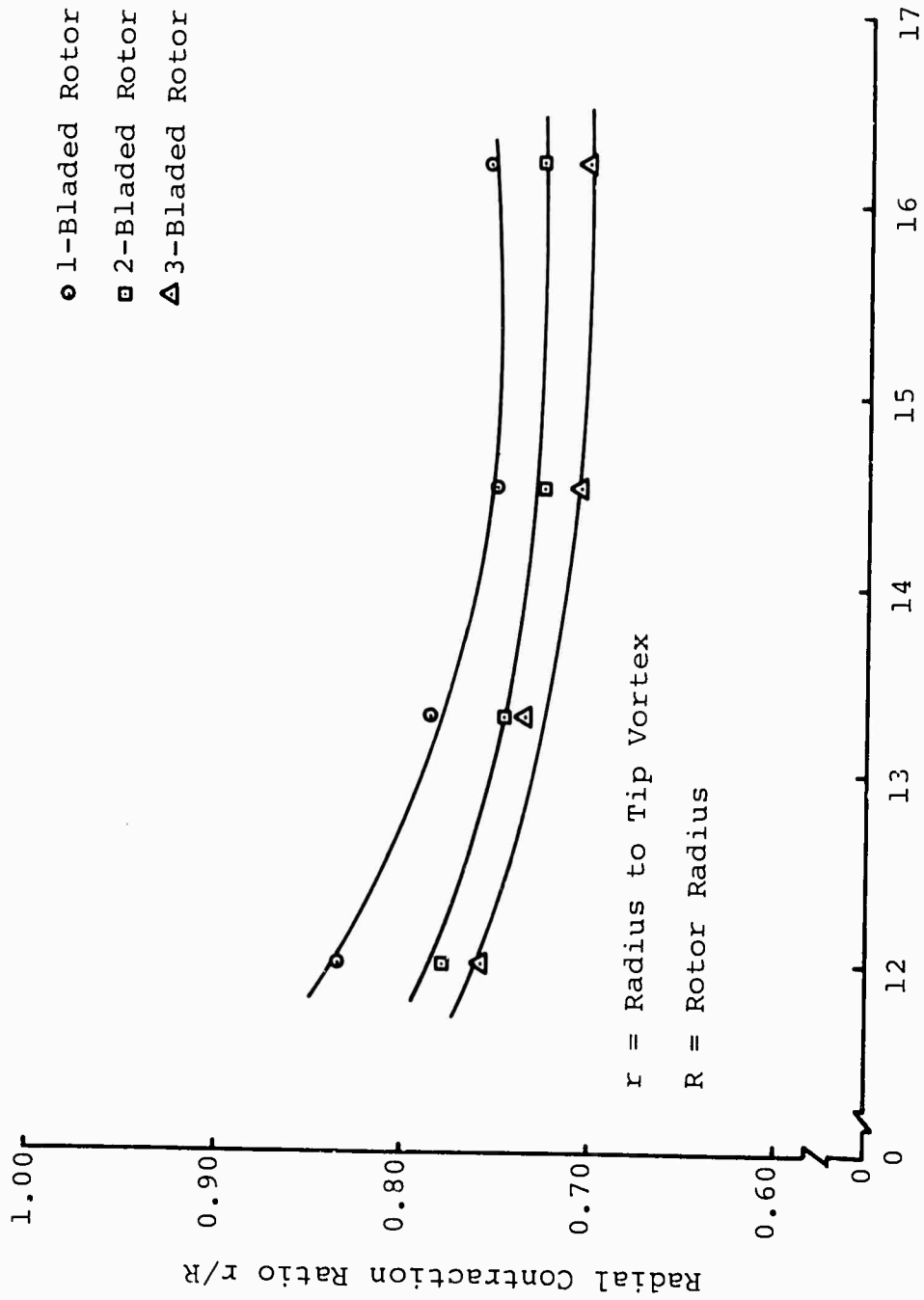


Figure 37. Plot of Radial Contraction Ratio Versus Collective Pitch Angle for 1-, 2-, and 3-Bladed Rotor at Hover

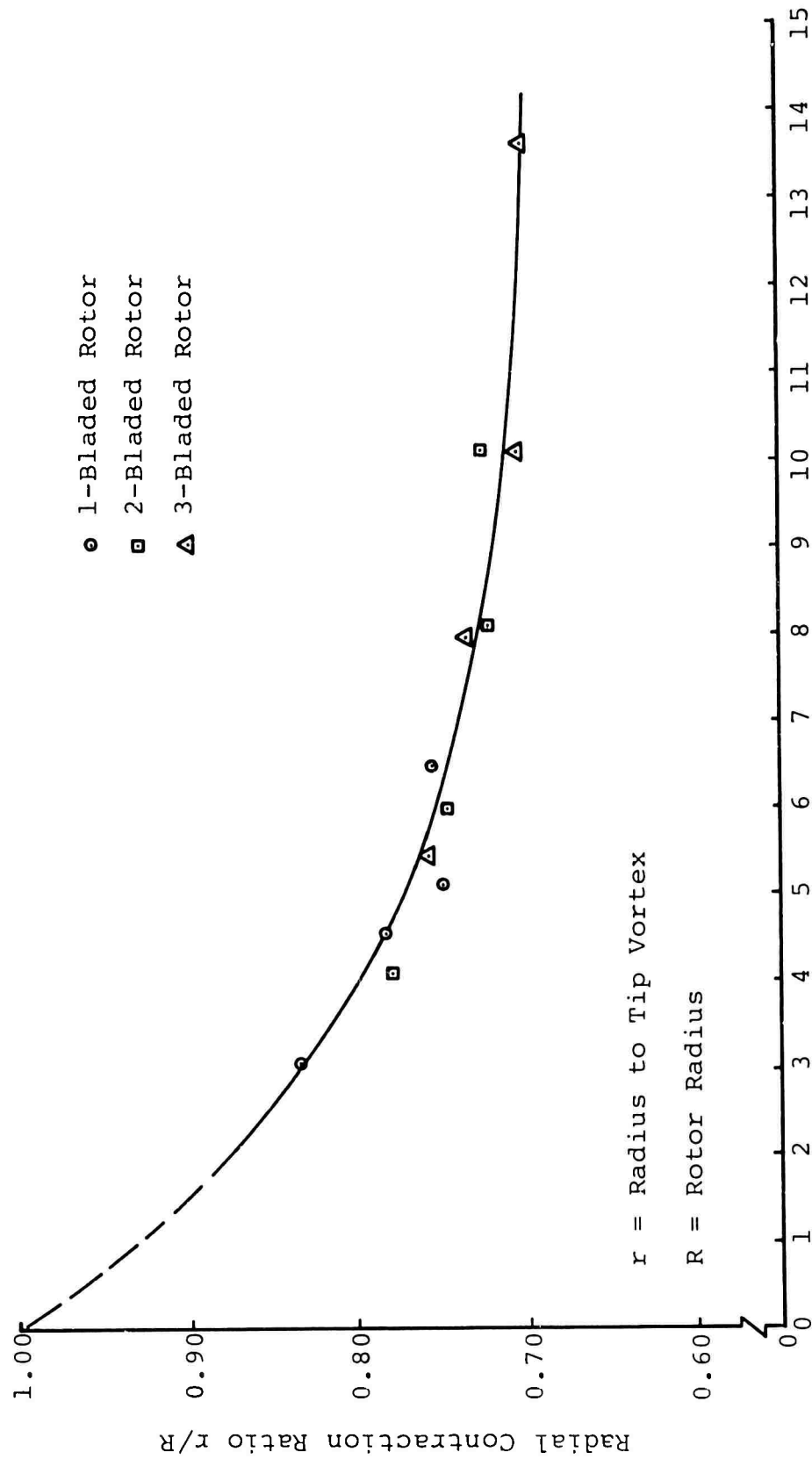


Figure 38. Plot of Radial Contraction Ratio Versus Equivalent Vertical Load for 1-, 2-, and 3-Bladed Rotor at Hover

All Rotor Blade Orientations
Correspond to \approx 4,000-lb Vertical
Lift with 2-Bladed Rotor

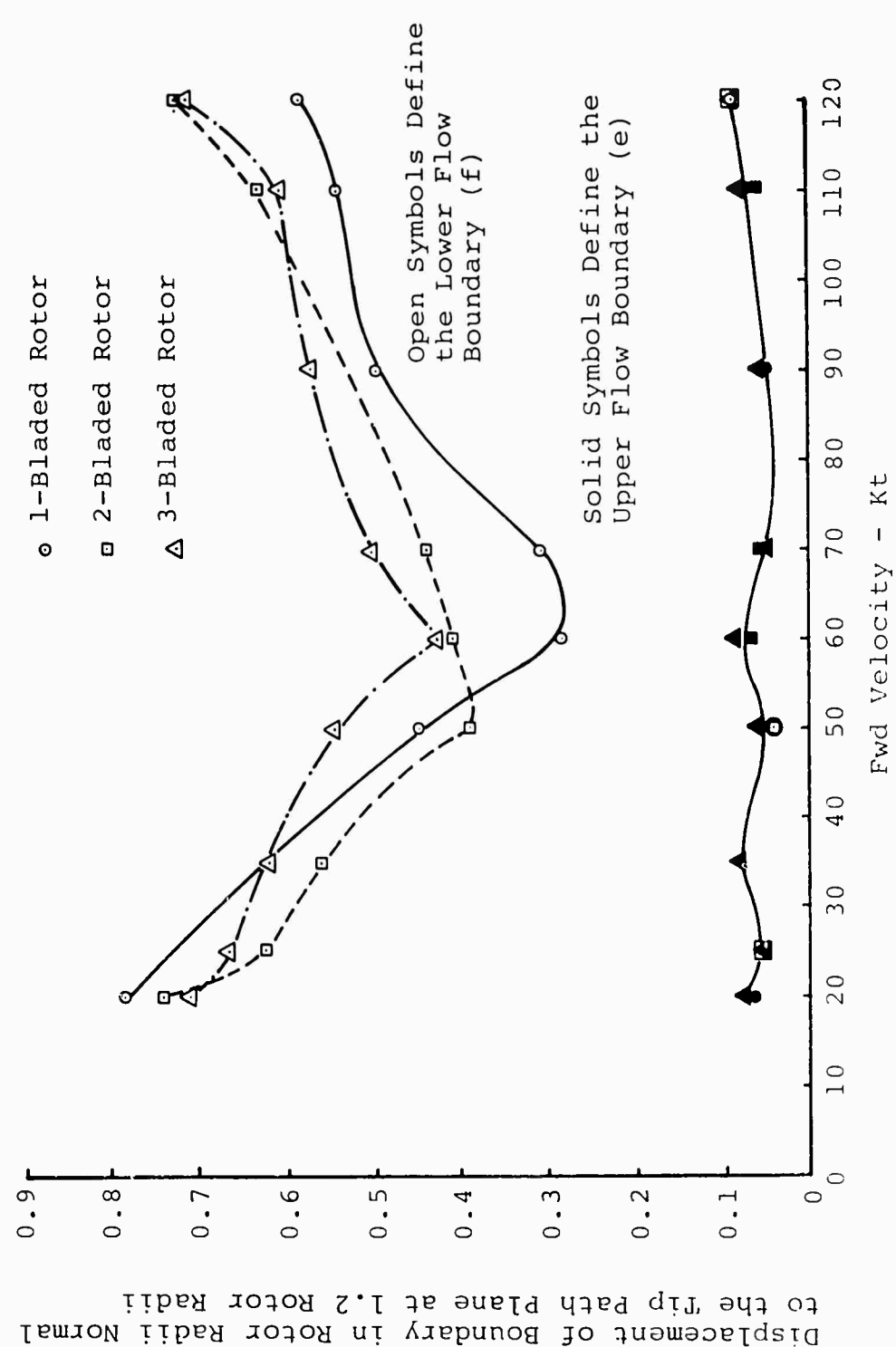


Figure 39. Displacement of the Upper and Lower Boundaries of the Flow Through the Rotor Versus Forward Velocity for a Nominal 4,000-Pound Lift for the 2-Bladed Rotor

Displacement of Boundary in Rotor Radii Normal to the Tip Path Plane at 1.2 Rotor Radii

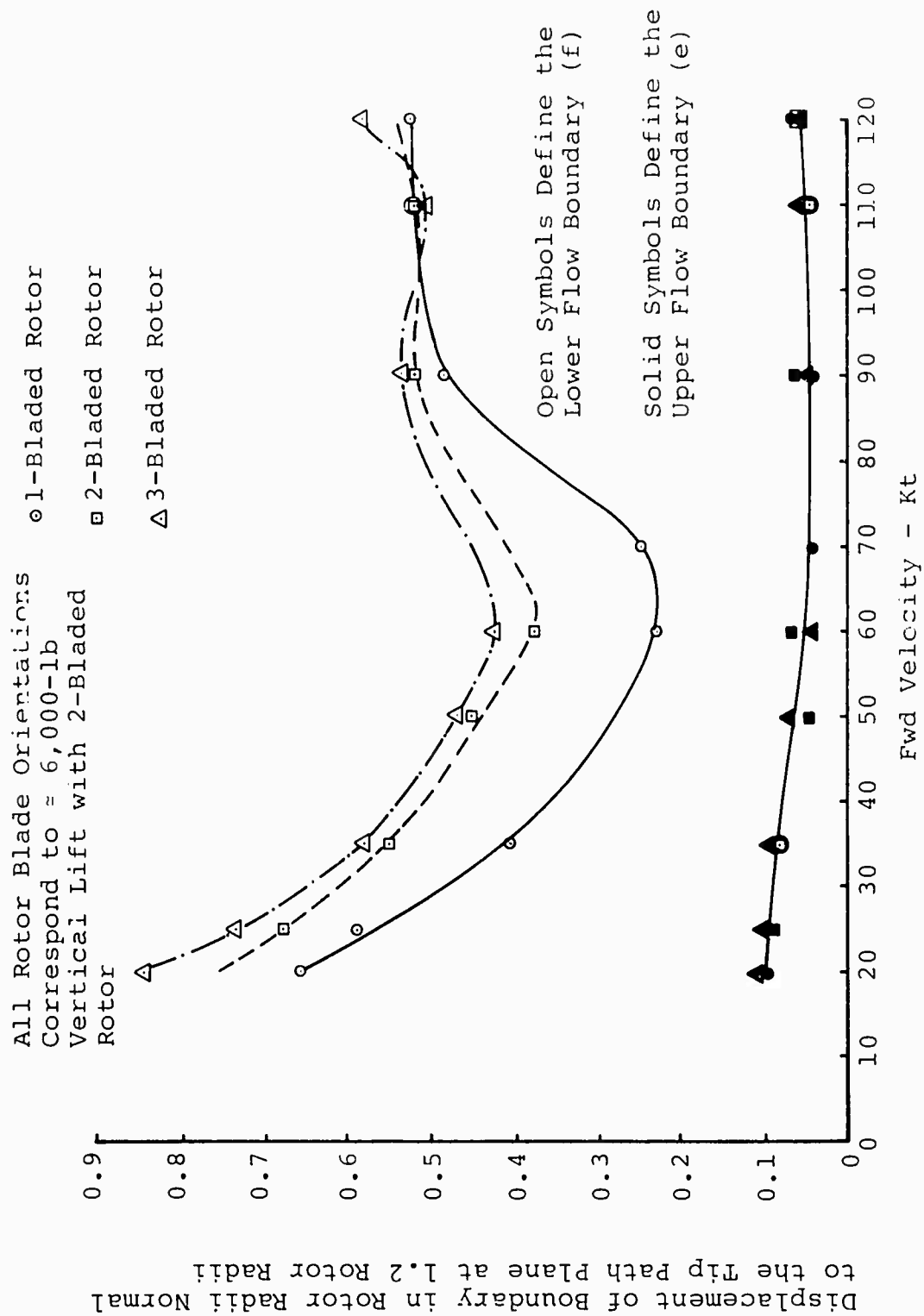


Figure 40. Displacement of the Upper and Lower Boundaries of the Flow Through the Rotor Versus Forward Velocity for a Nominal 6,000-Pound Lift for the 2-Bladed Rotor

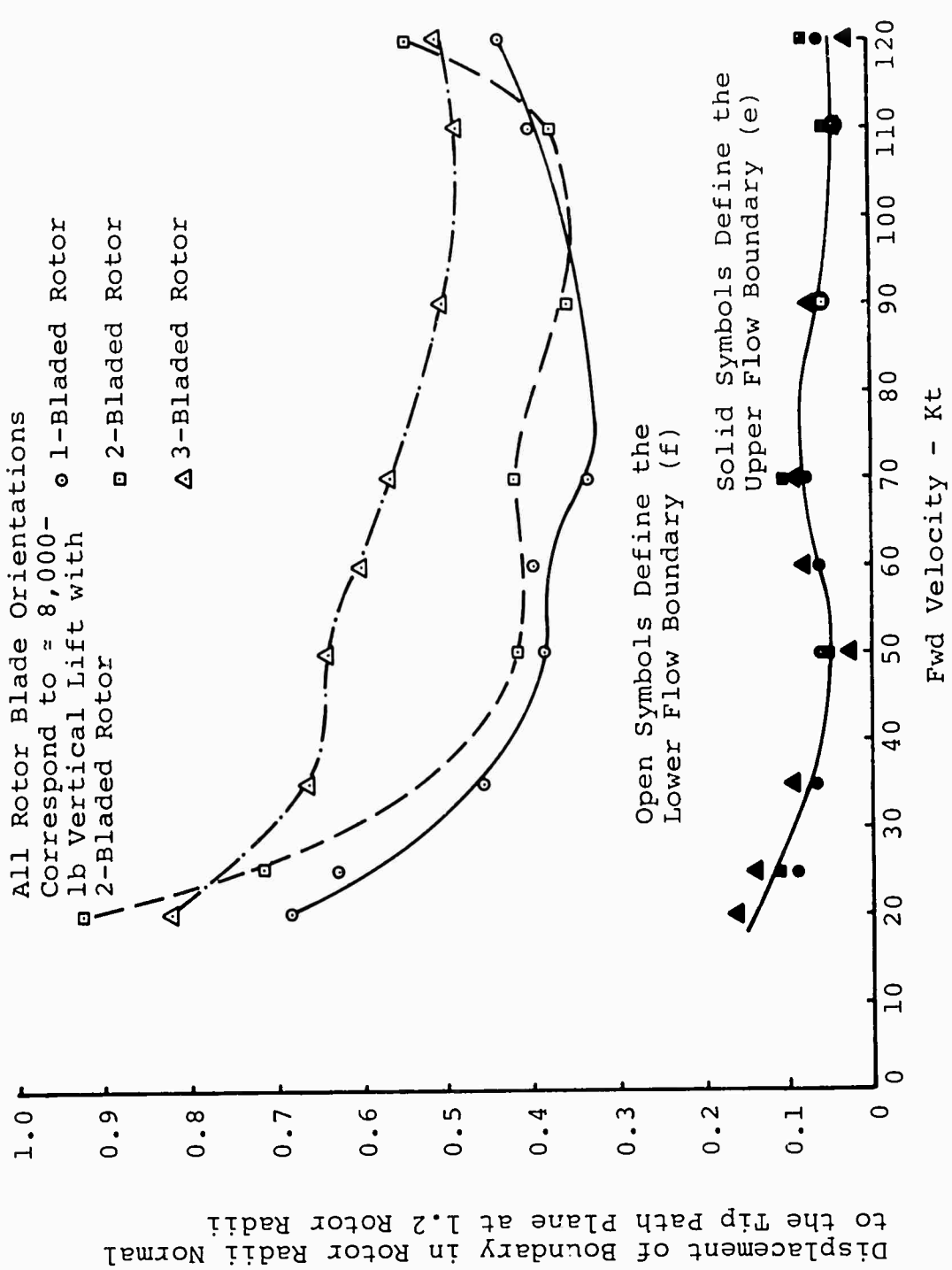


Figure 41. Displacement of the Upper and Lower Boundaries Defining the Flow Through the Rotor Versus Forward Velocity for a Nominal 8,000-Pound Lift for the 2-Bladed Rotor

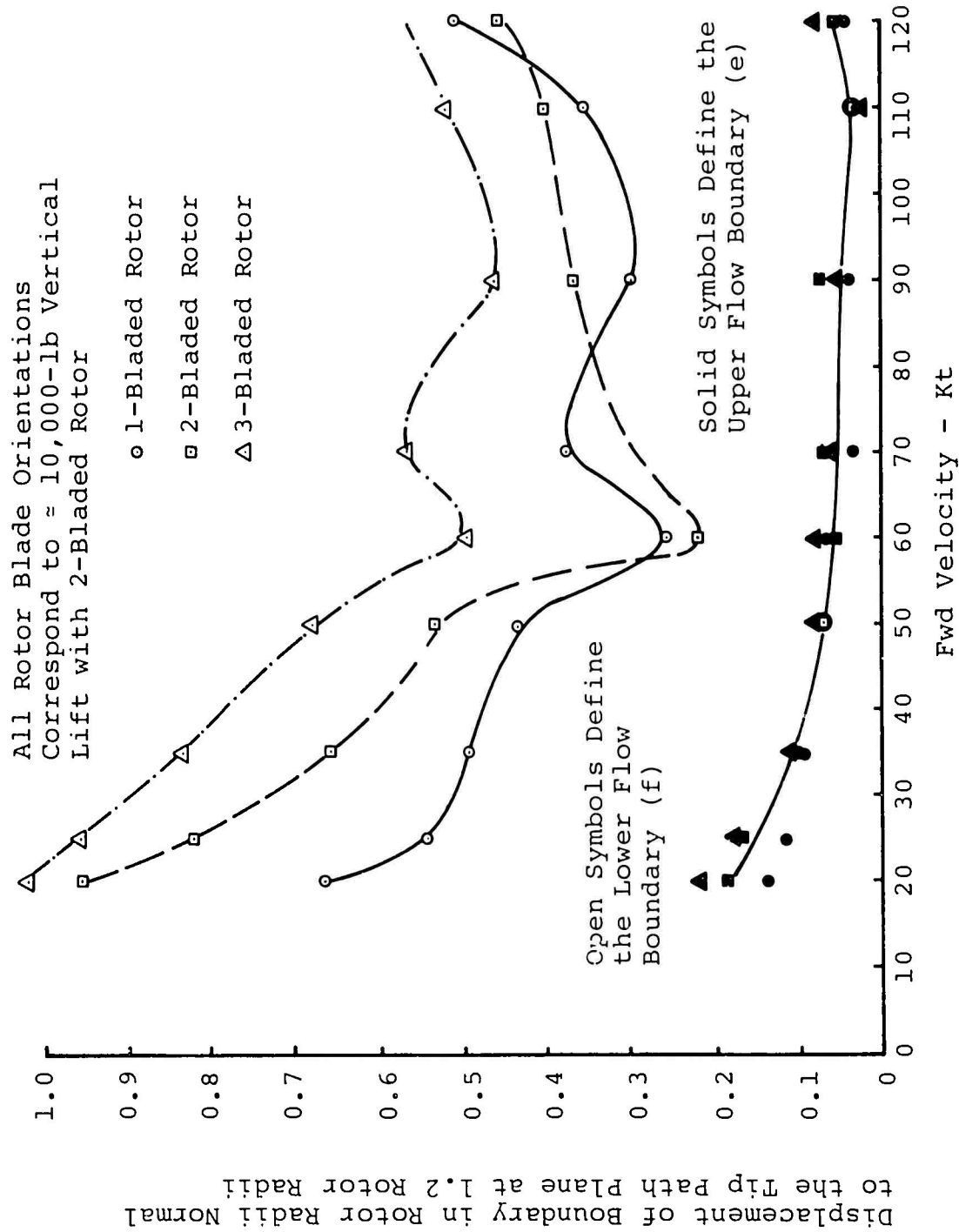


Figure 42. Displacement of the Upper and Lower Boundaries of the Flow Through the Rotor Versus Forward Velocity for a Nominal 10,000-Pound Lift for the 2-Bladed Rotor

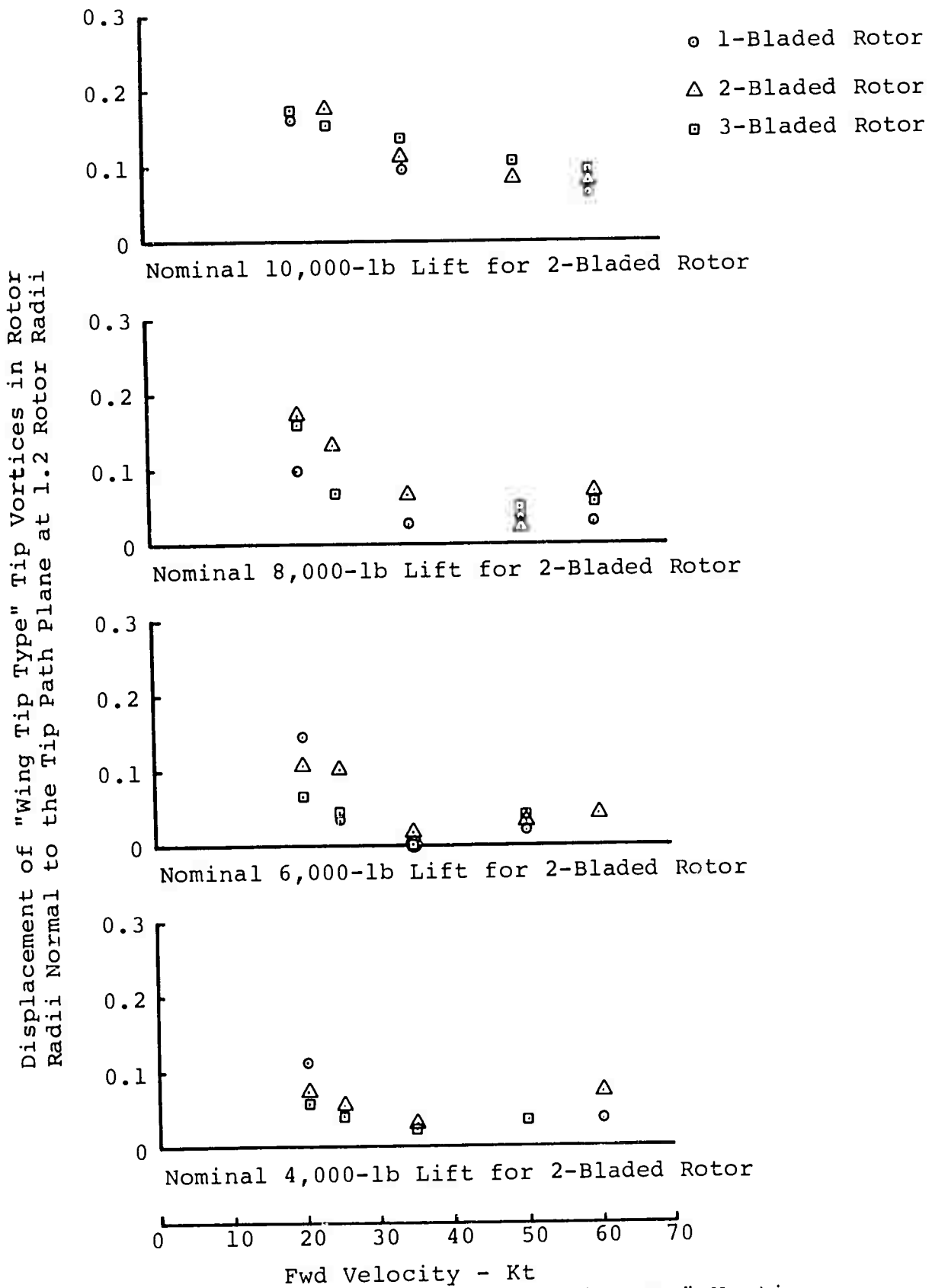


Figure 43. Displacement of the "Wing Tip Type" Vortices Versus Forward Velocity

APPENDIX I

HOVER AND FORWARD FLIGHT CONDITIONS

Line No.	No. of Blades on Rotor	Equiv Fwd Vel (kt)	Equiv Full-Scale Lift (lb)	Conditions Established for 2-Bladed Lift of ≈ (lb)	Viewing Position		Photograph Neg No.		Movie Clip
					Side	Top	Stop Action	Time Exp	
1	2	0	4,060	4,000	x		1	2	x
2	2	10	3,940	4,000	x		3	4	x
3	2	20	4,000	4,000	x		5	6	x
4	2	25	4,010	4,000	x		7	8	x
5	2	35	4,070	4,000	x		9	10	x
6	2	50	3,985	4,000	x		11	12	x
7	2	60	4,025	4,000	x		13	14	x
8	2	70	3,910	4,000	x		15	16	x
9	2	90	3,980	4,000	x		17	18	x
10	2	110	3,970	4,000	x		19	20	x
11	2	120	4,000	4,000	x		21	22	x
12	1	0	3,020	4,000	x		23	24	x
13	1	10	3,060	4,000	x		25	26	x
14	1	20	3,060	4,000	x		27	28	x
15	1	25	2,940	4,000	x		29	30	x
16	1	35	3,050	4,000	x		31	32	x
17	1	50	2,640	4,000	x		33	34	x
18	1	60	2,540	4,000	x		35	36	x
19	1	70	2,520	4,000	x		37	38	x

Line No.	No. of Blades on Rotor	Equiv Fwd Vel (kt)	Equiv Full-Scale Lift (lb)	Conditions Established for 2-Bladed Lift of = (lb)	Viewing Position		Photograph Neg No.		Movie Clip
					Side	Top	Stop Action	Time Exp	
20	1	90	2,590	4,000	x		39	40	x
21	1	110	2,580	4,000	x		41	42	x
22	1	120	2,560	4,000	x		43	44	x
23	3	0	5,400	4,000	x		45	46	x
24	3	10	5,240	4,000	x		47	48	x
25	3	20	4,960	4,000	x		49	50	x
26	3	25	4,760	4,000	x		51	52	x
27	3	35	5,000	4,000	x		53	54	x
28	3	50	5,240	4,000	x		55	56	x
29	3	60	5,440	4,000	x		57	58	x
30	3	70	5,400	4,000	x		59	60	x
31	3	90	5,800	4,000	x		61	62	x
32	3	110	5,890	4,000	x		63	64	
33	3	120	5,720	4,000	x		65	66	x
34	2	0	5,950	6,000	x		67	68	x
35	2	10	5,975	6,000	x		69	70	x
36	2	20	6,100	6,000	x		71	72	x
37	2	25	5,950	6,000	x		73	74	x
38	2	35	5,975	6,000	x		75	76	x
39	2	50	5,950	6,000	x		77	78	x
40	2	60	5,850	6,000	x		79	80	x
41	2	70	6,050	6,000	x		81	82	x

Line No.	No. of Blades on Rotor	Equiv Fwd Vel (kt)	Equiv Full-Scale Lift (lb)	Conditions Established for 2-Bladed Lift of = (lb)	Viewing Position		Photograph Neg No.		Movie Clip
					Side	Top	Stop Action	Time Exp	
42	2	90	5,800	6,000	x		83	84	x
43	2	110	6,100	6,000	x		85	86	x
44	2	120	5,850	6,000	x		87	88	x
45	1	0	4,520	6,000	x		89	90	x
46	1	10	4,210	6,000	x		91	92	x
47	1	20	4,330	6,000	x		93	94	x
48	1	25	4,110	6,000	x		95	96	x
49	1	35	4,220	6,000	x		97	98	x
50	1	50	3,760	6,000	x		99	100	x
51	1	60	3,650	6,000	x		101	102	x
52	1	70	3,820	6,000	x		103	104	x
53	1	90	4,210	6,000	x		105	106	x
54	1	110	3,300	6,000	x		107	108	x
55	1	120	3,690	6,000	x		109	110	x
56	3	0	7,930	6,000	x		111	112	x
57	3	10	7,650	6,000	x		113	114	x
58	3	20	7,590	6,000	x		115	116	x
59	3	25	7,480	6,000	x		117	118	x
60	3	35	7,630	6,000	x		119	120	x
61	3	50	7,760	6,000	x		121	122	x
62	3	60	8,040	6,000	x		123	124	x
63	3	70	8,570	6,000	x		125	126	x

Line No.	No. of Blades on Rotor	Equiv Fwd Vel (kt)	Equiv Full-Scale Lift (lb)	Conditions Established for 2-Bladed Lift of (lb)	Viewing Position		Photograph Neg No.		Movie Clip
					Side	Top	Stop Action	Time Exp	
64	3	90	8,540	6,000	x		127	128	x
65	3	110	8,900	6,000	x		129	130	x
66	3	120	8,530	6,000	x		131	132	x
67	2	0	8,090	8,000	x		133	134	x
68	2	10	7,750	8,000	x		135	136	x
69	2	20	7,900	8,000	x		137	138	x
70	2	25	7,950	8,000	x		139	140	x
71	2	35	7,930	8,000	x		141	142	x
72	2	50	8,175	8,000	x		143	144	x
73	2	60	8,000	8,000	x		145	146	x
74	2	70	7,825	8,000	x		147	148	x
75	2	90	7,875	8,000	x		149	150	x
76	2	110	7,900	8,000	x		151	152	x
77	2	120	8,150	8,000	x		153	154	x
78	1	0	5,050	8,000	x		155	156	x
79	1	10	5,100	8,000	x		157	158	x
80	1	20	4,140	8,000	x		159	160	x
81	1	25	5,540	8,000	x		161	162	x
82	1	35	5,180	8,000	x		163	164	x
83	1	50	4,980	8,000	x		165	166	x
84	1	60	4,900	8,000	x		167	168	x
85	1	70	4,680	8,000	x		169	170	x

Line No.	No. of Blades on Rotor	Equiv Fwd Vel (kt)	Equiv Full-Scale Lift (lb)	Conditions Established for 2-Bladed Lift of ≈ (lb)	Viewing Position		Photograph Neg No.		Movie Clip
					Side	Top	Stop Action	Time Exp	
86	1	90	4,920	8,000	x		171	172	x
87	1	110	5,000	8,000	x		173	174	x
88	1	120	4,560	8,000	x		175	176	x
89	3	0	10,480	8,000	x		177	178	x
90	3	10	10,450	8,000	x		179	180	x
91	3	20	10,250	8,000	x		181	182	x
92	3	25	10,200	8,000	x		183	184	x
93	3	35	9,800	8,000	x		185	186	x
94	3	50	10,520	8,000	x		187	188	x
95	3	60	10,230	8,000	x		189	190	x
96	3	70	10,720	8,000	x		191	192	x
97	3	90	11,500	8,000	x		193	194	x
98	3	110	11,180	8,000	x		195	196	x
99	3	120	11,280	8,000	x		197	198	x
100	2	0	10,075	10,000	x		199	200	x
101	2	10	9,960	10,000	x		201	202	x
102	2	20	10,150	10,000	x		203	204	x
103	2	25	10,175	10,000	x		205	206	
104	2	35	10,100	10,000	x		207	208	x
105	2	50	9,925	10,000	x		209	210	x
106	2	60	10,175	10,000	x		211	212	x
107	2	70	9,950	10,000	x		213	214	x

Line No.	No. of Blades on Rotor	Equiv Fwd Vel (kt)	Equiv Full-Scale Lift (lb)	Conditions Established for 2-Bladed Lift of (lb)	Viewing Position		Photograph Neg No.		Movie Clip
					Side	Top	Stop Action	Time Exp	
108	2	90	9,760	10,000	x		215	216	x
109	2	110	9,940	10,000	x		217	218	x
110	2	120	9,750	10,000	x		219	220	x
111	1	0	6,460	10,000	x		221	222	x
112	1	10	6,010	10,000	x		223	224	x
113	1	20	6,200	10,000	x		225	226	x
114	1	25	5,920	10,000	x		227	228	x
115	1	35	6,190	10,000	x		229	230	x
116	1	50	5,920	10,000	x		231	232	x
117	1	60	5,850	10,000	x		233	234	x
118	1	70	5,620	10,000	x		235	236	x
119	1	90	5,790	10,000	x		237	238	x
120	1	110	5,580	10,000	x		239	240	x
121	1	120	5,390	10,000	x		241	242	x
122	3	0	13,600	10,000	x		243	244	x
123	3	10	13,250	10,000	x		245	246	x
124	3	20	13,250	10,000	x		247	248	x
125	3	25	12,900	10,000	x		249	250	x
126	3	35	13,480	10,000	x		251	252	x
127	3	50	13,400	10,000	x		253	254	x
128	3	60	13,950	10,000	x		255	256	x
129	3	70	13,500	10,000	x		257	258	x

Line No.	No. of Blades on Rotor	Equiv Fwd Vel (kt)	Equiv Full-Scale Lift (lb)	Conditions Established for 2-Bladed Lift of = (lb)	Viewing Position		Photograph Neg No.		Movie Clip
					Side	Top	Stop Action	Time Exp	
130	3	90	13,650	10,000	x		259	260	x
131	3	110	13,700	10,000	x		261	262	x
132	3	120	13,300	10,000	x		263	264	x
133	2	0	4,060	4,000		x	265	266	x
134	2	10	3,940	4,000		x	267	268	x
135	2	20	4,000	4,000		x	269	270	x
136	2	25	4,010	4,000		x	271	272	x
137	2	35	4,070	4,000		x	273	274	x
138	2	50	3,985	4,000		x	275	276	x
139	2	60	4,025	4,000		x	277	278	x
140	2	70	3,910	4,000		x	279	280	x
141	2	90	3,980	4,000		x	281	282	x
142	2	110	3,970	4,000		x	283	284	x
143	2	120	4,000	4,000		x	285	286	x
144	1	0	3,020	4,000		x	287	288	x
145	1	10	3,060	4,000		x	289	290	x
146	1	20	3,060	4,000		x	291	292	x
147	1	25	2,940	4,000		x	293	294	x
148	1	35	3,050	4,000		x	295	296	x
149	1	50	2,640	4,000		x	297	298	x
150	1	60	2,540	4,000		x	299	300	x
151	1	70	2,520	4,000		x	301	302	x

Line No.	No. of Blades on Rotor	Equiv Fwd Vel (kt)	Equiv Full-Scale Lift (lb)	Conditions Established for 2-Bladed Lift of ≈ (lb)	Viewing Position		Photograph Neg No.		Movie Clip
					Side	Top	Stop Action	Time Exp	
152	1	90	2,590	4,000		x	303	304	x
153	1	110	2,580	4,000		x	305	306	x
154	1	120	2,560	4,000		x	307	308	x
155	3	0	5,400	4,000		x	309	310	x
156	3	10	5,240	4,000		x	311	312	x
157	3	20	4,960	4,000		x	313	314	x
158	3	25	4,760	4,000		x	315	316	x
159	3	35	5,000	4,000		x	317	318	x
160	3	50	5,240	4,000		x	319	320	x
161	3	60	5,440	4,000		x	321	322	x
162	3	70	5,400	4,000		x	323	324	x
163	3	90	5,800	4,000		x	325	326	x
164	3	110	5,890	4,000		x	327	328	x
165	3	120	5,720	4,000		x	329	330	x
166	2	0	5,950	6,000		x	331	332	x
167	2	10	5,975	6,000		x	333	334	x
168	2	20	6,100	6,000		x	335	336	x
169	2	25	5,950	6,000		x	337	338	x
170	2	35	5,975	6,000		x	339	340	x
171	2	50	5,950	6,000		x	341	342	x
172	2	60	5,850	6,000		x	343	344	x
173	2	70	6,050	6,000		x	345	346	x

Line No.	No. of Blades on Rotor	Equiv Fwd Vel (kt)	Equiv Full-Scale Lift (lb)	Conditions Established for 2-Bladed Lift of (lb)	Viewing Position		Photograph Neg No.		Movie Clip
					Side	Top	Stop Action	Time Exp	
174	2	90	5,800	6,000		x	347	348	x
175	2	110	6,100	6,000		x	349	350	x
176	2	120	5,850	6,000		x	351	352	x
177	1	0	4,520	6,000		x	353	354	x
178	1	10	4,210	6,000		x	355	356	x
179	1	20	4,330	6,000		x	357	358	x
180	1	25	4,110	6,000		x	359	360	x
181	1	35	4,220	6,000		x	361	362	x
182	1	50	3,760	6,000		x	363	364	x
183	1	60	3,650	6,000		x	365	366	x
184	1	70	3,820	6,000		x	367	368	x
185	1	90	4,210	6,000		x	369	370	x
186	1	110	3,300	6,000		x	371	372	x
187	1	120	3,690	6,000		x	373	374	x
188	3	0	7,930	6,000		x	375	376	x
189	3	10	7,650	6,000		x	377	378	x
190	3	20	7,590	6,000		x	379	380	x
191	3	25	7,480	6,000		x	381	382	x
192	3	35	7,630	6,000		x	383	384	x
193	3	50	7,760	6,000		x	385	386	x
194	3	60	8,040	6,000		x	387	388	x
195	3	70	8,570	6,000		x	389	390	x

Line No.	No. of Blades on Rotor	Equiv Fwd Vel (kt)	Equiv Full-Scale Lift (lb)	Conditions Established for 2-Bladed Lift of (lb)	Viewing Position		Photograph Neg No.		Movie Clip
					Side	Top	Stop Action	Time Exp	
196	3	90	8,540	6,000		x	391	392	x
197	3	110	8,900	6,000		x	393	394	x
198	3	120	8,530	6,000		x	395	396	x
199	2	0	8,090	8,000		x	397	398	x
200	2	10	7,750	8,000		x	399	400	x
201	2	20	7,900	8,000		x	401	402	x
202	2	25	7,950	8,000		x	403	404	x
203	2	35	7,930	8,000		x	405	406	x
204	2	50	8,175	8,000		x	407	408	x
205	2	60	8,000	8,000		x	409	410	x
206	2	70	7,825	8,000		x	411	412	x
207	2	90	7,875	8,000		x	413	414	x
208	2	110	7,900	8,000		x	415	416	x
209	2	120	8,150	8,000		x	417	418	x
210	1	0	5,050	8,000		x	419	420	x
211	1	10	5,100	8,000		x	421	422	x
212	1	20	4,140	8,000		x	423	424	x
213	1	25	5,540	8,000		x	425	426	x
214	1	35	5,180	8,000		x	427	428	x
215	1	50	4,980	8,000		x	429	430	x
216	1	60	4,900	8,000		x	431	432	x
217	1	70	4,680	8,000		x	433	434	x

Line No.	No. of Blades on Rotor	Equiv Fwd Vel (kt)	Equiv Full-Scale Lift (lb)	Conditions Established for 2-Bladed Lift of = (lb)	Viewing Position		Photograph Neg No.		Movie Clip
					Side	Top	Stop Action	Time Exp	
218	1	90	4,920	8,000		x	435	436	x
219	1	110	5,000	8,000		x	437	438	x
220	1	120	4,560	8,000		x	439	440	x
221	3	0	10,480	8,000		x	441	442	x
222	3	10	10,450	8,000		x	443	444	x
223	3	20	10,250	8,000		x	445	446	x
224	3	25	10,200	8,000		x	447	448	x
225	3	35	9,800	8,000		x	449	450	x
226	3	50	10,520	8,000		x	451	452	x
227	3	60	10,230	8,000		x	453	454	x
228	3	70	10,720	8,000		x	455	456	x
229	3	90	11,500	8,000		x	457	458	x
230	3	110	11,180	8,000		x	459	460	x
231	3	120	11,280	8,000		x	461	462	x
232	2	0	10,075	10,000		x	463	464	x
233	2	10	9,960	10,000		x	465	466	x
234	2	20	10,150	10,000		x	467	468	x
235	2	25	10,175	10,000		x	469	470	x
236	2	35	10,100	10,000		x	471	472	x
237	2	50	9,925	10,000		x	473	474	x
238	2	60	10,175	10,000		x	475	476	x
239	2	70	9,950	10,000		x	477	478	x

Line No.	No. of Blades on Rotor	Equiv Fwd Vel (kt)	Equiv Full-Scale Lift (lb)	Conditions Established for 2-Bladed Lift of (lb)	Viewing Position		Photograph Neg No.		Movie Clip
					Side	Top	Stop Action	Time Exp	
240	2	90	9,760	10,000		x	479	480	x
241	2	110	9,940	10,000		x	481	482	x
242	2	120	9,750	10,000		x	483	484	x
243	1	0	6,460	10,000		x	485	486	x
244	1	10	6,010	10,000		x	487	488	x
245	1	20	6,200	10,000		x	489	490	x
246	1	25	5,920	10,000		x	491	492	x
247	1	35	6,190	10,000		x	493	494	x
248	1	50	5,920	10,000		x	495	496	x
249	1	60	5,850	10,000		x	497	498	x
250	1	70	5,620	10,000		x	499	500	x
251	1	90	5,790	10,000		x	501	502	x
252	1	110	5,580	10,000		x	503	504	x
253	1	120	5,390	10,000		x	505	506	x
254	3	0	13,600	10,000		x	507	508	x
255	3	10	13,250	10,000		x	509	510	x
256	3	20	13,250	10,000		x	511	512	x
257	3	25	12,900	10,000		x	513	514	x
258	3	35	13,480	10,000		x	515	516	x
259	3	50	13,400	10,000		x	517	518	x
260	3	60	13,950	10,000		x	519	520	x
261	3	70	13,500	10,000		x	521	522	x

Line No.	No. of Blades on Rotor	Equiv Fwd Vel (kt)	Equiv Full-Scale Lift (lb)	Conditions Established for 2-Bladed Lift of (lb)	Viewing Position		Photograph Neg No.		Movie Clip
					Side	Top	Stop Action	Time Exp	
262	3	90	13,650	10,000		x	523	524	x
263	3	110	13,700	10,000		x	525	526	x
264	3	120	13,300	10,000		x	527	528	x

APPENDIX II

AIR BUBBLE STREAK STUDIES

Line No.	No. of Blades on Rotor	Equiv Fwd Vel (kt)	Equiv Full-Scale Lift (lb)	Photograph and Probe Position			Neg No. Position		Viewing Position	
				Port*	Center Line	Stbd*	Side	Top	Side	Top
265	2	0	4,060		673				x	
266	2	10	3,940		674				x	
267	2	25	4,010		675				x	
268	2	0	8,090	676	677	678			x	
269	2	10	7,750	679	680	681			x	
270	2	20	7,900	682	683	684			x	
271	2	35	7,930	685	686	687			x	
272	2	50	8,175	688	689	690			x	
273	2	70	7,825	691	692	693			x	
274	2	110	7,900	694	695	696			x	
275	2	0	10,075	697	698	699			x	
276	2	10	9,960	700					x	
277	2	25	10,175	701					x	
278	2	0	4,060		702					x
279	2	10	3,940		703					x
280	2	25	4,010		704					x
281	2	0	8,090		705					x

* Port and starboard probe positions were 0.45 rotor radii to either side of the center line.

Line No.	No. of Blades on Rotor	Equiv Fwd Vel (kt)	Equiv Full-Scale Lift (lb)	Photograph and Probe Position			Viewing Position	
				Port*	Center Line	Stbd*	Side	Top
282	2	10	7,750		706			x
283	2	20	7,900		707			x
284	2	35	7,930		708			x
285	2	50	8,175		709			x
286	2	70	7,825		710			x
287	2	110	7,900		711			x
288	2	0	10,075		712			x
289	2	10	9,960		713			x
290	2	25	10,175		714			x

* Port and starboard probe positions were 0.45 rotor radii to either side of the center line.

APPENDIX III

SIMULATED POWER FAILURE

Line No.	No. of Blades on Rotor	Equiv Fwd Vel (kt)	Equiv Full-Scale Lift (lb)	Equiv Rotor Tip Speed	Viewing Position		Photograph	
					Side	Top	Neg Stop Action	No. Time Exp
291	2	70	9,378	583.5	x		529	530
292	2	90	9,441	585.4	x		531	532
293	2	110	9,309	583	x		533	534
294	2	120	9,367	595	x		535	536
295	2	135	9,552	624	x		537	538
296	2	150	9,542	664	x		539	540
297	2	70	8,775	565.5	x		541	542
298	2	90	8,610	554.4	x		543	544
299	2	110	8,542	546	x		545	546
300	2	120	8,671	568	x		547	548
301	2	135	8,888	600	x		549	550
302	2	150	8,913	640	x		551	552
303	2	70	8,250	539.7	x		553	554
304	2	90	8,246	542.5	x		555	556
305	2	110	8,090	538.4	x		557	558
306	2	120	8,338	558	x		559	560
307	2	135	8,397	582	x		561	562
308	2	150	8,475	627	x		563	564
309	2	70	5,266	438	x		565	566

Line No.	No. of Blades on Rotor	Equiv Fwd Vel (kt)	Equiv Full-Scale Lift (lb)	Equiv Rotor Tip Speed	Viewing Position		Photograph	
					Side	Top	Neg Stop Action	No. Time Exp
310	2	90	5,299	449	x		567	568
311	2	110	5,324	454	x		569	570
312	2	120	5,316	452	x		571	572
313	2	135	5,347	487	x		573	574
314	2	150	5,545	534	x		575	576
315	2	70	4,901	420	x		577	578
316	2	90	4,969	428	x		579	580
317	2	110	4,806	428	x		581	582
318	2	120	4,855	439	x		583	584
319	2	135	4,937	467	x		585	586
320	2	150	5,055	511	x		587	588
321	2	70	4,423	402	x		589	590
322	2	90	4,412	401	x		591	592
323	2	110	4,367	407	x		593	594
324	2	120	4,514	421	x		595	596
325	2	135	4,605	451	x		597	598
326	2	150	4,507	484	x		599	600
327	2	70	9,377	583		x	601	602
328	2	90	9,441	585		x	603	604
329	2	110	9,309	583		x	605	606
330	2	120	9,367	595		x	607	608
331	2	135	9,552	624		x	609	610

Line No.	No. of Blades on Rotor	Equiv Fwd Vel (kt)	Equiv Full-Scale Lift (lb)	Equiv Rotor Tip Speed	Viewing Position		Photograph	
					Side	Top	Neg Stop Action	No. Time Exp
332	2	150	9,542	664		x	611	612
333	2	70	8,775	565		x	613	614
334	2	90	8,610	554		x	615	616
335	2	110	8,542	546		x	617	618
336	2	120	8,671	568		x	619	620
337	2	135	8,888	600		x	621	622
338	2	150	8,913	640		x	623	624
339	2	70	8,250	539		x	625	626
340	2	90	8,246	542		x	627	628
341	2	110	8,090	538		x	629	630
342	2	120	8,338	558		x	631	632
343	2	135	8,397	582		x	633	634
344	2	150	8,475	627		x	635	636
345	2	70	5,266	438		x	637	638
346	2	90	5,299	449		x	639	640
347	2	110	5,324	454		x	641	642
348	2	120	5,316	452		x	643	644
349	2	135	5,347	487		x	645	646
350	2	150	5,545	534		x	647	648
351	2	70	4,901	420		x	649	650
352	2	90	4,969	428		x	651	652
353	2	110	4,806	428		x	653	654

Line No.	No. of Blades on Rotor	Equiv Fwd Vel (kt)	Equiv Full-Scale Lift (lb)	Equiv Rotor Tip Speed	Viewing Position		Photograph Neg No.	
					Side	Top	Stop Action	Time Exp
354	2	120	4,855	439		x	655	656
355	2	135	4,937	467		x	657	658
356	2	150	5,055	511		x	659	660
357	2	70	4,423	402		x	661	662
358	2	90	4,412	401		x	663	664
359	2	110	4,367	407		x	665	666
360	2	120	4,514	421		x	667	668
361	2	135	4,605	451		x	669	670
362	2	150	4,507	484		x	671	672

Unclassified
Security Classification

DOCUMENT CONTROL DATA - R & D		
<i>(Security classification of title, body of abstract and indexing annotation must be entered when the overall report is classified)</i>		
1. ORIGINATING ACTIVITY (Corporate author) Oceanics, Inc. Technical Industrial Park Plainview, New York		2a. REPORT SECURITY CLASSIFICATION Unclassified
		2b. GROUP
3. REPORT TITLE Model Studies of Helicopter Rotor Flow Patterns		
4. DESCRIPTIVE NOTES (Type of report and inclusive dates) Final Technical Report		
5. AUTHOR(S) (First name, middle initial, last name) August F. Lehman		
6. REPORT DATE April 1968	7a. TOTAL NO. OF PAGES 118	7b. NO. OF REFS 16
8a. CONTRACT OR GRANT NO. DA 44-177-AMC-426(T)	9a. ORIGINATOR'S REPORT NUMBER(S) USAAVLABS Technical Report 68-17	
b. PROJECT NO. Task 1F125901A14232	9b. OTHER REPORT NO(S) (Any other numbers that may be assigned this report) 67-38	
c.		
d.		
10. DISTRIBUTION STATEMENT This document has been approved for public release and sale; its distribution is unlimited.		
11. SUPPLEMENTARY NOTES	12. SPONSORING MILITARY ACTIVITY US Army Aviation Materiel Laboratories Fort Eustis, Virginia	
13. ABSTRACT This report discusses an experimental program undertaken in a water tunnel wherein the tip vortex patterns were made visible through air bubble injection at the rotor tips. The model was a scaled version of the 48-foot-diameter Bell UH-1D rotor. The rotor configuration was tested as a standard 2-bladed unit and also as a 1- and 3-bladed unit. Correlation was established by comparing full-scale vertical lift values (at hover conditions) with scaled model values, where the model was mounted above the tunnel floor at a distance equivalent to "out of ground" effects for the full-scale vehicle. Employing solely a Prandtl-Glauert correction factor produced excellent lift value agreement between the model and the full-scale vehicle. Different aspects of the tip vortex patterns were visible from 2 to 6 diameters downstream, thus the technique appears promising for both near and far field studies. High speed movies and stop and time exposure photographs were used to document the variation in vortex patterns. Discrete tip vortex patterns are created for forward flight regimes in the general ranges of hover to 10 knots, 10 to 50 knots, and above 50 knots. Tip vortices shed from one blade do intersect with following blades (under certain conditions), thus verifying a limitation in the commonly employed mathematical models, where this limitation has been hypothesized by certain other investigators.		

DD FORM 1473
1 NOV 65

REPLACES DD FORM 1473, 1 JAN 64, WHICH IS
OBSOLETE FOR ARMY USE.

Unclassified

Security Classification

Unclassified
Security Classification

14 KEY WORDS	LINK A		LINK B		LINK C	
	ROLE	WT	ROLE	WT	ROLE	WT
Flow Visualization Helicopter Rotor Rotor Flow Patterns Aerodynamics Water Tunnel Tests						

Unclassified
Security Classification

4760-68